Predicting the Effectiveness of Post-Weld Treatments Applied under Load

by

Kasra Ghahremani

A thesis

presented to the University of Waterloo

in fulfillment of the

thesis requirement for the degree of

Master of Applied Science

in

Civil Engineering

Waterloo, Ontario, Canada, 2010

AUTHOR'S DECLARATION

I hereby declare that I am the sole author of this thesis. This is a true copy of the thesis, including any required final revisions, as accepted by my examiners.

I understand that my thesis may be made electronically available to the public.

Abstract

Existing steel bridges are subjected to both increasing traffic loads and natural aging, both are capable of causing severe durability problems. Dependable rehabilitation methods are attracting attention as the promising methods to enhance structural durability and/or structural performance. One possible rehabilitation method, for improving fatigue performance, is the use of residual stress-based post-weld treatments such as peening. A number of studies has been performed and it has been proven that residual stress-based treatments are an effective way of increasing the fatigue lives of newly built steel bridges, and even enhancing the fatigue performance of existing structures. Provisions have been developed to ensure the proper execution of peening and several codes have considered its beneficial effect in the fatigue design of welded structures.

Various analytical approaches are used to predict the fatigue performance of welded structures and the beneficial effects of residual stress-based post-weld treatments. In most codes and recommendations, variations of the "S-N curve" approach are employed. Linear elastic fracture mechanics (LEFM) and strain-based fracture mechanics (SBFM) are widely accepted approaches for making more precise predictions of the treatment benefit. Cohesive zone fatigue models are also recently introduced for predicting fatigue crack growth in as-received and peened welds.

Despite all the research conducted, there are still two main unanswered questions related to the application of peening treatments. First, it is claimed that peening can be more effective for civil structures where a considerable portion of the total applied stress is due to permanent loads and thus peening is applied under load. However, most of research done so far has studied effects peening prior to the introduction of the structural self weight. Secondly, considering the nature of these treatments, some concerns have been raised regarding their effectiveness under actual in-service loading conditions, as most of the reported test-based studies only demonstrated the fatigue performance improvement under constant amplitude tension-only loading conditions.

The current study was undertaken to examine the fatigue performance of welds peened-under load and to determine the effectiveness of peening for improving the fatigue performance of welds subjected to realistic in-service loading conditions. Moreover, a previously developed strain-based fracture mechanics (SBFM) model for predicting fatigue performance of welded details under different loading and treatment conditions, and a previously developed damage-based cohesive zone model for steel specimens were evaluated and calibrated.

Fatigue tests were conducted on welded steel specimens, simulating different loading and peening conditions. Dye penetrant was used to stain cracked specimens upon detection of cracks and a crack front marking loading scheme was used to study the crack front shape. The alternating current potential drop (ACPD) method was used for continuous crack growth monitoring for both as-welded and peened specimens under different loading schemes. It was observed that cracks propagated at different rates in specimens treated under load than in the normally peened and as-welded specimens. Material tests were also conducted to determine the mechanical properties of the steel base metal. Secondary effects of peening were investigated by microhardness measurements and weld toe measurements. A number of typical weld toe defects was also detected. Residual stress measurements showed a uniformly distributed tensile residual stress near the surface of the untreated specimen. Needle peening the specimen resulted in a significant change in the residual stress distribution through the specimen thickness.

In all cases, peening resulted in a significant increase in the fatigue life. However, greater fatigue life improvements were observed in lower stress ranges. Of the specimens tested under constant amplitude loading, those peened under load experienced the largest fatigue lives. For the variable amplitude loading tests, the untreated specimens had mean fatigue lives slightly less than observed in the constant amplitude tests.

A previously developed strain-based fracture mechanics (SBFM) model was used to estimate analytically the effectiveness of peening applied to welded details. The model was able to predict the fatigue lives for both the as-welded and peened specimens for all loading conditions. It correctly estimated the additional benefit of peening when applied under a relatively small prestress level. The model predictions were used to estimate the additional benefit of peening under load.

A previously developed cohesive zone model was introduced and applied to predict fatigue crack growth in a weld detail under cyclic loading. Fatigue tests were simulated using the finite element program ABAQUS. The material parameters α and β were chosen by iteration. Other fatigue tests were simulated and the model correctly predicted the effects of varying the applied stress range, R ratio, and residual stress level on the fatigue behaviour.

Acknowledgements

I would like to thank the following persons for their contributions to this work:

- God. Also my parents and my brother for their unconditional love and unwavering support throughout my life.
- Dr. Scott Walbridge and Dr. Katerina Papoulia, invaluable co-supervisors of this thesis, for their guidance, technical support, and for always believing in me during the past two years.
- The readers of my thesis, Prof. Tim Topper and Prof. Carl T. Haas, for their insightful comments and suggestions.
- Civil Engineering Structures Lab technicians, Richard Morrison, Dough Hirst, and Rob Sluban for their assistance during the experimental phase of this program.
- Victor Baltazar for his assistance with the microhardness measurements, Amin Eshraghi for his guidance with ABAQUS modelling, Max Hsu for his assistance with the weld toe geometry measurements, and Jeff Luckai for reading my thesis.
- Solmaz for all her help and support.
- My colleagues and officemates Farhad, Reid, Matthew, Alan, Greg, and Richard for their friendship.

Dedicated to my parents,

who gave me the two greatest things in the world:

roots and wings.

Table of Contents

List of Figures

List of Tables

Chapter 1
Introduction

1.1 Background and motivation

The rehabilitation of existing steel bridges is recently attracting increased attention. These structures are subjected to both increasing traffic loads and natural aging, both of which are capable of causing severe durability problems. Based on the 2009 Annual Report of the Office of the Auditor General of Ontario [Auditor General of Ontario, 2009], more than 70% of the bridges in Ontario were built between 1950 and 1980, giving an average age of about 40 years. Indeed there is a need for immediate action to build new infrastructure, decrease the traffic loading on existing structures, or use safe, economical, and dependable rehabilitation methods to enhance their durability and/or structural performance.

One possible rehabilitation method for improving fatigue performance that has received recent attention is the use of residual stress-based post-weld treatments such as hammer peening, needle peening, and Ultrasonic Impact Treatment (UIT) (See Figure 1.1). By introducing permanent plastic deformation at the expected crack location, these treatments keep the crack tip closed. Thus, fatigue cracks are not allowed to open and close during cyclic loading and thus, cannot propagate. A number of studies have been performed and it has been shown that although the effectiveness of these treatments is highly dependent on the loading conditions, in some realistic in-service loading conditions, fatigue life can be increased by more than 100% [Manteghi and Maddox 2004].

Several studies have shown that residual stress-based treatments are an effective way of increasing the fatigue lives of newly built steel bridges, and even enhancing the fatigue performance of existing ones. In addition, when compared to other weld treatments such as “grinding” and “dressing”, peening is more cost effective, easier to perform, faster, and does not require highly skilled technicians. Provisions have been developed to ensure the proper execution of peening [IIW 2005] and several codes have considered its beneficial effect in the fatigue design of welded structures. For example, the use of UIT as a rehabilitation method for existing highway bridges has been recently permitted by AASHTO.

Figure 1.1: View of the zone of repair (welding +UP treatment) of fatigue crack in welded element of bridge span (left) [Kudryavtsev et al. 2005], and needle peening a weld toe in [Walbridge 2005] (right)

Various analytical approaches are used to predict the fatigue performance of welded structures and also the beneficial effects of residual stress-based post-weld treatments. In most codes and recommendations, variations of the "detail category" or "S-N curve" approach are employed. Linear elastic fracture mechanics (LEFM) is one of the most widely used approaches for making more precise predictions of the treatment benefit. A strain-based fracture mechanics(SBFM) approach, which is similar to LEFM in many ways, can be used to account for non-linear material behaviour, which may be significant at the weld toe under high applied stress ranges. Thus, SBFM is suitable for considering the effects of the large overloads and underloads that may occur under in-service loading histories typical of bridge structures. Cohesive zone fatigue models are also introduced in this thesis as an alternative approach for predicting fatigue crack growth in as-received and peened welds. Damage-based cohesive models are based on the traction–separation relationship ahead of the crack tip, rather than Paris model typically employed in LEFM and SBFM analyses.

Despite all the research conducted to date, there are still some unanswered questions related to the application of peening treatments that should be addressed before their routine use is expanded to a broader scale. Two of these issues are as follows:

- Most of research done so far has studied effects of "shop-peening", i.e. peening prior to the introduction of the structural self weight. However, for civil structures where a considerable portion of the total applied stress is due to permanent loads, it is claimed that peening can be even more effective [Maddox, 1998 and Ummenhofer et al., 2006].

Until now, however, no design curves exist for considering this additional fatigue life increase.

- Most of the reported test-based studies only demonstrate the fatigue performance improvement under constant amplitude tension-only loading conditions. Considering the nature of these treatments, i.e. residual stress based, some concerns have been raised regarding their effectiveness under actual in-service loading conditions.

1.2 Objectives

Based on the background presented in the previous Section, the current study was undertaken with the following research objectives:

1- *to examine the fatigue performance of welds peened-under load;*

2- *to determine the effectiveness of peening for improving the fatigue performance of welds subjected to realistic in-service loading conditions;*

3- *to evaluate and calibrate a previously developed strain-based fracture mechanics (SBFM) model for predicting fatigue performance of welded details under different loading and treatment conditions; and*

4- *to validate a previously developed damage-based cohesive zone model for steel specimens and evaluate its ability to predict the effects of different loading and treatment conditions.*

1.3 Scope

The fatigue tests performed for the current study were conducted at the University of Waterloo, primarily using the MTS 810 Material Testing System with load capacity of 100 kN. For test series that required a higher load capacity, the MTS 322 with a capacity of 500 kN was used. The small scale test specimen geometry studied herein is a welded stiffener detail, representing a non load-carrying transverse web stiffener in a web girder. Both the web and stiffeners were made from 350W, steel which is similar to the steels commonly used in Canadian bridges [Walker et al. 2008]. The post-weld treatment method that is investigated in this study is needle peening, performed using a compressed air needle gun and following the procedure recommended by the IIW [IIW 2005]. Crack growth measurements were made using the alternating current potential drop (ACPD) method. A TSC ACPD Mk IV instrument was used to monitor crack propagation during testing.

The focus of the analysis is on modelling the effects of the needle peening of the welded details. Both treated and untreated welded details are considered, and effectiveness of the peening when applied under different loading conditions is predicted. Other assumptions and calculations are based on the Canadian Highway Bridge Design Code [CAN/CSA-S6-06].

1.4 Organization of thesis

In this thesis, first a number of key concepts are introduced and a literature review of articles on post-weld treatments is presented in Chapter 2. Next, in Chapter 3, test and measurements procedures are described. Chapter 4 presents the experimental results. In Chapter 5, a previously developed strain-based fracture mechanics(SBFM) model is introduced and its predictions are compared with the test results. This model is then used to predict the additional benefit that results from applying peening under load. A previously developed cohesive zone model is reviewed in Chapter 6 and its ability to predict fatigue crack growth in steel welds is investigated. Finally, in Chapter 7, conclusions are presented along with recommendations for future works in this field.

Chapter 2
Background and Literature Review

2.1 Introduction

This chapter introduces a number of key concepts and reviews the existing literature on post-weld treatments and other research fields addressed in this thesis.

In Section 2.2, key concepts related to the fatigue design of structures are discussed. In Section 2.3, fatigue improvement methods are introduced, and Section 2.4 reviews residual stress-based post-weld treatment (PWT) methods. A general literature review on test based fatigue studies is presented in Section 2.5, which focuses on the following research fields:

- effect of variable amplitude loading spectrum on fatigue behaviour of welded details,
- effect of different peening conditions,
- crack profile and growth measurement methods,
- effect of peening on surface hardness of the material,
- effect of peening on weld toe geometry, and
- residual stress distribution in welded details before and after peening.

2.2 Fatigue design of structures

Fatigue failure of metals is defined as *"the formation of a crack or cracks as a result of the repeated application of loads, each of which is insufficient, by itself, to cause normal static failure"* in [Gurney 1979]. ASTM defines fatigue life, N_f, as "the number of stress cycles of a specified character that a specimen sustains before failure of a specified nature occurs". Fatigue of metals has been studied for over 170 years, after the first fatigue failures were identified in the railway industry. These studies were accelerated after the first fatigue fractures recognized in Liberty ships, during WWII in 1943, in which an all-welded hull was used instead of the traditional riveted hull construction. Soon after, it was realized that all welded details subjected to cyclic loading are susceptible to fatigue cracking and special consideration must therefore be made in the design. Bridges are one of these repeatedly loaded structure types that need special fatigue design consideration.

Three methods that are widely used for the fatigue design of bridges are: the Classification method, the hot-spot stress method, and fracture mechanics. Each method has its advantages and disadvantages as briefly described in the following paragraphs.

The Classification method is based on S-N (characteristic stress versus fatigue life) curves, associated with a 95 or 97.5% survival probability. In this method, a calculated design stress range, induced by the live loads for the detail of interest and a corresponding number of stress cycles that the detail is supposed to endure during its service life are compared to the S-N curve for the appropriate detail category.

Figure 2.1 illustrates an example design by this method using design S-N curves provided in [CAN/CSA-S6-06]. First a detail category is chosen based on the actual design geometry, here a transverse stiffener, which is a class C detail category. This categorization implicitly considers crack location and stress concentrations due to the geometry and nature of the detail. Nominal stresses are used for calculating design stress ranges, i.e. global stresses in the loaded member not including the effects of openings or sudden changes in geometry. Using the S-N curves, the number of cycles to failure can be calculated for a given design stress range or vice versa.

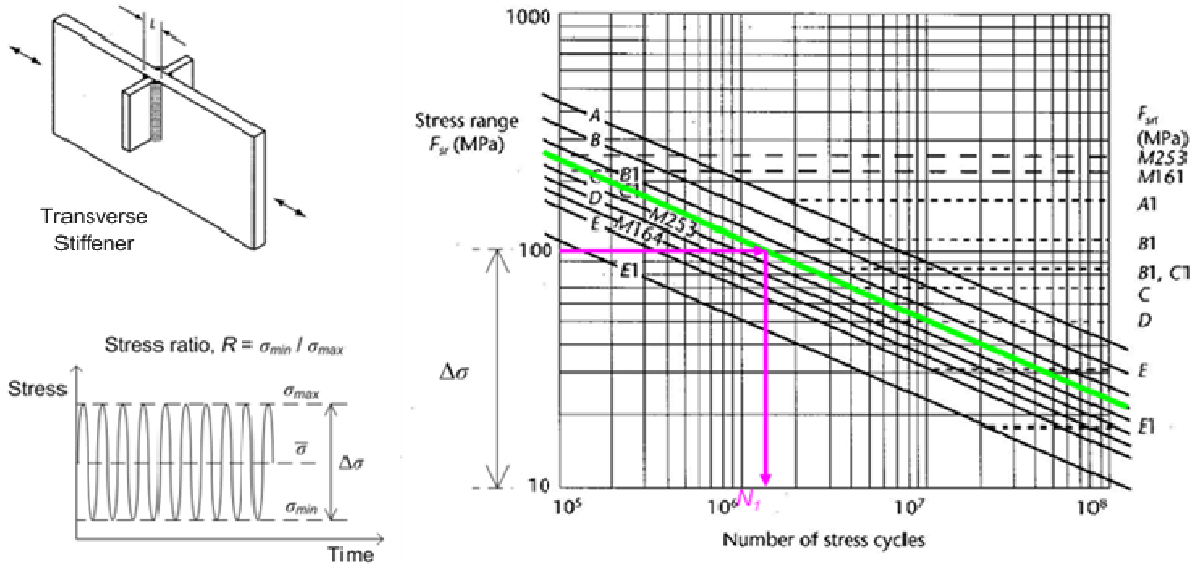

Figure 2.1: Sample use of the design S-N curves; definition of stress range (Δσ) and a detail category C example (left) and design S-N curve for different categories (right) [CAN/CSA-S6-06]

The Classification method based on the nominal global stress in the detail is the most commonly used method for fatigue design of structures. This method is widely accepted as a reliable one for common structures and similar curves are also provided in other design codes such as [AASHTO 1992] and [ECCS 1985].

Though the Classification method is a widely used one because of its simplicity, and is backed by large fatigue test result databases for various common structural details, it has certain disadvantages. The first major disadvantage of this method is that S-N design curves can only be used to design details listed in the codes, and cannot be used to design unusual structural details that are not covered in the codes and fatigue test result databases. Additionally, using these curves does not give any information about the crack depth evolution over the course of the fatigue life [Walbridge 2006].

The hot-spot stress method is suitable for the fatigue design of welded joints in unusual structural details, especially those not covered in the design code detail categories. “Hot-spot” refers to the critical point in the welded joint where the fatigue crack is expected to initiate. The design hot-spot stress can be determined by using one the following three methods: finite element analysis, strain gauge measurements from prototype or real structures, and the application of structural stress concentration factors (SCF),usually resembled by K, according to Equation 2.1 [Partanen and Niemi, 1996]:

$$\sigma_{hs} = K_s \cdot \sigma_{nom} \qquad (2.1)$$

where σ_{hs} is the hot-spot stress, K_s is the structural stress concentration factor for the specific change in the geometry, and σ_{nom} is the nominal stress in the detail. K_s can be determined from direct strain measurements, an analytical formula, or the finite element analysis.

For a welded detail, the method involves calculating the hot-spot stress range based on the structural stress range at the weld toe, including all of the effects of the structural detail, but excluding all stress concentrations due to the weld profile, and a corresponding number of loading cycles for the detail.

Approaching the hot-spot, the actual stress changes (increases) rapidly. The hot-spot stress should be estimated by a suitable extrapolation scheme. Usually, the stress is calculated at two or

three points in the vicinity of the hot-spot and hot-spot stress is then estimated by linear or quadratic extrapolation. Figure 2.2 shows a linearly extrapolated hot-spot stress.

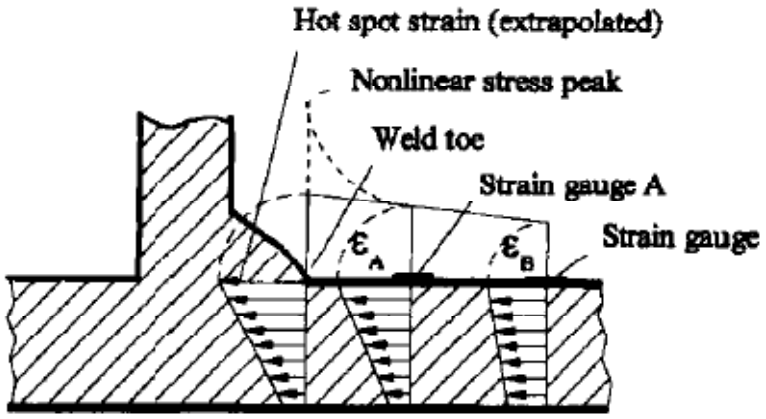

Figure 2.2 : Linearly extrapolated hot-spot [Partanen and Niemi 1996]

Once the hot-spot stress is calculated, it is then compared with a design hot-spot S-N curve, similar to ones used in Classification method. Since it is assumed that the weld toe geometry is identical in all weld joints, a single hot-spot S-N curve can be used for all structural details. This curve should be consistent with the weld type and quality level of the test specimens used in the S-N curve determination and the actual structure. Additionally, to account for size effect, it is possible that the hot-spot S-N curve should be shifted vertically along the stress axis [Walbridge 2005].

Since the stress state is more precisely determined in the hot-spot stress method, using this method leads to fatigue life predictions with less scatter than the Classification method. It is stated in [Partanen and Niemi 1996] that the hot-spot method is mainly appropriate for the analysis of weld toe cracking, where the alternating principal stress due to cyclic loading acts across a weld toe line.

The hot-spot stress method is a relatively simple method to use and is generally more versatile than the Classification method. However, as stated in [Walbridge 2005], it still has a number of short comings such as being only adapted for the design of structural details resembling weld toes and giving “inconsistent results” in some cases due to the current approach for considering the size effect.

The hot-spot approach has been used successfully for welded details in various engineering fields, but with limited application to bridges, in particular in North America. The Classification method is confined to existing detail categories, making it unable to deal with innovative designs. Moreover, the Classification method is limited in dealing with out-of-plane distortion fatigue, another common form of cracking in steel girder bridges. Using the hot-spot method, gives more reliable designs for a wider range of geometries and loading modes, facilitates the use of FEA in design, provides a method for assessing secondary distortion stresses, and makes full analysis of novel configurations possible. For these reasons, the hot-spot stress method is being more widely used in designing structures and an increasing number of studies is being undertaken for fatigue analysis of existing structures and for the fatigue design of special structures and special structural members (e.g. [Nazari and Durack 2007] and [Lotsberg and Sigurdsson 2006]).

Neither the Classification method nor the hot stress approach give precise information about crack size and crack growth in different stages of the structure's service life. Fatigue test results have shown that there are other parameters, e.g. loading scheme, influencing the fatigue behaviour of structures than the design stress range and detail geometry. Moreover, there are a number of fatigue rehabilitation methods that enhance the fatigue behaviour of the structures. The effect of these methods can only be fully understood by using analytical models, flexible enough to account for all these variables. Linear elastic fracture mechanics (LEFM) is such an analytical tool, with the ability to predict the behaviour of propagating cracks in structures.

Fracture mechanics deals with the formation and propagation of cracks in materials by calculating a crack driving force and characterizing the material's resistance to fracture. Linear elastic fracture mechanics assumes that the material is isotropic and linear elastic. Based on these assumptions, the stress field near the crack tip is calculated using the theory of elasticity. In LEFM, most formulas are derived for either plane stress or plane strain conditions, associated with the three basic modes of loading on a cracked body: opening, sliding, and tearing. LEFM is valid only when the inelastic deformation is small compared to the size of the crack, or under a condition commonly referred to as small-scale yielding. If large zones of plastic deformation develop in the vicinity of the crack, other methods such as elastic plastic fracture mechanics (EPFM) or strain-based fracture mechanics (SBFM) must be used.

Fracture mechanics is known to have been first developed by Griffith, an English aeronautical engineer, during the 1920's while working on glass specimens to study the failure of this brittle material [Smith and Kulak 1993]. Based on his experiments, Griffith suggested that microscopic flaws are always present in the bulk material and these flaws cause a low fracture strength and a size dependency of strength. Additionally, he observed that the product of the stress at fracture and square root of the crack (flaw) length was almost constant. i.e.:

$$\sigma_f \cdot \sqrt{a} \sim constant \qquad (2.2)$$

where σ_f is the stress at fracture and a is the initial surface crack (flaw) length.

Griffith's theory provided excellent agreement with experimental data for brittle materials which behave elastically, i.e. theoretically infinite stress at the crack tip, but did not work well for ductile materials. In the late 1950's, Irwin discovered the key role of plasticity in the fracture of ductile materials. He also introduced the concept of the stress intensity factor (SIF), K and stated that the stress distribution in the vicinity of the crack tip is a function of the SIF. Moreover, as long as the small-scale yielding condition holds, cracks with the same K but with different length and loading conditions behave in the same way [Walbridge 2005].

For a central crack with length a in an infinitely large plate under a uniform nominal stress σ, it can be shown that the stress intensity factor can be determined by following expression:

$$K = \sigma \cdot \sqrt{\pi \cdot a} \qquad (2.3)$$

Equation 2.4 shows a more general form of this equation, which can be applied for other specimen geometries and loading conditions. Y is a correction factor that accounts for the geometry of the specimen and the crack and other assumptions such as the presence of a free surface, the finite thickness of the plate, and non-uniformity of the stress distribution:

$$K = Y \cdot \sigma \cdot \sqrt{\pi \cdot a} \qquad (2.4)$$

The relationship between crack growth rate under cyclic loading conditions and stress intensity factor was established in [Paris & Erdogan 1963]. Introducing the stress intensity factor range:

$$\Delta K = K_{max} - K_{min} = Y \cdot \sigma_{max} \cdot \sqrt{\pi \cdot a} - Y \cdot \sigma_{min} \cdot \sqrt{\pi \cdot a} = Y \cdot \Delta\sigma \cdot \sqrt{\pi \cdot a} \qquad (2.5)$$

(σ_{max} , $\sigma_{min,,\ and}$ $\Delta\sigma$ are the maximum nominal applied stress, minimum nominal applied stress, and nominal applied stress range, respectively). The following expression can be used for calculating crack growth rate, *da/dN* (the Paris-Erdogan equation):

$$da/dN = C \cdot \Delta K^m \qquad (2.6)$$

where N is the number of load cycles and C and m are material constants, obtained from experiments. Using Eq. (2.6), it is possible to predict the number of cycles to failure, N_f, by integrating this equation, for a crack that grows from an initial value a_i to the final value, a_f :

$$da/dN = C \cdot \Delta K^m \rightarrow N_f = \int_{a_i}^{a_f} \frac{da}{C \cdot \Delta K^m} \qquad (2.7)$$

It should be noted that a basic assumption of LEFM in the fatigue analysis of welds is that cracks or crack-like defects are present at the very beginning of the fatigue life. In other words, no crack initiation period is considered. Research has shown that this is a reasonable assumption for welded structures [Smith & Smith 1982, Bremen 1989, Haagensen 1989].

Actual crack growth measurements have shown that three distinct phases can be identified in *da/dN – ΔK* curve (see Figure 2.3), namely: slow growth, stable growth, and rapid growth phases. Eq. 2.7 is valid for the stable growth phase of the fatigue life of a crack. As illustrated in Figure 2.3, by considering a threshold stress intensity factor, Eq. 2.7 still can be modified to consider the first phase. With similar modifications considering the effects of crack closure and residual stresses, Paris law's prediction can be improved even more. Details on such modifications can be found in [Stephens et al. 2001, Walbridge 2005].

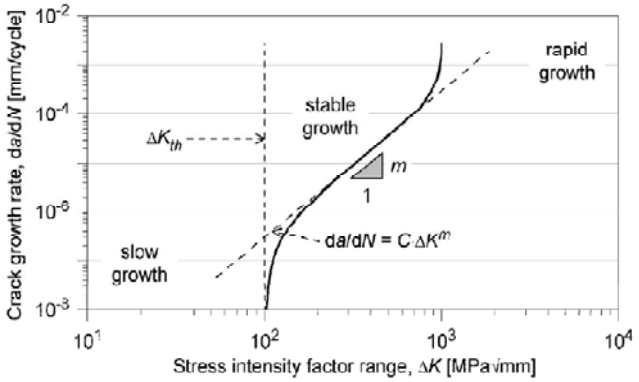

Figure 2.3: Three phases of fatigue crack growth [Walbridge 2005]

2.3 Fatigue improvement techniques

Welds in structures are considered as weak spots in terms of brittle fracture and fatigue strength. Fatigue strength normally does not increase with steel strength and can thus be a limiting factor in the design of high strength steel structures. The fatigue performance of a welded structure can be improved by reducing the nominal stress range, using a detail with a higher fatigue strength, or using post-weld fatigue improvement techniques. Fatigue improvement techniques offer the possibility of improving the fatigue performance of a structure without increasing its self weight. They can be applied to new structures or existing structures to improve fatigue performance in view of changing service requirements or detected deficiencies.

By definition, any special action taken after the completion of weld to improve its fatigue performance is called a "post-weld treatment method" [Walbridge 2005]. There are several fatigue improvement techniques for extending fatigue lives of structures which are categorized based on the aspect of the treated weld that they improve. In [Manteghi and Maddox 2004], the three main causes for fatigue cracking at weld toes are listed as follows:

- Abrupt changes in geometry due to welding at discontinuities often cause geometric stress concentrations. As the stresses are much higher in the regions close the welded zone, fatigue cracks are more likely to initiate and propagate in the vicinity of the welded zone. This makes the weld toe region the most fatigue critical area as the geometrical notch of the weld toe region is less uniform than a notch in a machined component.
- Welded joints have a variety of defects formed during welding operation. These crack-like discontinuities are always present in the welded joints in the form of non-metallic inclusions, and most of them are sharp enough to start growing right after the structure is subjected to cyclic loads. Thus, the crack initiation stage of the fatigue life is reduced or eliminated.
- Residual stresses are present in and near the weld toe because of the contraction of the weld metal, as it cools to ambient temperature, and can be as high as the yield stress in magnitude. These residual stresses intensify fatigue cracking by keeping the crack faces always open. Moreover, since applied cyclic stresses are added to these high tensile static stresses, tensile applied stress cycles become more damaging and compressive applied stress cycles can also contribute to fatigue cracking. In fact, residual stresses affect the

fatigue behaviour in a similar manner to externally imposed mean loads, i.e. a tensile residual stress reduces fatigue life while a compressive stress increases life.

Other factors such as metallurgical changes in the material in the heat affected zone (HAZ) and environmental effects (e.g. corrosive environment) may also affect fatigue behaviour of the component or limit the fatigue strength that can be obtained by improvement techniques.

As mentioned earlier, the low fatigue strength of welded connections is generally due to the very short crack initiation period, i.e. about 10 to 30% of the total life compare to the more than 90% typically observed in smooth specimens tested at low stresses. Thus, fatigue life can be increased by using fatigue improvement techniques that either slow the crack propagation rate or introduce a significant crack initiation period by reducing the stress concentration factor of the weld, removing crack-like defects at the weld toe, removing harmful tensile welding residual stresses, or introducing beneficial compressive stresses.

The first two approaches both involve changing the local geometry and the second two deal with residual stress modification. Thus, treatment methods are divided in two main groups: weld toe geometry modification methods and residual stress based methods.

In the following sections, a number of fatigue improving post-weld treatment techniques with wide range industrial application are discussed. Weld toe grinding and remelting are classed as weld toe geometry modification methods. Peening is considered to be a residual stress-based technique.

2.3.1 Weld toe grinding

Two objectives are targeted by using grinding methods; first to modify the weld profile and consequently reduce the stress concentration at the weld toe, and second, to remove, or at least reduce, the small crack-like flaws existing in the weld. Grinding is an effective, relatively simple to perform, and inexpensive improvement method that gives large increases in fatigue life, typically from 15 to 100% at long lives (see Figure 2.4). However, it is mainly applicable to planar joints and cannot be employed to details without sufficient access to the weld.

Grinding has to be carried out to a minimum depth of 0.5 mm below the plate surface or any visible undercut to ensure removal of the slag inclusions. Two forms of grinders are currently used; disc and rotary burr. Burr grinding is a relatively slow and expensive method, which results

in large improvements for all types of welds, whereas disc grinding is a fast but less effective method and improper use of it may remove too much material and cause serious damage to the part.

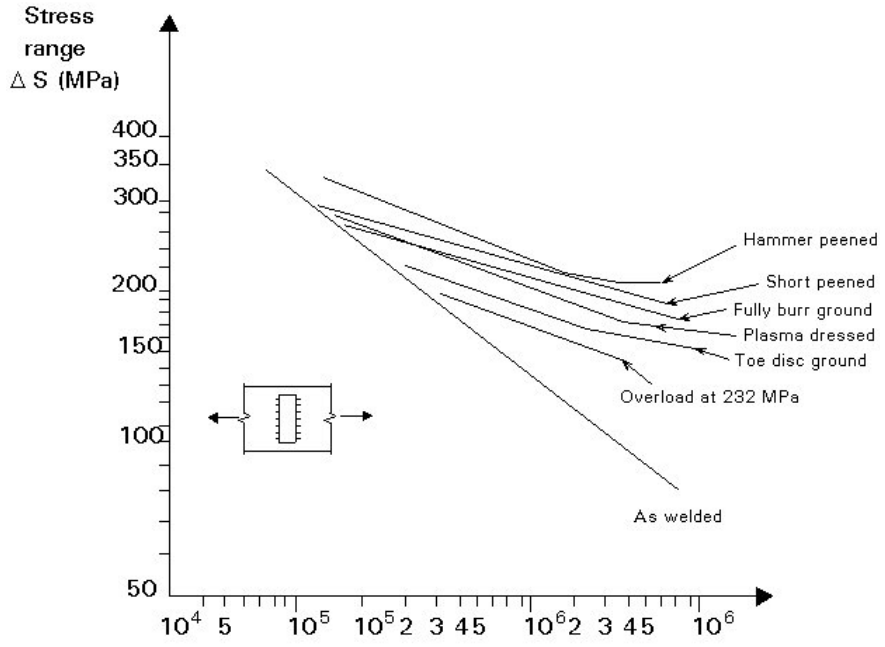

Figure 2.4: Comparison of results obtained by some improvement methods [ESDEP]

2.3.2 Weld toe remelting

The fact that the TIG (Tungsten Inert Gas) and plasma welding processes do not leave slag inclusions, brought up the idea of using TIG or plasma torch to re-melt the potential crack sites, i.e. weld toes made by other welding processes, to produce a slag inclusion free surface. Remelting the weld toe, using either a TIG or plasma torch, results in a smoother weld toe transition and thus a smaller stress concentration factor, as well as the removal of slag inclusions and undercuts. Plasma dressing generally tends to give better results than TIG dressing. Remelting methods give large improvements; however, immobile equipment and the expensive skilled manpower needed for both TIG and plasma dressing along with the possible risk of over hardening the material as reported in [Haagensen 1989] are the main disadvantages of these methods. [Walbridge 2005].

Like other PWT methods, the magnitude of fatigue life improvement depends primarily on the weld toe condition and base material strength ranging from about 10% for butt welds in mild

steel plates to about 100% for fillet welded high strength. Figure 2.5 shows typical results for fillet welds [Haagensen 1978].

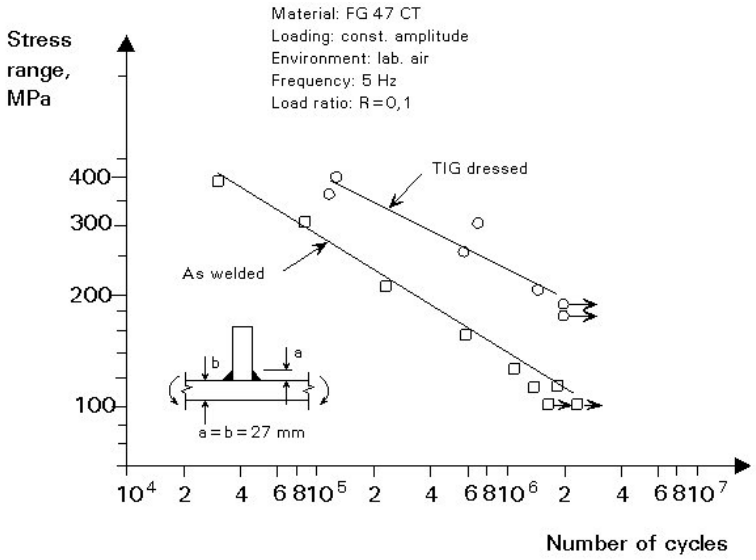

Figure 2.5: Effect of TIG dressing on the fatigue strength of a medium strength steel [ESDEP]

2.3.3 Residual stress-based PWT methods

Residual stress-based post-weld treatment (PWT) methods aim to mitigate the effect of welding induced tensile residual stresses. Some of them relax residual stresses, while others go further and introduce compressive residual stresses to the treated region, usually the weld toe. The latter methods are more efficient because, in contrast with tensile residual stresses, compressive residual stresses keep the crack faces closed during low applied stress cycles.

Stress relief by vibratory techniques or by post-weld heat treatment are stress relaxation methods, and tensile overloading, spot heating, local compression, and peening are examples of residual stress field modification near the weld toe. Of these, peening is probably the most practical and widely used residual stress-based PWT technique. Peening is a cold work process that can improve or change a metal's surface to improve its material properties, usually by mechanical means such as hammer blows. In this process, the surface of the component is impacted using the peening tool with sufficient force to create plastic deformation. Expansion of the deformed material is restrained by the surrounding material. As a result, compressive residual stresses are created in the surface layer, which are then balanced by tensile residual stresses elsewhere. If the

compressive stresses are large enough in magnitude, they can slow down, or even stop, the growth of small fatigue cracks.

The four main peening methods that are listed in [Manteghi and Maddox 2004] are as follows:

- Hammer and needle peening

  Hammer peening involves hammering of the surface using a solid pneumatically operated tool with a rounded tip having a 6-14 mm radius. A similar technique consists of using a wire bundle instead of a solid tool (needle peening). The solid tool results in more severe deformation and gives better improvements than both needle and shot peening [Knight 1978]. Optimum results for hammer peening are obtained after four passes, which severely deforms the weld toe, resulting in a smooth dent. An almost uniform indentation depth of about 0.6mm provides a simple inspection criterion. Like burr grinding, hammer peening is a noisy operation. The improvements resulting from hammer peening are among the highest reported (see Figure 2.5). Even larger improvements are possible for higher strength steels [Knight 1978].
- Shot peening

  The shot peening process involves bombarding the surface of a part with high velocity shot (round metallic, glass, or ceramic beads) with force enough to create plastic deformation and thus compressive residual surface stresses of about 70 to 80% of the yield stress. In fact, each bead acts as a small hammer. Shot peening is done by placing the part in a chamber and performing the shot peening automatically. Other equipment suitable for site treatment of structures is also available [Walbridge 2005]. Significant improvements can be achieved by shot peening. Typically an increase between 30 to 100% in fatigue strength is expected in long life region, however, at shorter lives ($N < 10{,}000$ cycles) there is almost no improvement.

  Large areas can be covered by shot peening at low cost. There are some arguments regarding stress relaxation but fatigue tests carried out in [Grimme et al. 1984] showed that induced compressive residual stresses are not relaxed even with large tensile overloads.

- Ultrasonic peening

  Ultrasonic peening or ultrasonic impact treatment (UIT) is essentially similar to hammer peening. A major difference is that the vibrating frequency of the impacting needles is significantly increased from 25-100 Hz to 27,000 Hz. It has some advantages over the previous mentioned methods such as better control and less noise. The primary effect of UIT is modification of the residual stresses, although it has been argued that additional improvements may results from the beneficial effects of UIT on the weld toe geometry and near-surface microstructures.

2.3.4 Compounding

Two improvement methods can be combined to give even larger improvements, especially when weld toe geometry method and a residual stress-based method are combined together. An example is reported in [Gurney 1968] in which the fatigue strength of fillet welds in mild steel was restored to that of the base metal by first full profile grinding followed by hammer peening. Other combinations are also reported such as grinding and peening and AWS weld profile control and shot peening [Haagensen et al 1987] and the resulting improvement was double that of using a single method.

2.4 Fatigue behaviour of welds under variable amplitude (VA) loading

2.4.1 Design consideration

Available design curves and fatigue limits are mostly based on constant amplitude (CA) loading fatigue studies. In CA loading, all load cycles have the same stress range, $\Delta S = S_{max} - S_{min}$, equal to that induced by the maximum live load and log-log bilinear S-N curves are deduced based on this assumption. As the S-N data suggests, there is a specific stress range (hereafter called the fatigue limit) below which cracks do not propagate and no fatigue damage is assumed to occur. For stress ranges greater than the fatigue limit, all stress cycles cause fatigue damage and the number of cycles to failure can be determined from the inclined part of the design S-N curve.

Fatigue design of the welded details in actual structures using constant amplitude (CA) loading results can be performed, however, by employing a cumulative damage rule. To determine the fatigue life of a detail from a design S-N curve, first an equivalent stress range that accounts for all of the stress ranges in the VA histogram that contribute to fatigue damaging is needed.

Miner's rule is a widely used cumulative damage rule. According to Miner's rule, structure will be safe if the following inequality, often referred to as Miner's sum, holds:

$$\frac{n_1}{N_1}+\frac{n_2}{N_2}+\frac{n_3}{N_3}+\ldots+\frac{n_k}{N_k}=\sum_{n=1}^{k}\left(\frac{n_i}{N_i}\right)\leq 1.0 \qquad (2.8)$$

Where n_i is the number of cycles at stress range of S_i and N_i is the fatigue life of the component if it was subjected to CA fatigue loading with stress range of S_i, according to the design S-N curve. This rule assumes that there are no interactions between load cycles of different stress ranges. Based on Miner's rule and assuming a slope of 3 for steel, [Yamada 1975] proposed that variable amplitude (VA) fatigue lives correlate well with the CA data when the former is plotted in terms of RMC (root-mean-cube) stress, i.e.

$$S_{eq} = (\Sigma S_i^3 y_i)^{1/3} \qquad (2.9)$$

Where S_{eq} is the equivalent stress range for the load spectrum, S_i is the stress range for stress block i, and y_i is the ratio of the number of cycles with a stress range of S_i to the total number of cycles in the load spectrum. It was reported in a number of studies that VA data correlated well with the CA data when plotted in terms of RMC [Albrecht and Lenwari 2009].

Figure 2.6 shows the design S-N curves according to two well known specifications: [AASHTO 1992] and [ECCS 1985]. The AASHTO S-N curves have two linear parts intersected at a point called the transition point: a sloped S-N line and a horizontal line representing the fatigue limit for each detail category. Based on the corresponding fatigue life to the transition point, two life regimes can be defined: the finite-life regime for stress ranges greater than fatigue limit and fatigue lives greater than N_{tr} and the infinite-life regime. The ECCS S-N curves differ from AASHTO in that they have three linear parts: a sloped S-N line for stress ranges greater than the CA fatigue limit and another sloped but shallower line for stress ranges between the CA and VA fatigue limits, followed by a horizontal line representing VA fatigue limit.

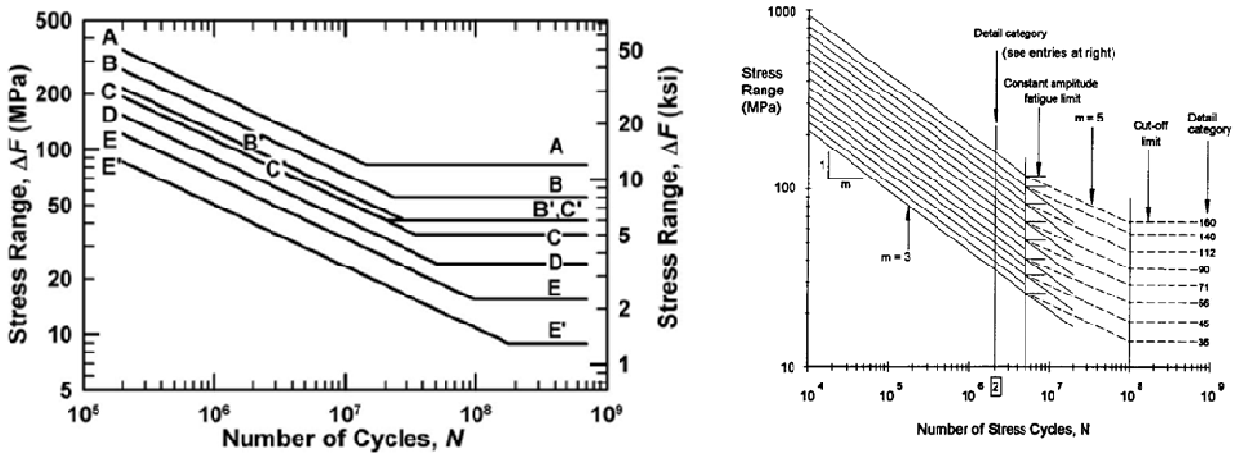

Figure 2.6: Fatigue design S-N curves according to AASHTO (left) [Albrecht and Lenwari 2009], and ECCS specification (right) [Kulak and Smith 1993]

In both the AASHTO and ECCS design S-N curves, the fatigue limit for VA loading is less than that for CA loading. This means that that load cycles with stress ranges less than CA fatigue limit can contribute to fatigue damage in the VA loading spectrum. In the AASHTO specification, the "transition life" can be determined using following expression:

$$N_{tr} = \frac{A}{(0.5\Delta F_{TH})^3} \qquad (2.10)$$

where A is a detail constant and ΔF_{TH} is the CA fatigue threshold [Albrecht and Lenwari 2009]. Eq. 2.4 implies that the VA fatigue limit is half of the CA fatigue limit ($0.5 \cdot \Delta F_{TH}$). While transition lives for different AASHTO detail categories vary from 14.6 million cycles for A to 178.5 million cycles for E', ECCS specifications considers 100 million cycles as the fixed transition life for all detail categories.

2.4.2 Correlating VA and CA fatigue

There are different methods for correlating VA and CA testing. RMS (root-mean-square) and the pre-mentioned RMC method are the examples of the following general expression

$$\Delta S_{eq} = (\Sigma \Delta S_i^m y_i)^{1/m} \qquad (2.11)$$

in which m is the slope of the CA S-N curve. In the RMS method, m is taken 2 [Fisher et al. 1970] and in the RMC method it is taken as 3. More accurate values can be considered subjected

to the availability of data, as in [Zhang and Maddox 2009] m = 2.728. In [Albrecht et al. 1990] and [Yamada and Albrecht 1977] it was concluded that VA data plotted in terms of RMC and CA data correlate well on the short-life regime but not in the infinite life domain where the VA fatigue limit is almost half of that for CA [Albrecht and Lenwari 2009].

[Dowling 1988] developed random stress histories and studied methods of correlating the data between random and CA loading such as the maximum stress level method, the most damaging stress level method, and the half damage stress level method. However, use of an effective stress range is suggested because of its ability to combine several sets of fatigue data.

[Albrecht and Friedland 1979] reported that RMC can be used as a convenient transfer function between CA data and VA data when the following conditions are approximately met: 1) the crack initiation phase is negligible, 2) block sizes are small enough to prevent interaction in high-low stress ranges sequences, 3) the inverse slope of the S-N curve and the slope of the crack growth curve are about equal, and 4) all stress ranges are above the CA fatigue limit. Once these conditions are met, the RMC method can be used for stress ranges greater than the CA fatigue limit to calculate equivalent stress and the corresponding N only accounts for these large cycles. Also they reported that RMC stress range works best if it is equal to or greater than the CA fatigue limit. Otherwise, the VA data diverges from the straight extension of the CA S-N line. Later, [Albrecht and Rubeiz 1990] reported a good correlation between VA and CA data using an equivalent stress range of the entire spectrum when 50% or more of the cycles exceeded the fatigue limit. Fisher et al. also suggested that all stress cycles above 50% of the fatigue limit should be considered to cause fatigue damage and their effect must be considered in RMC calculation. This is consistent with the AASHTO specifications, suggesting that the VA fatigue limit lies a factor of two below the CA fatigue limit [Albrecht and Lenwari 2009].

Figure 2.7 shows the example test results for tensile plates with transverse stiffeners reported in [Klippstein and Schilling 1989] representing a good correlation between VA data and CA data. To plot the VA test data in this figure, the RMC method was used.

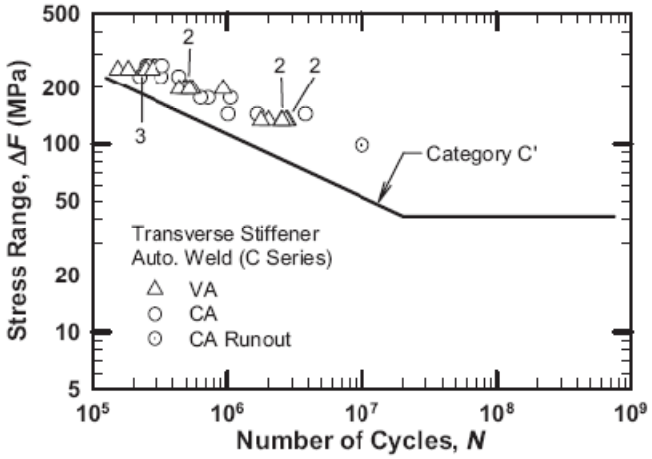

Figure 2.7: S-N data for tensile specimens with transverse stiffeners [Klippstein and Schilling 1989]

2.4.3 Effect of load spectrum

As mentioned earlier, there is strong evidence that the interactions between load cycles of different stress ranges influence fatigue behaviour. Some of the main parameters influencing the fatigue behaviour of structures are: the occurrence of periodic overloads and underloads, the load history shape, mean stress, minimum stress, and maximum stress.

Effect of periodic overloads

According to [Abtahi et al. 1976], the effect of periodic overloads should be studied in two cases. First, when the structure is designed for infinite fatigue life, meaning all stresses are below the CA fatigue limit. In this case, only overloads can contribute to fatigue crack propagation. Thus, if the number of overloads is restricted, there would be no fatigue problem. Another case is when the structure is susceptible for fatigue cracking under normal loading conditions and then the overloads can have both advantageous and disadvantageous effects on the structure fatigue behaviour, depending on their frequency. An overload can delay crack initiation by creating a residual compressive stress and thus reducing tensile portion of the effective stress range at the weld toe. The same mechanism can explain the effect of single overloads in delaying crack growth (crack retardation). On the other hand, overloads can accelerate crack propagation by separating poorly bonded regions. Thus, a limit in the frequency of the overload occurrence should exist above which the overall effect would be considered damaging. To find this limit, overloads with the magnitude of $\sigma_{max,OL} = \sigma_{min} + 1.67\sigma_r$, where σ_{min} and σ_r represent dead load stress range and live load stress range respectively, were applied for different stress ranges and

at the different intervals. It was observed that applying overloads at the beginning of the test and spaced every 1000 cycles or more, increased the fatigue life, while a decrease in the fatigue life was observed when they were spaced at 100 or less cycles. The most beneficial reported frequencies were every 10^4 to 10^5 cycles for the tested stress ranges. Like overloads, underloads can also accelerate crack growth rate. One possible mechanism could be related to the introduction of tensile residual stresses around the crack tip [Zhang and Maddox 2009].

Similar results are also reported by [Albrecht and Rubeiz 1990], however, as mentioned earlier, the beneficial and damaging effects of periodical overloads and underloads are not predicted with the equivalent stress range concept. Thus, overloading bridges is not allowed.

Effect of loading history

[Yamada 1975] used a stress histogram consisting of four blocks similar to that recorded on a three-span continuous girder bridge in Maryland and reported that block sequence and histogram size did not affect the results. Additionally, no significant difference in crack initiation and crack propagation were observed between specimens subjected to CA and VA stresses for the tested cover plated beams with finished end welds. [Schilling et al. 1978] used three Rayleigh probability curves with normalized equivalent stress ranges of 0.50, 0.60, and 0.72 to model the narrow band, medium band, and wide band Raleigh-type spectra respectively. Each spectrum consisted of 500 hundred randomly arranged cycles. Later [Schilling et al. 1978] showed that for that loading history, band width and sequence of blocks had no statistically significant effect on the fatigue strength. However, [Albrecht and Rubeiz 1990] used another set of normalized equivalent stress ranges for Rayleigh curves and reported that specimens subjected to wide band Rayleigh-type spectra had higher fatigue strength than those subjected to medium-band and narrow-band spectra. Additionally, the effect of increasing the minimum stress on the VA loading fatigue limit was studied. For a 70 MPa increase in minimum stress, no significant effect was reported, but for an increase of 276 MPa in minimum stress, the VA fatigue limit was significantly lowered. However because that minimum stress was not comparable to the actual dead load induced stresses in bridges, it was concluded that there was no need to include the minimum stress as a new variable in bridge design.

To prevent interaction in high-low stress range sequences, [Albrecht and Yamada 1977] suggested that block loading spectra should not exceed 1200 cycles. According to [Albrecht and Rubeiz 1990], spectra of 1000 cycles or less, with ten randomly ordered blocks, were free of load interaction in high-low stress range sequences, indicating that the random-order VA truck loading of bridges can be simulated in laboratory tests by repeatedly applying a 1000-cycle spectrum of nine randomly ordered blocks and it is not necessary to apply single, randomly ordered stress ranges. Moreover, block sequence in the investigated nine-block spectrum of 1000 cycles did not appear to affect the result.

Fatigue damage accumulation

Codes and specifications normally use Miner's sum (Eq. 2.8), with S-N curves determined from CA tests, to consider fatigue damage accumulation. According to Miner's rule, a structure will be safe against fatigue failure if Miner's sum is less than 1. However Miner's rule does not consider stress cycle interaction. In other words, fatigue damage caused by a particular stress cycle in a VA loading is assumed to be exactly the same as that due to the same stress cycle under CA loading. However, as discussed earlier, there is strong evidence that a stress cycle can be more (or less) damaging under VA loading than the same stress cycle under CA loading. Hence, Miner's rule and the RMC method might lead to conservative or non-conservative results depend on the load spectrum.

[Zhang and Maddox 2009] used three VA loading sequences, all based on the same spectrum in terms of stress ranges and cycle sequences but with different mean stresses, to investigate the effect of mean stress on the fatigue life of steel details under VA loading. These sequences were: 1) Sequence A: stresses cycling down from a constant maximum tensile stress of 280 MPa, 2) Sequence B: stresses cycling about a constant mean stress of 175 MPa, and Sequence C: stresses cycling up from a constant minimum stress of 70 MPa. A maximum stress range of 210 MPa was used in all VA loading tests. These three loading sequences are shown in Figure 3. Two types of specimen representing two different detail categories were tested and crack initiation and crack growth were monitored. Residual stress measurements were also carried out.

The VA test results were analysed in terms of Miner's rule and the stress range corresponding to a fatigue endurance of 10^7 cycles was considered as the CA fatigue limit. N_i's, for use in Eq. 2.8,

were determined based on three S-N curves: 1) a single curve without any slope change, 2) a bi-linear curve with a slope change from m to (m+2) at the CA fatigue limit, here m = 2.728, and 3) a single curve cut-off at the CA fatigue limit where all stress ranges below it were assumed to be non-damaging. The test results showed that Miner's rule was generally non-conservative (with values as small as 0.30 at failure) for all tests under sequence A. Showing that some stress cycles were more damaging than expected. Comparing Miner's sum calculated using the single slope S-N curve with the two other curves confirmed that small stress ranges below the fatigue limit, as small as 8.4 MPa, were still as damaging as implied by the CA S-N curve extrapolated beyond the CA fatigue limit without changing the slope. Miner`s rule was non-conservative for specimens tested under load sequence B too, though its values (around 0.80) were greater than those under load sequence A. However, Miner`s rule was very conservative (more than 1.30) for tested specimens under load sequence C, even when the S-N curve with the cut-off was used. Figure 3 compares the VA test results with the CA S-N curve expressed in terms of equivalent stress range. (Note: Based on the equivalent stress definition, Miner's rule gives a safe estimate of the actual fatigue life if an experimental results lies on or above the CA S-N curve).

Residual stresses were monitored during testing and under sequence A, a 73% decrease in the residual stress was observed before 1% of the total fatigue life. However, the remaining residual stress (76 MPa after 10 blocks of VA loading), was still big enough in comparison with the small stress ranges in the spectrum, to have a significant effect on the specimen fatigue behaviour. A change in the mean stress did not influence the fatigue performance of the specimens, mainly because of the existence of these residual stresses.

Results from crack growth measurements showed that growth rates obtained under CA loading are significantly smaller than those obtained under sequence A, marginally smaller than those obtained under sequence B, and significantly larger than those obtained under sequence C, in proportion with the Miner's sum values at failure. Additionally, significant crack growth acceleration was observed for tests under sequence A, moderate acceleration under sequence B, and crack growth retardation under sequence C, indicating that stress interaction had the most significant effect on the fatigue performance of the specimens.

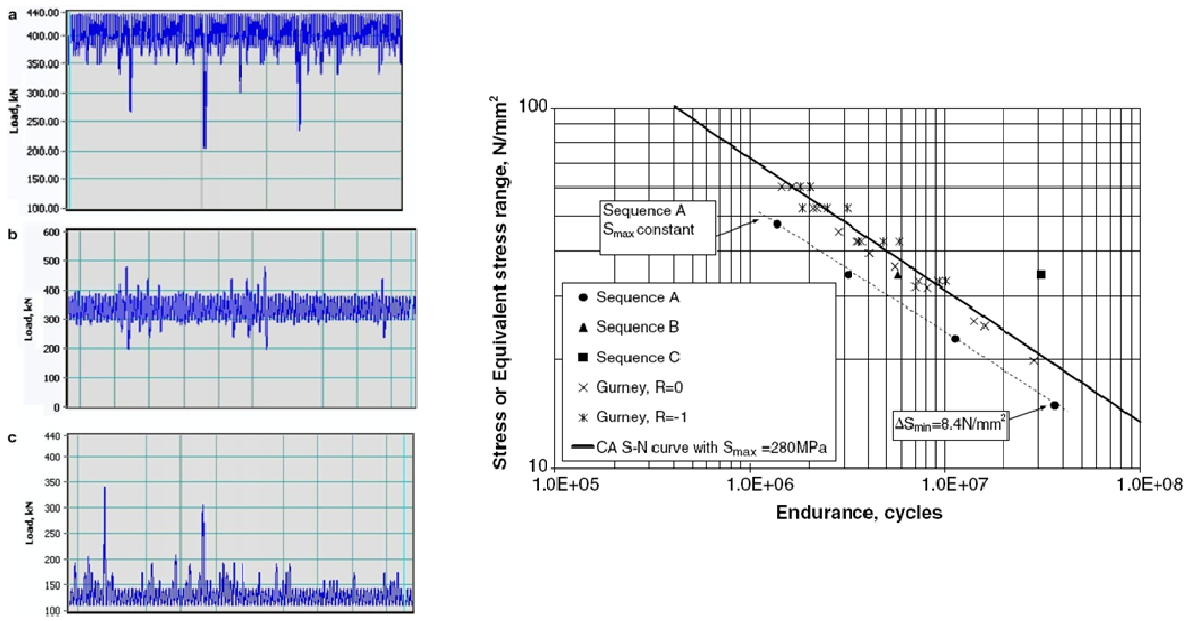

Figure 2.8: Examples showing three loading sequences (left) and comparison of VA test results with the CA S-N curve (right) [Zhang and Maddox 2009]

In another similar study, [Agersov 2000] performed VA loading fatigue tests on various types of welded plate under realistic loading conditions, simulating actual loading in offshore structures, similar to sequence B in the previous study, and loading in highway bridges and chimneys, similar to sequence C. The results showed that the fatigue performance of structures is highly dependent on the applied loading type. A total of 540 fatigue tests on welded plate specimens and tubular joints were carried out and the results illustrated a significant difference between CA and VA fatigue behaviour. Equivalent stress range and Miner's sum were used to correlate VA and CA test results. For offshore load histories, the Miner's rule was non-conservative for all three load histories. Values ranges reported for Miner's sum were ~0.40-0.85 for tests under offshore load histories and ~0.50-1.0 for tests under highway bridge and chimney load histories.

Fracture mechanics analysis showed that crack closure mechanisms were the most important factors in crack acceleration (and crack retardation) due to high tensile (and compressive) stresses in the VA histories, which in turn, were the main reason for the different fatigue behaviour of the details under CA and VA loading.

2.4.4 Fatigue limit for VA loading

The fatigue limit effect is reported to have a significant influence on the VA long life behaviour of structural steel details [Albrecht and Rubeiz 1990]. There appears to be a VA fatigue limit for the equivalent stress range, below which fatigue cracks will not propagate regardless of the number of applied cycles.

For CA loading, the fatigue limit (also called the fatigue strength or endurance limit) is the range of cyclic stresses that can be applied to the component without causing any fatigue damage. In other words, structures have infinite fatigue life for stress ranges equal or below the fatigue limit. For VA loading, as Figure 2.6 implies, a fatigue limit still exists. According to [AASHTO 1992] specifications, the stress range derived by extrapolating the S-N curve beyond the CA fatigue limit without changing the slope and corresponding to 10^8 cycles is the VA fatigue limit. Therefore two parameters should be compared with the CA fatigue limit for fatigue analysis under VA loading: the effective stress range and the maximum stress range.

Three different cases are possible:

1) effective stress range > fatigue limit,

2) effective stress range < fatigue limit and maximum stress range > fatigue limit, and

3) effective stress range < fatigue limit and maximum stress range < fatigue limit.

These three cases are shown in Figure 2.9.

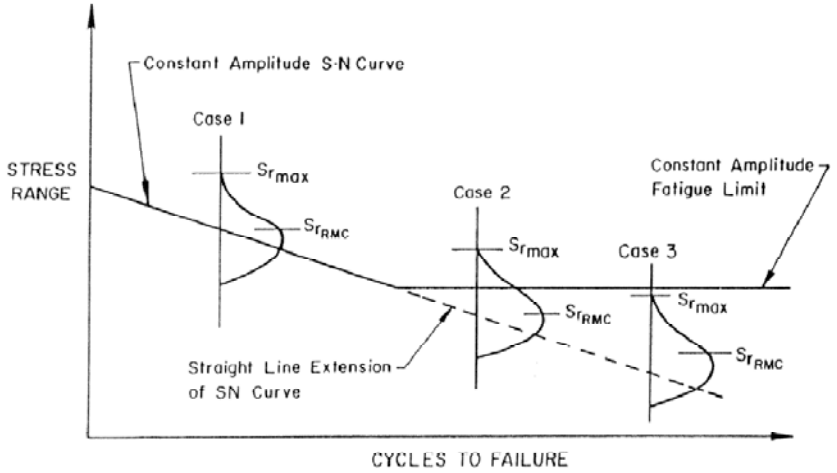

Figure 2.9: Three cases of VA stress spectra [Yamada 1975]

For case 3, no fatigue crack growth will occur and the structure is safe, but, for the first two cases, the S-N curve and its extension should be used to determine the fatigue life of the structure. Based on [Albrecht and Rubeiz 1990], the VA fatigue limit can be calculated using the following expression:

$$f_{VAFL} = \rho_e f_{FL} \qquad (2.12)$$

where f_{VAFL} and f_{FL} are fatigue limits for VA and CA loading, respectively, and ρ_e is the ratio of equivalent stress range to the maximum stress range. It is obvious from Eq. (2.12) that the VA fatigue limit depends on the loading spectrum unlike the CA fatigue limit.

Though design S-N curves in specifications are normally bilinear, it was reported in [Albrecht et al. 1994] and also in [Albrecht and Friedland 1979] that there is actually a gradual transition between the finite-life and infinite-life regimes. Albrecht and Friedland 1979] reported that once 15% or fewer cycles exceed the VA fatigue limit, the fatigue life begins to become increasingly longer than the straight-line extension of the CA S-N line predicts.

[Albrecht and Lenwari 2009] proposed a simplified model that accounts for this gradual change in the S-N curve. [Albrecht and Simon 1981] proposed the use of fatigue notch factors for specifying the relationship between the allowable stress range and the number of loading cycles. The fatigue notch factor for detail category X, $K_{f,x}$ is defined as:

$$K_f = \frac{\Delta F_A}{\Delta F_X} \qquad (2.13)$$

Where ΔF_A and ΔF_x are stress ranges at a fixed number of cycles for categories A and X, respectively. Substituting Eq. 2.10 into Eq. 2.13 gives

$$K_f = \left(\frac{A_A}{A_X}\right)^{1/3} \qquad (2.14)$$

where A_A and A_X are detail constants for categories A and X, respectively.

From fracture mechanics, the crack growth rate can related to stress intensity factors as in [Klesnil and Lukas 1972]

$$\frac{da}{dN} = C\ (\Delta K^m - \Delta K_{th}^m) \qquad (2.15)$$

where C and m are material constants, ΔK is the stress intensity factor range, and ΔK_{th} is the threshold stress intensity factor range.

Similar to Eq. 2.14, the proposed simplified model for detail category X is given in the notation of the AASHTO specifications, similar to Eq. 2.10, as

$$N = \frac{A_X}{\Delta F^m - (0.5\Delta F_{TH})^m} \qquad (2.16)$$

By substituting Eq. 2.13into 2.16 and for m = 3 it gives

$$\Delta F = \left(\frac{A_A}{K_f{}^3 N} + (0.5\Delta F_{TH})^3 \right)^{1/3} \qquad (2.17)$$

This model predicts the same transition behaviour for all detail categories and matches well with the testing results, as shown in Figure 2.10.

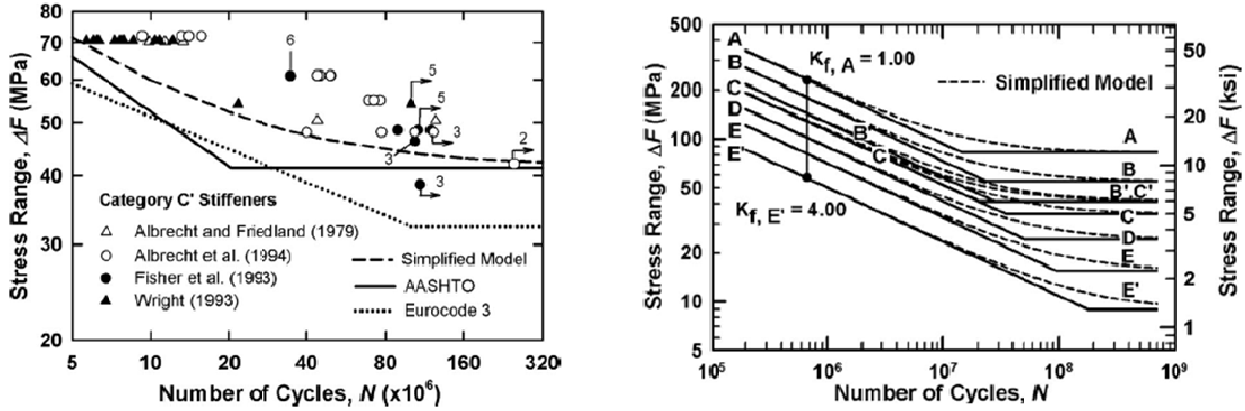

Figure 2.10: Application of simplified model to S-N data for category C' stiffeners in transition region (left) and simplified model for each AASHTO detail category (right) [Albrecht and Lenwari 2009]

2.5 Improvement methods and design rules

The current knowledge on PWT methods has been obtained mostly from experiments on small scale specimens. In extending the conclusions to actual structures, two important differences

should be considered; size effect, e.g. presence of higher notch effects and other residual stresses due to forcing members together, and possible failure at other locations than the weld toe, e.g. at weld roots. Obviously using PWT methods on the weld toe of a specimen that is likely to fail at the weld root does not improve the fatigue behaviour of the structure.

The beneficial effects of residual stress-based PWTs on fatigue performance are recognized in a number of design standards for welded structures. The International Institute of Welding (IIW) recommendation allows a vertical shift of the design S-N curve for needle and hammer peened welds. Specifically, this recommendation allows a 1.3-1.6 times fatigue strength increase, up to a treated fatigue strength of 100 MPa (at a fatigue life of 2 million cycles). A similar benefit for hammer peening is allowed in the CSA structural welding code.

AWS design rules account for the weld profile improvement method in terms of X curves; two X curves can be used, the upper one is for when profile control is performed. These curves intersect at roughly 10,000 load cycle, implying that post-weld treatment is not effective for low cycle-high stress fatigue improvement.

In the Swedish design code [74 StBk-N2, 1974], ten S-N curves are presented each identified by a factor. Four basic weld quality system classes are also included together with an additional class (Class U) that accounts for improved fatigue strength. Use of this class is subjected to fulfilling four welding control requirements.

The UK Department of Energy has provided a simple rule for considering the effect of fatigue improvement methods: an increase factor of 1.3 on strength and 2.2 on life [HMSO 1984]. This method results in two parallel curves.

The IIW recommendation on the post weld improvement of steel and aluminium structures [Haagensen and Maddox 2002] provides guidelines on number of passes, speed, air pressure provided to the pneumatic peening tool, training, and quality control for needle and hammer peening treatment. The standard CSA for welded steel construction [CSA W59-03, 2003] also includes rules on the depth of the groove left by the peening tool for hammer peening (0.5, 0.25, and 0.1 mm for low, medium and high strength steel). In terms of quality control of the

treatment, this code encourges weld inspection by magnetic particle or dye penetrant testing prior to peening.

2.6 Test based studies of residual stress-based post weld treatment

Early test based studies on fatigue improvement methods were carried out in "Effect of Grinding and Peening on the Fatigue Strength of Fillet Welded Joints" by Gurney in 1968 [Gurney 1968]. In [Gurney 1979] butt welds and fillet welds were peened using three different peening methods. Hammer peening resulted in 85-100% increase in fatigue strength and was found to be the most effective peening method, followed by shot peening with 15-25% and needle peening with 15-25% [Walbridge 2004].

During the 80's, [Booth 1981] reported fatigue tests carried out on transverse non-load carrying fillet welded specimens made from steel to BS 4360 and Grade 43A. Two methods of PWT and three load ratios (R) were investigated; heavy disc grinding and four-pass hammer peening under R = 0 (pulsating loading) , 0.5 (half tensile loading), and -1 (alternating load). It was concluded that the mean stress had no influence on the fatigue strength of the as-welded joints, but significantly influenced the behaviour of the peened joints. The best results were observed for both peened and ground specimens under alternating loading. Under half tensile loading, both treatment methods were not that much effective at high stresses, however, small increases in fatigue life were reported at low stresses. Finally, it was concluded that peening resulted in an increase in the CA fatigue limit to a value close to the static design stress for the steel.

[Maddox 1985] studied the effectiveness of shot peening and hammer peening. Test results showed large improvements in fatigue strength and CA fatigue limit. Test results also showed the improvement increased with an increase in the steel tensile strength, reduction in the applied stress range, or reduction in the R ratio. Hammer peening was found to be both more effective and easier to control than shot peening and a depth of about 0.6 mm was reported as the "sufficient deformation depth" that can be achieved by four passes of hammer peening.

[Braid et al. 1998] conducted fatigue testing on two series of T-joints with fillet-welded longitudinal attachments made from 350 MPa grade structural steel and 550 MPa grade high strength steel. As welded and "weld repaired and hammer peened" specimens were tested under constant amplitude loading with various stress ranges between 50 and 300 MPa. The same fatigue behaviour was reported for as-welded specimens for both types of steel; however,

hammer peening resulted in more improvement for high strength steel (175% improvement in fatigue life). The repair welding procedure involving hammer peening worked well in restoring the fatigue strength of fatigue-cracked joints to that of the original welded joints. Also it was noted that unlike as-welded and weld repaired fatigue tests in which cracks were detected at the weld toe, in the hammer peened joints, fatigue cracks initiated and propagated at the weld root.

Two other test based studies conducted at ICOM are summarized in [Walbridge 2005]. [Bremen 1989] studied the effect of hammer, needle, and shot peening on welded specimens under CA loading with R = 0.1 at $\Delta\sigma$ = 180 MPa. The same as the previous study, hammer peening resulted in significant improvements with 310% to 1500% improvements in fatigue life followed by shot peening with 30% to 200% and needle peening with 0 to 160%. As there was "no systematic" increase in fatigue life for the needle and shot peened specimens, [Bremen 1989] pointed out the need for better quality controls method for these PWTs. It was also concluded that residual stress-based PWT methods extend the fatigue life by modification of the crack growth and the other parameters such as geometry modification or local surface hardening make only a minor contribution to the fatigue behaviour improvement (if any). The change in crack growth rate is a function of the residual stress distribution. A deterministic LEFM model was also proposed for predicting the fatigue behaviour of the peened specimens. Additionally, an empirical model is also proposed for the residual stress distribution due to peening with a value of 0.5·fy (compressive) at the surface to a depth of 0.1 times the indent diameter and then linearly decreased to the original tensile residual stress due to welding at a depth equal to the diameter of the imprint.

[Huo et al. 2004] compared the effectiveness of ultrasonic peening under the CA and VA loading conditions. The load spectrum used for VA loading was consisted of three blocks of CA stress, referred to as the minimum, medium, and maximum, applied in sequence. The results showed that generally ultrasonic peening was less effective under VA loading than under CA loading. As can be seen in Figure 2.11, at $2x10^6$ cycles, TIG dressing increased the fatigue limit by 37% and increased the fatigue life by 2.5 times, when it was applied under CA loading, while those numbers decreased to 34% and 1.7-1.9 times under VA loading. Similarly, ultrasonic peening increased the fatigue limit by 84% and increased the fatigue life by 3.5-27 times, when it was applied under CA loading, while those numbers dropped to 80% and 2.5-17 times under VA loading.

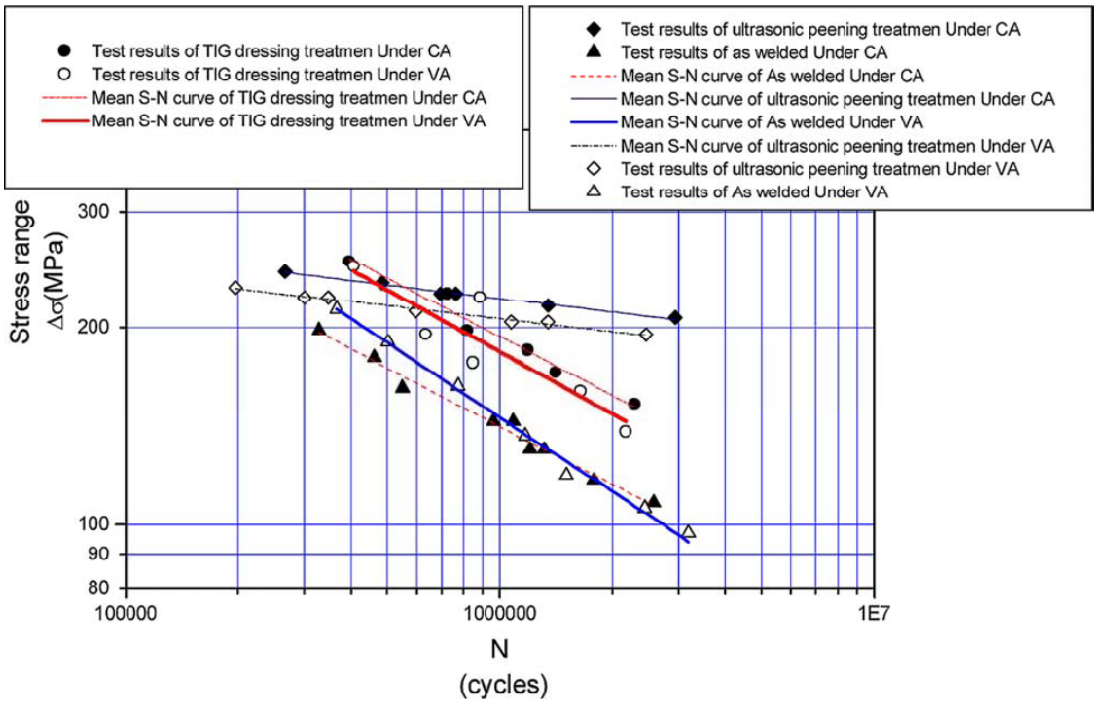

Figure 2.11: S-N curve of the fillet welded joints [Huo et al. (2004)]

Another experimental study at ICOM targeted the effectiveness of peening methods under variable amplitude (VA) loading. As-welded and peened fatigue tests were carried out and the results are reported in [Dubois 1994]. Two different variable amplitude loading schemes were used to study the effect of "underloads" and "overloads". Each loading spectrum consisted of 10 large cycles with $\Delta\sigma$ = 180 MPa followed by 350 small cycles with $\Delta\sigma$ = 60 MPa. Large load cycles were created by keeping either the maximum or the minimum applied load constant (i.e. the same as the other 350 small cycles), modelling underload and overload events, respectively. Both peened and as welded specimens tested under the loading history with overloads, had shorter fatigue lives but and the difference was more significant for the peened welds, implying that overloads resulted in the loss of part of the treatment benefit.

[Manteghi and Maddox 2004] conducted a pilot study of PWT methods mainly for evaluating different PWT methods applied to high strength steel components. Two types of specimens were fabricated using two steel grades and two different electrodes, and were tested under both constant amplitude (R = 0.1) and variable amplitude loadings. VA loading spectrum used in this

study was a modified version of the offshore WASH-W spectrum. The main conclusions made in this study are as follows:

- As-welded test results showed little scatter, indicating a negligible effect of steel grade and electrode type.
- Miner's rule did a good job in correlating VA and CA test results only for the as-welded joints. However, it over estimated the fatigue lives of the hammer peened specimens under VA loading by as much as 10 times.
- Although hammer peening resulted in significant fatigue life increase (around two times longer) for the treated specimens under VA loading, that benefit was less than under CA (around eight times longer).
- Fillet welds with hammer peened weld toes can be upgraded from UK class F to B with a fatigue limit corresponding to the stress range at a fatigue life of two million cycles.

[Wright 1996] reported an average of eight-times increase in fatigue life by UIT over the untreated weld at stress range of 130 MPa. In other words, a category C' detail in AASHTO fatigue S-N curves, behaved like a category B detail.

[Anami et al. 2000] studied TIG-dressing and hammer peening effects on the fatigue strength of out-of-plane gusset welded joints. As Figure 2.12 illustrates, TIG-dressing resulted in a fatigue performance increase of one or two classes according to JSSC (Japanese Society of Steel Construction) design code, regardless of the applied stress range. As illustrated in Figure 2.16, large improvements were also reported for both one-pass and three-pass hammer peened specimens, however, these improvements were highly dependent on the applied stress range. For one-pass hammer peened specimens, not only less fatigue improvement was observed, but also it was found that a steep "ditch" was always induced by peening and fatigue cracks initiated from it. Failure surfaces were also examined and by observing the "beach marks", crack aspect ratios (depth/surface length) were found to be larger for the hammer peened specimens than for the as-welded ones, mainly due to the introduced compressive stresses and decreased stress concentration at the peened surface.

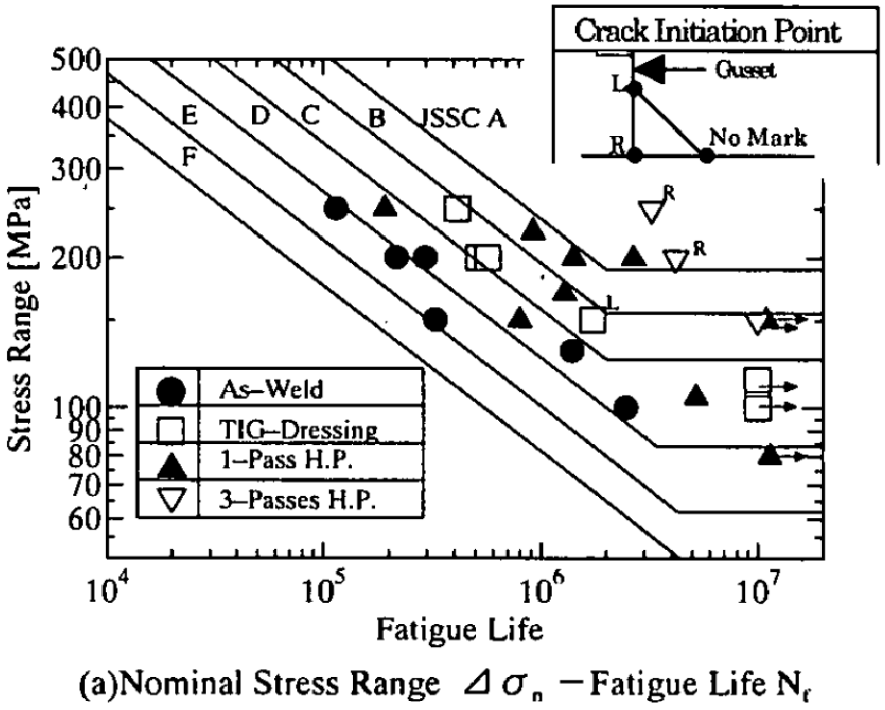

Figure 2.12: Fatigue test results by [Anami et al. 2000]

The magnitude and subsurface distribution of residual stresses induced by UIT and shot peening were measured using X-ray and neutron diffraction techniques for the first time in [Cheng et al. 2003]. Both peening methods resulted in a near surface peak compressive residual stress that was higher than the yield stress, however the depth of the compressive layer due to UIT was almost double of that for the shot peened specimen. Based on the measurements made in this study, the compressive region due to UIT application was as wide as ±12 mm and as deep as 1.5-1.7 mm for the base metal specimen. That depth was reduced to about 1 mm in welded specimens due to the presence of tensile weld residual stress. This thin layer of compressive stress suggests that peening methods are most effective in the crack initiation phase and early crack growth stages.

The application of UP (Ultrasonic Peening) to existing welded structures was studied in [Kudryatsev et al. 2005]. Fatigue testing conducted on three series of welded specimens in as welded condition, peened before testing, and peened after 50% of the fatigue life in as welded condition. By looking at Figure 2.13, UP was even more effective when applied after fatigue loading. This suggests that UP can be as efficient when applied to the existing welded structures as it is when applied during construction, and thus, is a promising method for both rehabilitation

and repair of the existing structures. The practical application of UP to two existing bridges, one in USA and one in Ukraine, were also reviewed in this reference.

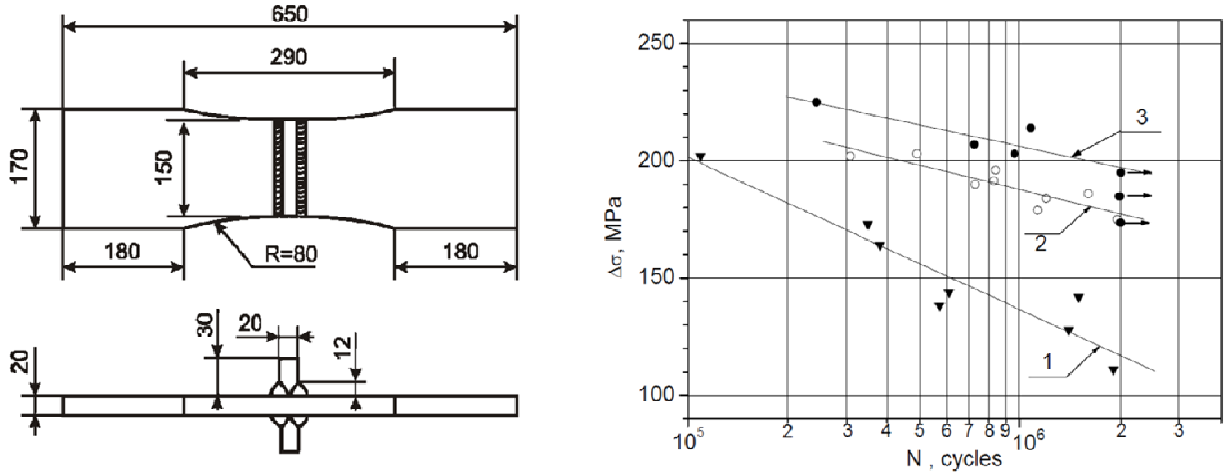

Figure 2.13: Specimen geometry (left) and fatigue test results (right) reported by [Kudryatsev et al. 2005]: 1- as welded condition, 2- UP applied before fatigue testing, 3- UP applied after fatigue testing for 50% of the expected as-welded fatigue life

The effect of hammer peening applied under load was addressed in [Maddox 1998] and fatigue testing on specimens treated under 120 MPa prestress showed that hammer peening was even more beneficial when applied under load in comparison with its application before loading.

The fact that residual stress-based post-weld treatments are even more efficient when applied to already loaded structures, together with their applicable nature and easiness of use, shows the possibility and advantage of using these methods for fatigue rehabilitation of the existing bridges, without any reduction in their serviceability. Though only non-cracked structural members were considered here, several studies, e.g. [Branco et al. 2002] and [Braid et al. 1998], have reported the usefulness of these methods in already cracked welded-joints.

A fatigue study on the rehabilitation of non load carrying fillet welded joints was carried out by [Branco et al. 2002]. Previous studies by the same authors had indicated that hammer peening can be used as an efficient repair method for the as-welded joints with fatigue cracks of known size. However, re-application of hammer peening to the initially peened specimens with fatigue cracks did not lead to a further increase in the fatigue life. Weld toe radius and angle measurements showed a very small difference between the as-welded and hammer peened

specimens, confirming that peening methods enhance the fatigue behaviour of welded joints primary by introducing favorable compressive residual stresses rather than geometry modification. Hardness tests were also conducted and the results showed that the hardness of the material was increased in a ~ 2.5 mm deep hardened zone, with its peak value of ~320 HV at the surface gradually decreasing to ~240 HV for the base metal (Figure 2.14). It can be deduced that hammer peening could be effective as long as fatigue cracks are inside this hardened zone. Residual stress measurements were made using the X-ray diffraction method and the results showed residual compressive stresses as large as the yield stress in magnitude at the surface, localized at a distance of 5 mm away from the weld toe where the treatment was applied.

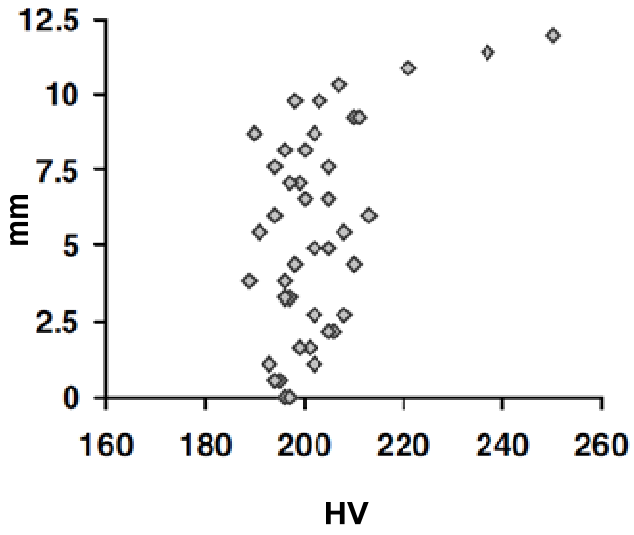

Figure 2.14: Hardness profile of a peened weld toe [Branco et al. 2002]

[Ummenhofer et al. 2006] studied the application of weld improvement methods (specifically UP) to extend the fatigue life of cyclically loaded structures. Fatigue tests were conducted on as-welded, normally peened, and preloaded and then peened specimens. The test results proved that the application of UP to the preloaded specimens increased the fatigue life, similar to normally peened specimens. Microhardness measurement results showed an increase in the hardness of the material in a ~2 mm deep hardened zone, with a peak value of ~320 HV at the surface, gradually decreasing to ~225 HV for the base metal. Residual stress measurements revealed the presence of the compressive stresses close to the yield stress near the surface of the weld toe.

Chapter 3
Test Procedures and Measurements

3.1 Introduction

A number of fatigue tests under various loading and treatment conditions were conducted to evaluate the effectiveness of needle peening for improving fatigue performance. Additionally, using the analytical models discussed in Chapters 5 and 6 to predict the fatigue behaviour of the specimens requires a number of input parameters that can only be determined from various experiments and measurements. Towards this end, materials tests were conducted to determine accurate material properties and to get a better understanding of the material cyclic behaviour. Microhardness measurements were also made to study the effect of peening on the microstructure of the material in the vicinity of the peened weld toe. Weld toe geometry measurements were made to investigate the weld shape properties and weld defects. Crack growth and crack shape measurements were also made to obtain a better understanding of the fatigue crack initiation and propagation behaviour. Finally, residual stress measurements were obtained to determine the actual residual stress distribution on and below the weld toe surface.

In this chapter, the fatigue and materials test procedures and measurements are described. First in Section 3.2, test specimen dimensions and fabrication procedures are described. Then, in Section 3.3, fatigue tests procedures, loading, and treatment conditions and Section 3.4 is devoted to explaining test procedures for cyclic and static materials tests. In Section 3.5, the methods used to measure crack growth are described, followed by microhardness measurements in Section 3.6. Weld toe geometry and crack aspect ratio measurement procedures are discussed in Sections 3.7 and 3.8, respectively. Finally, the residual stress measurements performed for this thesis project are discussed in Section 3.9.

3.2 Description of test specimens

The fatigue specimen geometry used in this study was a Detail Category ‘C’ non-load carrying fillet welded transverse stiffener fatigue specimen representing a transverse web stiffener in a bridge girder (see Figure 3.1). This Detail Category is considered to be representative for welded bridges [Klippstein and Schilling 1989] and was the same geometry used in the tests reported in [Walker et al. 2008, Walbridge 2008]. The specimens were constructed of 9.5 mm (3/8”) 350W

steel plate and had a width of 30 mm. They were fabricated by saw cutting 30 mm wide slices from larger (300 mm wide) welded joints fabricated using the FCAW welding process. The rolling direction of the plate was oriented in the longitudinal direction of both the loaded plates and the stiffeners (see figure 3.1).

During testing, failure at the grips was observed for number peened specimens under certain loading conditions, mainly due to the high stress concentration at this location. To avoid this, another specimen with wider gripping surfaces was designed and used in subsequent testing. These specimens were 10 cm longer in overall length but had same 30 mm weld width sections. They were fabricated by saw cutting 50 mm wide slices from 300 mm wide welded joints, and were then "dog-boned" using a CNC machine for a gradual decrease in cross section in accordance with ASTM E8 [ASTM E8 2004]. The welding procedure and rolling direction were the same as for the Type 1 specimens. Figure 3.1 illustrates the geometry both fatigue specimen types.

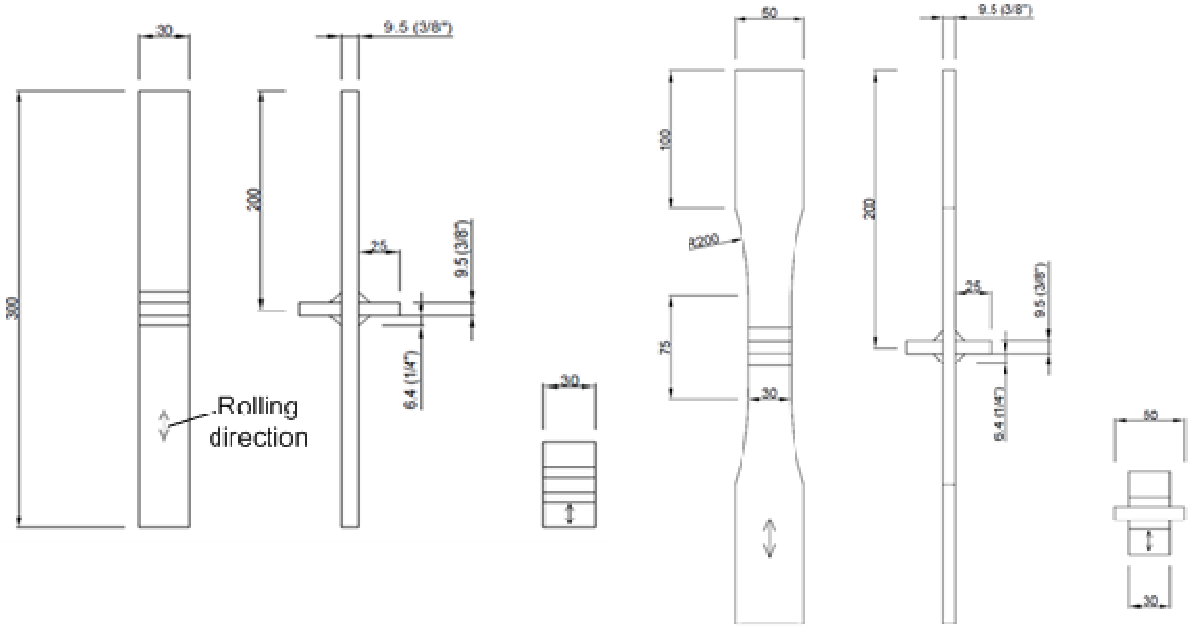

Figure 3.1: Fatigue specimen geometry; (left) Type 1, (right) Type 2 (dimensions are in mm u.n.o.)

For the materials static tests, five standard, sheet-type, 12.5mm wide, tension coupons were fabricated of the same 350W steel used in the fabrication of fatigue specimens. Figure 3.2 shows the shape of these coupons used in the static material tests. Static tension and cyclic tests were conducted in accordance with ASTM E8.13005-1 [ASTM E8 2003].

Polished smooth cylindrical, variable width specimens (see Figure 3.3) were fabricated from the same material for cyclic materials testing.

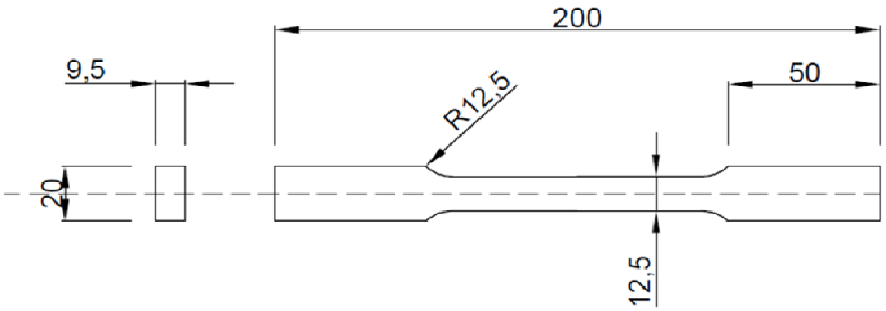

Figure 3.2: Tension coupon for static material testing (dimensions are in mm)

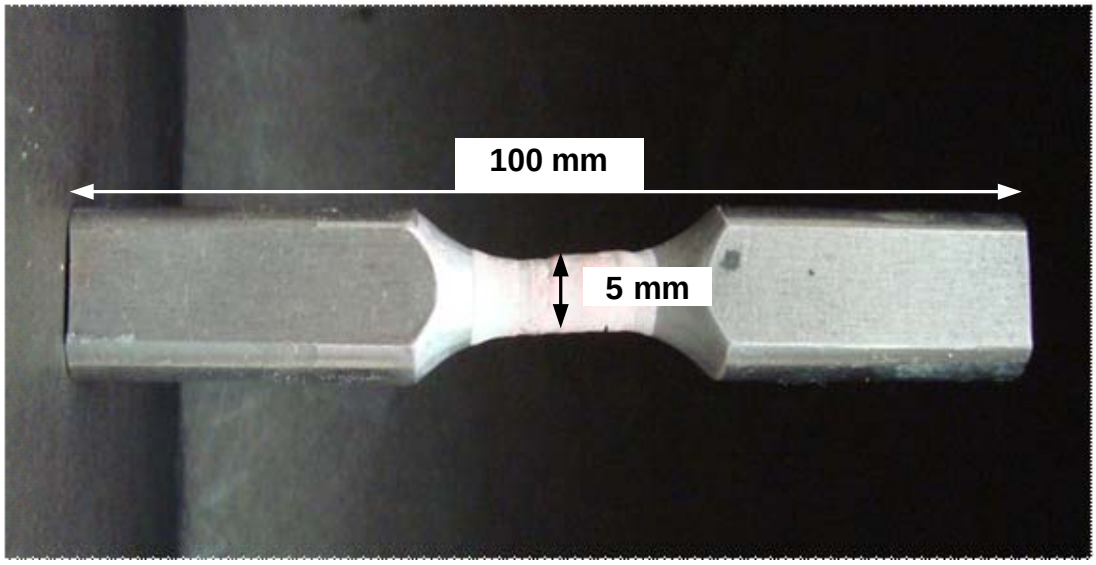

Figure 3.3: Specimens used for cyclic materials testing (dimensions are in mm)

3.3 Fatigue tests

A total number of 47 fatigue tests were carried out under different cyclic loading and treatment conditions. Each test is identified by a loading scheme and the treatment it received. In total, thirteen different combinations of treatment and loading were tested. Each treatment/ loading combination was repeated on a set of at least three specimens. The specimens assigned to each set were selected at random, but in such a way that each set contained specimens from each of

the larger stiffened plates from which the smaller specimens had been cut. The tests were performed using an MTS 810 Material Testing System.

3.4 Static and cyclic materials tests

The static tension and cyclic materials tests were conducted in accordance with ASTM E8 [ASTM E8 2003] to determine the static material properties (E, σ_y, σ_u) and to obtain the Ramberg-Osgood cyclic stress-strain curve constants (K', n'). All specimens were carefully inspected and their dimensions were measured at three different points along the reduced cross section prior to testing.

Using an MTS 810 Material Testing System (see Figure 1.5), each static tension coupon was loaded to a point well beyond the yield point, then was unloaded, and reloaded to failure with the prescribed loading rates. Forces in N and displacements in mm were read and recorded using the attached extensometer (gauge length= 50.80 mm) during testing. Table 3.1 summarizes static tension coupon dimensions before testing and loading rates at each stage for each specimen.

Table 3.1: Static tension coupon description and loading details

	Dimensions before testing (mm)			Loading rates (mm per minute)		
Specimen	Average width	Average thickness	Gauge length	Loading	Unloading	Reloading
S 1	12.75	9.64	50.80	0.5	1	1-5
S 2	12.76	9.65	50.80	0.5	1	1-5
S 3	12.76	9.61	50.80	0.5	1	1-5
S 4	12.80	9.36	50.80	1.5	3	3-15
S 5	12.75	9.42	50.80	1.5	3	3-15

For the cyclic materials tests a 7.6 mm (0.3") extensometer was used. Specimens were cycled in strain increments up to $\pm$ 1% strain.

3.4.1 Loading

Four different types of fatigue loading were employed, namely: constant amplitude (CA) cyclic loading, constant amplitude cyclic loading with periodic underloads (CA-UL), variable amplitude cyclic loading (VA), and a crack marking loading spectrum (CA-M). These types of

loading are illustrated in Figure 3.4. Each loading block was repeated until either the specimen failed or until roughly $3 \cdot 10^6$ cycles were applied, at which point an infinite fatigue life was assumed and the specimen was considered as "run out".

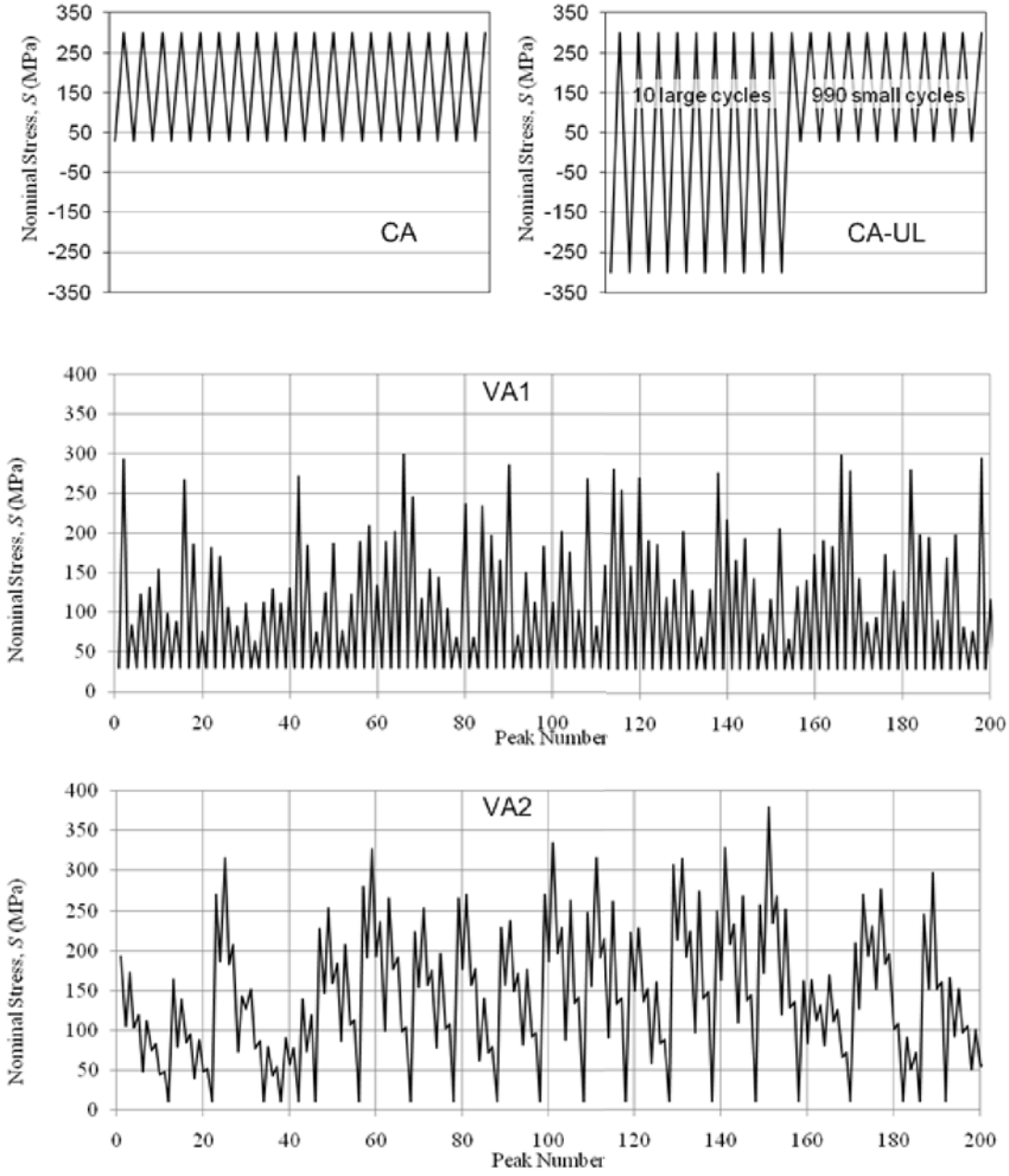

Figure 3.4: Types of fatigue loading; Top left: Constant amplitude (CA), top right: Constant amplitude with periodic underloads(CA-UL), Middle: Variable amplitude load history 1(VA1), Bottom: Variable amplitude load history 2(VA2)

CA loading tests were performed at a frequency of 8 Hz and stress ranges of 400, 270, and 180 MPa with stress ratios ($R = S_{min} / S_{max}$) of -1, 0.1 and 0.4. The maximum nominal applied tension stress was 300 MPa due to the limited capacity of the testing machine.

The second aforementioned loading type, CA-UL, involved repeating the same 1000 cycle loading block. Each block consisted of 990 tensile-only cycles with a stress range of 180 or270 MPa (with R = 0.1) and 10 compressive underload cycles with stress range of 400 or 600 MPa (with R = -1.0). The same testing frequency of 8 Hz was used.

Two different variable amplitude loading spectrums were applied. These spectrums involved the repetition of two 100 cycle spectrums, randomly extracted from larger in-service loading histories. These nominal stress histories, used to simulate in-service loading conditions, were generated using traffic data from Ontario, Canada obtained from a survey of truck axle spacings and loads conducted in 1995 with total number of 10198 trucks [Ministry of Transportation of Ontario 1995]. Figure 3.5 shows a gross truck weight histogram based on this survey data. A 1000 truck representative sample was used in this study. The truck weights in Figure 3.5 are static weights, therefore to approximate the corresponding dynamic load effects, each axle load should be multiplied by an impact factor of 1.25, in accordance with CAN/CSA-S6-06 [CSA 2006].

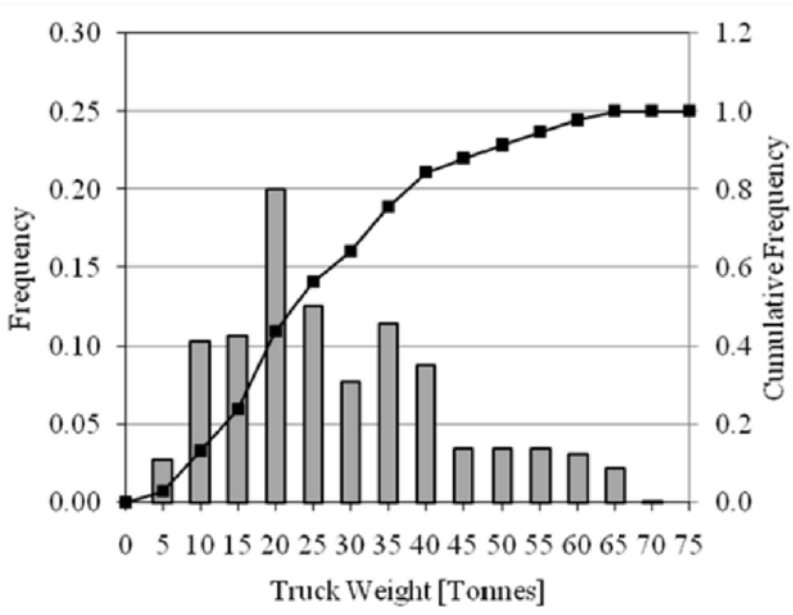

Figure 3.5: Gross vehicle weight histogram based on 1995 Ontario survey [Ministry of Transportation of Ontario 1995]

To generate in-service load effect histories, the trucks in the sample were successively passed over influence lines for two locations on a 1-span simply supported bridge. These influence lines, illustrated in Figure 3.5, were for: moment at the mid-span (ps-m) and the support reaction (ps-r). For load history LH1, the ps-m influence line was assumed, along with a bridge span of L = 40m. For the 1Hz load history, the ps-r influence line was used with a bridge span of L = 15 m.

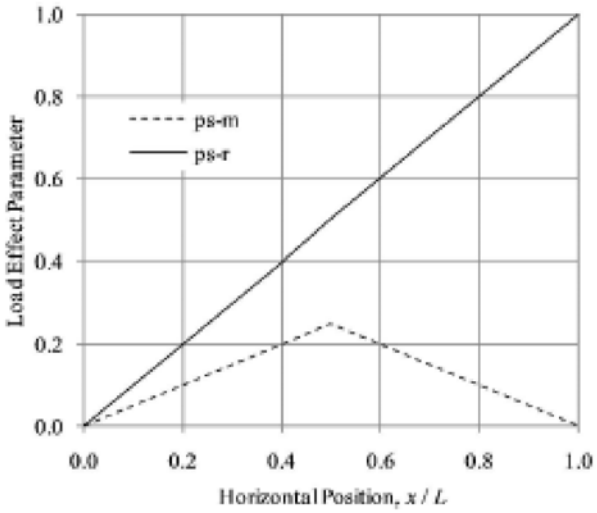

Figure 3.6: Influence lines used to generate in-service load effect histories for a 1-span simply supported girder

Load effect history data can be generated without specifying the cross-sectional properties of the bridge girder. Analyses at different stress levels can then be performed in a generic method by simply scaling the load effect history. By conducting a rainflow analysis of the load effect history multiplied by the scaling factor, the equivalent stress range determined using Miner's sum (for example) can be calculated.

Variable amplitude load histories 1 and 2 (VA1 and VA2) are based on the load effect histories generated from the ps-m and ps-r influence lines, respectively. For load history VA1, all load effect parameters were multiplied by a factor of 19.85 and then shifted up to maintain maximum and minimum loads of 85.5 and 8.55 kN (300 and 30 MPa in terms of nominal stresses). The calculated equivalent stress resulting from this loading spectrum was 159.43 MPa. For load history VA2, the factor to be multiplied by all load effect parameters was chosen in such a way that the resultant load history gives a close equivalent stress to VA1's to make these two histories comparable. This was done by first performing a rainflow analysis to count the number of cycles in the spectrum, then calculating the equivalent stress range, and multiplying all stress ranges in

the spectrum by a factor to obtain an equivalent stress range of around 160 MPa. A factor of 15.11 was found by trial and error and then was multiplied by all load effects parameters, maintaining an equivalent stress range of 161.05 MPa. Maximum and minimum loads in this load spectrum were found to be 108.30 and 2.85 KN (380 and 10 MPa in terms of stresses), respectively. Since the VA2 load history required the specimens to be subjected to loads greater than 108 kN, and the MTS 810 load capacity was limited to 100 kN, another MTS 322 machine with a 500 kN loading capacity was used for the six VA2 fatigue tests. Final spectrums were inputted into the MTS control loading program as profiles with sinusoidal peaks and an 8 Hz frequency.

In parallel with the main fatigue testing program, two different marking spectrums were tested; one for an as-welded specimen test and one for a normally peened specimen. Using these spectrums, a "beach-marked" crack surface was produced for specimen S-Fm1 from the beginning of the test and for specimen S-E32 after 1,825,000 cycles following the procedure proposed by [Husset et al. 1985], which can be summarized as follows:

- Cycling begins at ΔS = 270MPa, R = 0.1;
- Stress amplitude is then decreased by half, i.e. to 135 MPa;
- Maximum stress is kept at the same level however, i.e. 300 MPa, to eliminate possible crack retardation;
- These loading conditions are alternated for an equal number of cycles: 10,000 cycles for the untreated specimen (S-Fm1) and 100,000 cycles for the peened specimen (S-E32).

The marking spectrum was continued until failure. Equivalent stress ranges were then calculated for both tests using Miner's rule, similar to the produced followed for the VA loading tests. Figure 3.6 presents a schematic view of the marking load spectrum.

This procedure takes advantage of the beach-marks generated on the fracture surface by overloading and is an easy one to employ without requiring special complicated equipment. Crack initiation sites, evolution of the shape parameter (a/c) during the test, and variation of crack depth (a) can be determined by crack front marking, without any disturbance of the crack growth rate and evolution of the crack front [Husset et al. 1985].

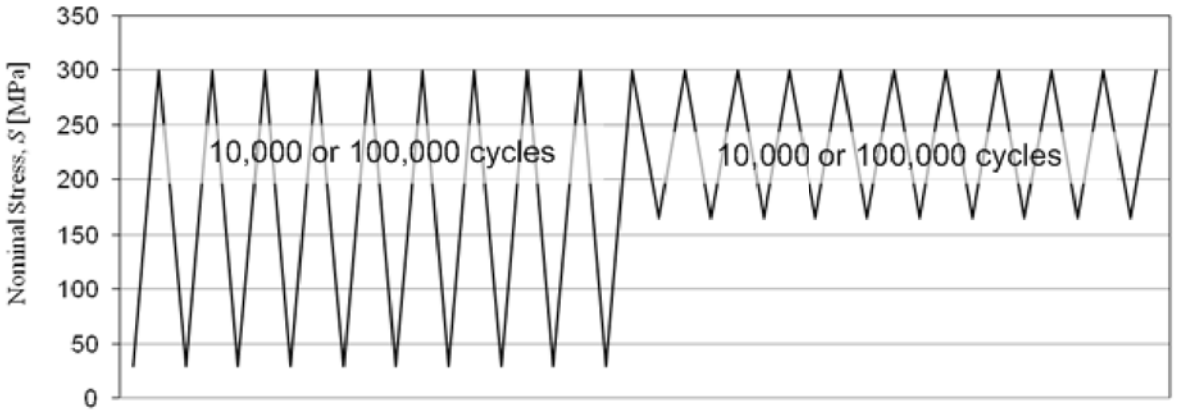

Figure 3.7: Crack front marking loading scheme

This procedure takes advantage of the beach-marks generated on the fracture surface by overloading and is an easy one to employ without requiring special complicated equipment. Crack initiation sites, evolution of the shape parameter (a/c) during the test, and variation of crack depth (a) can be determined by crack front marking, without any disturbance of the crack growth rate and evolution of the crack front [Husset et al. 1985].

3.4.2 Weld treatment

Weld treatment by needle peening was performed using a compressed air needle gun; following the procedure recommended by the International Institute of Welding [Haagensen and Maddox 2002]. Each treated weld toe, received four passes of peening, each pass lasting approximately 3 seconds. The treatment was performed by the same individual to ensure consistency. Four different treatment conditions were studied: untreated (as-welded), treated under zero axial load (normal peening), treated under 15% of the maximum axial load (45 MPa prestress), and treated at the mean axial load level (165 MPa prestress) for a CA loading test at $\Delta s = 270$ MPa and $R = 0.1$. For the specimens treated under load, in order to simulate peening of existing structures with the dead load stress present, the specimens were loaded to the desired prestress level, peened while in the testing machine (without removing the tensile prestress), and then cyclic loaded right after peening. Figure 3.7 shows the peening tool used in this study. Sample weld toes before and after peening are shown in Figure 3.8.

Figure 3.8: Needle peening tool used in this study

3.5 Crack growth monitoring

To monitor crack growth, three different techniques were used; ink marking (dye penetrant staining), crack front marking (beach-marking), and the alternating current potential drop (ACPD) method. These methods can be used both independently and in conjunction with each other.

Figure 3.9: *Fatigue specimen weld toe; Left: untreated, Right needle peened (photo: [Walker et al. 2008])*

Ink marking was used to obtain more information on crack shape and depth. This was done by staining already cracked specimens using SPOTCHECK dye penetrant sprays by MAGNAFLUX (Figure 3.9). To do this, cracked weld toes were first cleaned using the cleaner (SKC-S) and left for a couple of hours to dry. Next, the (dye) penetrant (SKL-SP1) was applied and then left for at least 24 hrs to dry. Finally, the specimens were put back into the MTS testing machine and cyclically loaded until complete fracture (separating into two parts). The fractured surfaces were then studied to obtain information about the crack shape and depth at the time of staining.

Figure 3.10: SPOTCHECK sprays for crack detection

As mentioned in Section 3.4.1, the crack front marking technique is based on the concept that any change in the fatigue test loading parameters, e.g. amplitude and mean stress, results in another crack surface aspect, resulting in a "beach-mark". The crack front marking technique was used to mark the crack front at other depths. Here, by changing the stress amplitude while keeping the maximum stress unchanged, it can be assumed that the plastic zone at the crack tip does not change and thus the possibility of crack retardation is eliminated.

Both the ink marking and beach-marking methods are accurate methods for studying crack shape and depth, but they do not provide continuous real time information regarding the crack depth. The ink marking method can only be applied to cracked specimens where the crack is large enough to be measured after breaking the specimen. The crack front marking method gives more information about crack properties and can be applied from the beginning of testing, however, it does have two main limitations. First, similar to ink marking, it does not give clear information about crack depth, especially at the early stages, and secondly, it needs to be calibrated for the test duration. In other words, tests should be long enough so that the formed beach-marks can be distinguished from each other. Facing these limitations, another technique was also used for monitoring crack growth during fatigue tests. The alternating current potential drop (ACPD) method was employed as a way of continuously monitoring crack depths during the fatigue tests on untreated and needle peened welds. As discussed earlier, the basic principle is to introduce an

alternating current (AC) to flow between two electrodes (field probes) and measure the local voltage drop over the area adjacent to the weld and over the crack by means of voltage probes.

To implement the ACPD method specimens were first sand blasted to remove millscale and to decrease the electrical resistance of specimens so that an almost uniform suitable electrical current field can be generated using ACPD unit box and field probes. Special care was taken to protect the weld toes and to keep them untouched during sand blasting by duct taping a narrow region around weld toes (see Figure 3.10). Next, four 2-site ACPD arrays, one for each weld toe, were attached to the specimens, straddling the weld toes as shown in Figure 3.11, and used, in conjunction with a TSC ACPD Mk IV instrument and LIMOS data acquisition software, to monitor the fatigue crack growth. Each array recorded the crack depth at two different points, spaced 10 mm apart, every 20 seconds from the beginning of the test until failure. This was done for different test series. The ACPD equipment [TSC 2008] is shown in Figure 3.12.

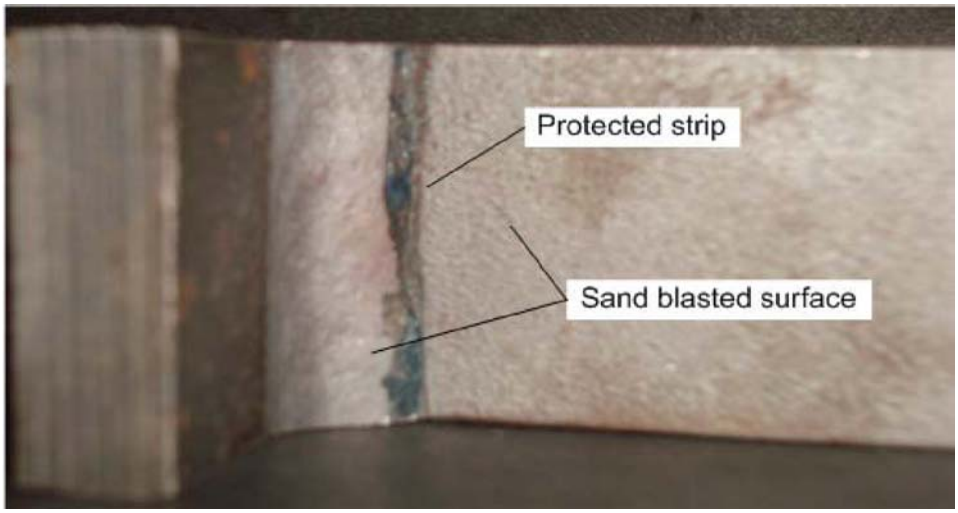

Figure 3.11: Sand blasted specimen (weld toes remained untouched by using a narrow duct tape)

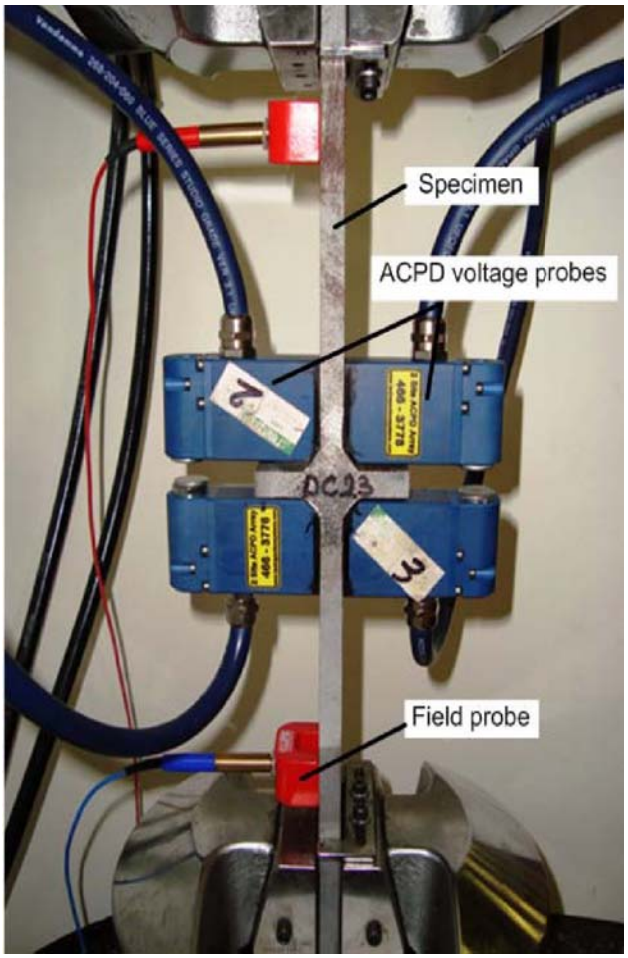

Figure 3.12: ACPD measurements tools; ACPD probes attached to the specimen (top); Acquisition box (bottom)

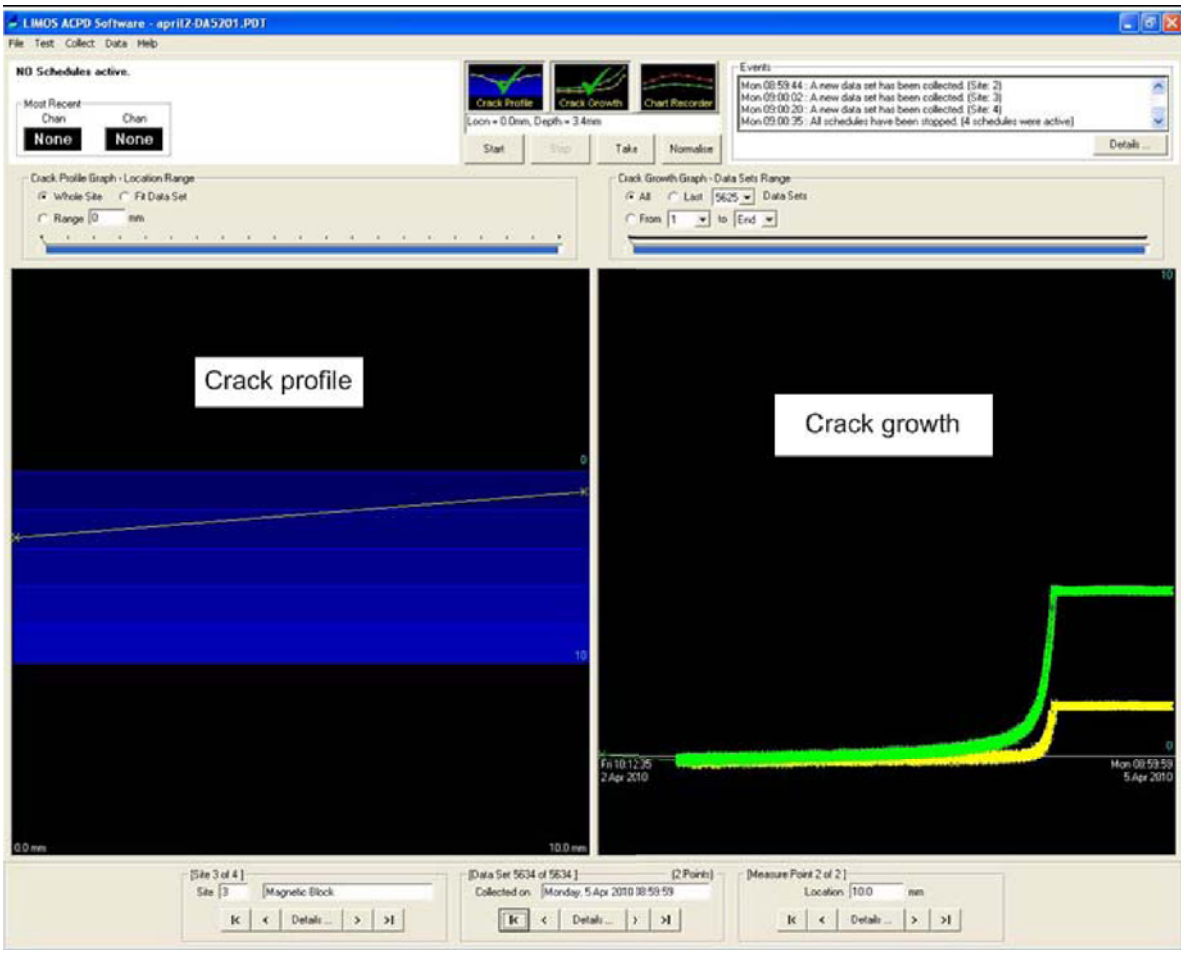

Figure 3.13: LIMOS software interface

Electrical Current Potential Drop (Direct Current Potential Drop, DCPD, and Alternating Current Potential Drop, ACPD) techniques have been widely used for crack sizing and crack growth monitoring in laboratory experiments for many years, e.g. [Martin 1978], [Husset 1986], and [Costa Borges 2008].

ACPD theory and formulation can be found in the literature (e.g. in [Michael et al. 1981]). The basic principle is to introduce an alternating current (AC) to flow between "field probes" and measure the local voltage drop over the area closest to the weld and over the crack by voltage probes (see Figure 3.13) [Costa Borges 2008] and [Lugg 2002].

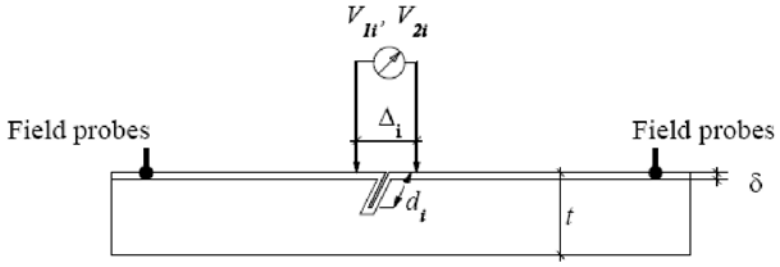

Figure 3.14: ACPD theory and notation [Costa Borges 2008]

The probes are organized in pairs (cross crack and reference) and the voltages from each pair are used to calculate crack depth using the following simple formula, applicable to high aspect ratio cracks in ferritic steel:

$$d_i = \Delta_r/2\ (V_c/V_r - \Delta_c/\Delta_r) \qquad (3.1)$$

where d_i is the crack depth at location i, V_r and Δ_r are the measured potential difference measured by and probe spacing for the cross crack probe, respectively, and V_c and Δ_c are the potential difference measured by and probe spacing for the reference probe, respectively.

Formula (3.1) gives an accurate estimate for cracks with aspect ratios (a/c) smaller than 0.1 in the specimens with a simple geometry. For complicated geometries and for cracks with higher aspect ratios, the formula underestimates crack depth and a calibration factor is then needed [Costa Borges 2008].

Passing an alternating current through a conductor, current is forced to flow in a thin layer on the outer surface by the so-called "skin effect". The thickness of this layer (skin depth) is given by:

$$\delta = (\pi \sigma \mu_r \mu_o f)^{-1/2} \qquad (3.2)$$

Where δ is the skin depth, σ is the electrical conductivity of the material, μ_r is the relative magnetic permeability of the material, μ_m is the permeability of the free space, and f is the frequency of the applied alternating current.

As Eq. (3.2) implies, the skin depth is relatively small for materials with a high permeability and it becomes bigger as conductivity increases. For example, at a frequency of about 5 kHz, ferromagnetic mild steel has a skin depth of ~ 0.1 mm, high conductivity materials such as

aluminium have skin depths of 1-2 mm, and low conductivity metals stainless steel have skin depths of 5-8 mm.

A two point contacting probe measures the surface voltage produced by the input current. This value is dependent on the magnitude of the input current, the spacing between the two measuring points, the skin depth, the material conductivity and the specimen geometry [Lugg 2002]. Given a uniform current distribution, if the current and the probe spacing are kept constant, then the measured voltage will be dependent only on the conductive metal path length between the probe tips. This path length is clearly longer for a surface-breaking crack than for a surface without any crack. By reading the two voltages, one across the crack and the other on an adjacent uncracked surface, the effect of the crack can be separated from the other effects [Lugg 2002].

To evaluate the device accuracy, dye penetrant staining was used upon crack detection in three specimens and the actual crack depths were compared with the ACPD readings after complete specimen fracture. A number of additional fatigue tests employing the beach-marking technique were also conducted to provide a second means of validating the ACPD device.

3.6 Microhardness measurements and microstructure

To study the effect of peening on the near-surface hardness of the fatigue specimens, microhardness tests were conducted on the base metal and heat affected Zone (HAZ) of the untreated (AW) and needle peened (NP) welds.

To perform these measurements, two untested fatigue specimens, one as-welded and one needle peened, were sectioned and cast in epoxy. The samples were then polished using four successively finer grades of emery paper to produce a smooth, pit-free surface. Hardness tests were then performed using a Vickers microhardness tester. Sample preparation was in accordance with ASTM E3-01 [ASTM 2007]. Following the procedure in ASTM E384 – 10 [ASTM 2010], indentations were made at a depth of ~0.1 mm below the surface and then every 0.2 mm up to ~2 mm in depth. Using a microscope at X50 magnification, indent dimensions were measured and the Vickers hardness (HV) was calculated for each depth using (3.3).

$$HV = 1854.4 \cdot P/d^2 \qquad (3.3)$$

Where HV is the Vickers hardness number, P is the applied force in grams-force (gf), and d is mean diagonal length of the indentation in μm. All hardness measurements were done with the same applied force of $P = 200\ gf$.

To study the microstructure of the treated weld toe, after performing microhardness measurements, the specimen surface was etched with a 2% Nital solution to reveal the microstructure (grains and grain boundaries). Photos were then taken through a microscope at X10 magnification to observe grain boundaries in the microstructure of the steel were. Figure 3.15 shows the prepared microhardness specimens.

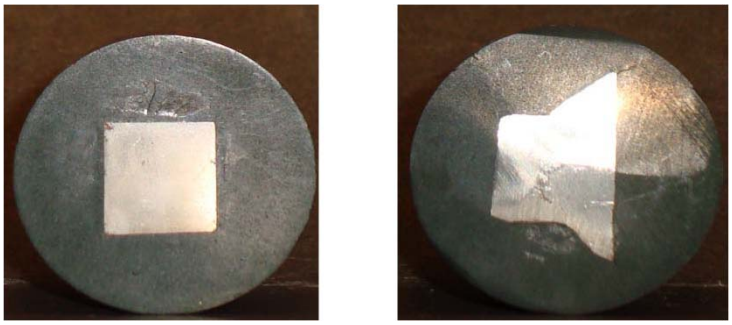

Figure 3.15: Microhardness specimens: base metal (left), weld toe (right)

3.7 Weld toe geometry

The weld toe angle and weld toe radius are two important parameters for describing the local conditions at the weld toe. These parameters can be measured using photographs of saw-cut sections. To do this, three as-welded specimens, two untested and one cracked, and three normally peened specimens, two untested and one cracked, were cut into halves and then polished to get a smooth enough surface. Photos were then taken of all of the exposed and polished weld toes (12 photos for each specimen) at X5 magnification, and then carefully examined to measure the weld toe radius and angle. Moreover, possible visible initial defect and/or any irregularities that could act as initial cracks were also investigated and measured using these photographs.

Weld toe angle is defined as the angle between the extension of the parent plate surface and the line representing the shape of the weld near the toe area. There are different methods for measuring weld toe radius based on different definitions of this parameter. Herein, the same as in [Martinez and Korsgren 1994], the weld toe radius is defined as the radius of the largest circle

fitted to the transition between the parent plate and the weld metal, as illustrated in Fig. 3.15. Defect depths were defined as the longest dimension perpendicular to the intended direction of loading from a horizontal projection of the base plate line. Defect root radii were taken to be the radius of the largest circle enclosed by the defect at its point of maximum depth.

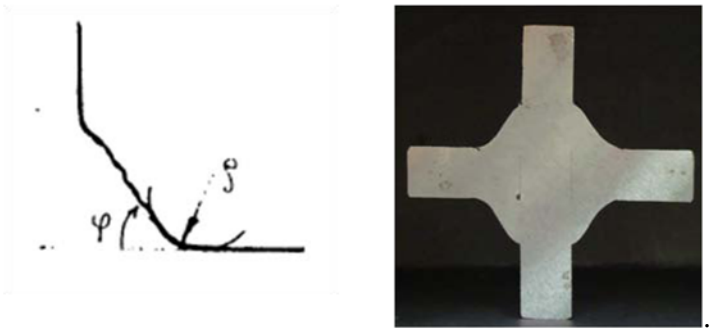

Figure 3.15: Typical weld profile and recording of weld geometry [Martinez and Korsgren, 1994] (left) and prepared specimen for weld toe geometry measurements (right)

3.8 Crack aspect ratio

The crack aspect ratio for a through crack is defined as the ratio of the deepest crack point, *a*, to the half crack length, *c*. To investigate *a/c* values, cracked sections were inspected, and photos were taken from failed specimens' surfaces. Those photos were then used to determine values for *a* and *c* for final crack fronts. For specimen S-E32, the crack front marking technique was used so that *a/c* ratios could be calculated at multiple crack depths.

3.9 Residual stress measurements

The X-ray diffraction method was used to measure residual stress using the distance between crystallographic planes, i.e. d-spacing, as a strain gauge. X-ray diffraction was chosen because of its appropriate spatial and volumetric resolution to fully and adequately characterize the residual stress distributions often found in the areas of critical importance.

Three specimens, one as-welded and two normally peened, one untested and one tested under CA-UL loading (Δs_{eq} = 186 MPa) but not cracked, were sent to Proto Manufacturing Ltd., the external laboratory that performed the residual stress measurements. Seven measurements were taken at two locations on each specimen at depths of approximately 0, 0.1, 0.2, 0.5, 1.0, 1.5, and 1.8 mm below the surface. Measurements were made using the Laboratory X-Ray Diffraction

(LXRD) system at Proto, following the procedure recommended in ASTM- E915 and SAE J784a [SAE 1971]. Each measurement location was first electro-polished to the desired depth, the measurement was then made and the location was polished again to get to the next 3.16 depth.

Figure 3.17 shows a specimen in the LXRD system. As can be seen in this figure, to maintain enough space for measurements, one of the transverse stiffeners was removed by saw cutting. To confirm that this procedure does not affect the residual stress distribution at the location of interest, strain measurements were made at the same location on the specimen before and after saw cutting. The results showed no significant error due to this procedure.

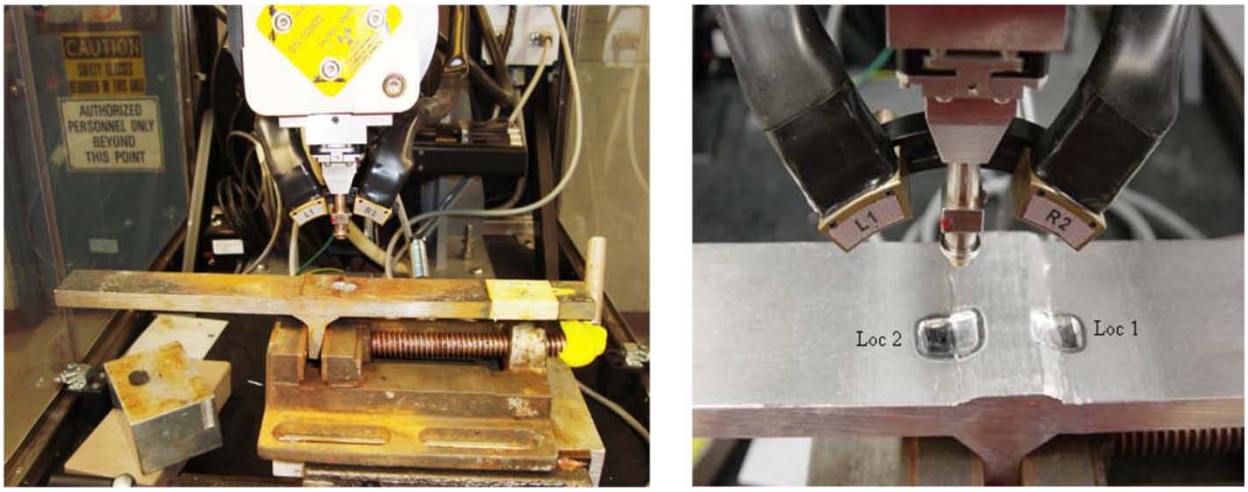

Figure 3.16: LXRD system for residual stress measurements

Chapter 4
Test Results and observations

4.1 Introduction

The results and observations of the tests conducted for the current study are presented in this chapter. Recall that the main goal of these tests was to investigate the effectiveness of needle peening in enhancing the fatigue performance of welded details, when applied under different conditions. Moreover, they were also performed to provide a means for calibrating and evaluating the two fatigue prediction models used herein. The tests and measurement procedures were explained in the Chapter 3. The focus of the current chapter is on the test results.

The fatigue test results presented in Section 4.2 encompass a range of loading and treatment conditions. The results illustrate how parameters, such as the loading history type, stress range, and R ratios, and peening under different prestress levels, influence the fatigue life. In Section 4.3, static and cyclic properties of the 350W steel are determined based on materials tests. This gives accurate measurements for a number of the input parameters for the two analytical models. In Section 4.4 results for the different crack growth measurements methods, described in Chapter 3, are presented. These results not only show how fatigue cracks grow under different loading and treatment conditions, but are also essential for calibrating fatigue models and understanding the fatigue behaviour of welded joints. Section 4.5 presents the microhardness measurement results, while highlighting one of the secondary effects of peening. Weld toe angle and radius measurements, along with weld toe defect measurements, are presented in Section 4.6. Section 4.7 is devoted to studying the crack front profiles, and finally in Section 4.8, the residual stress measurement results are presented.

4.2 Fatigue test results

The fatigue tests results are presented in this section. In order show the effects of the different loading and treatment conditions separately, two different sets of graphs are provided. Figures 4.5, 4.7, and 4.8 show test results for the three loading conditions i.e. CA, CA-UL, and VA, respectively. The next three Figures (Figure 4.9 to 4.11) present test results based on the treatment type (as-welded, normally peened, and peened under load).

Failure was defined as the detection of a crack larger than 1 mm caught by eye inspection in the specimen. Cracks initiated in one or several of the following locations; the weld toe of the loaded plate, the weld toe of the stiffener, or the base metal. The different failure types are shown in Figure 4.1. If the specimen did not fail after more than 3 million load cycles, it is marked as a "runout" in the S-N graph. Specimens that failed in stiffener weld toe or base metal are also considered runouts. (see Figure 4.5 and Figures 4.3 to 4.8).

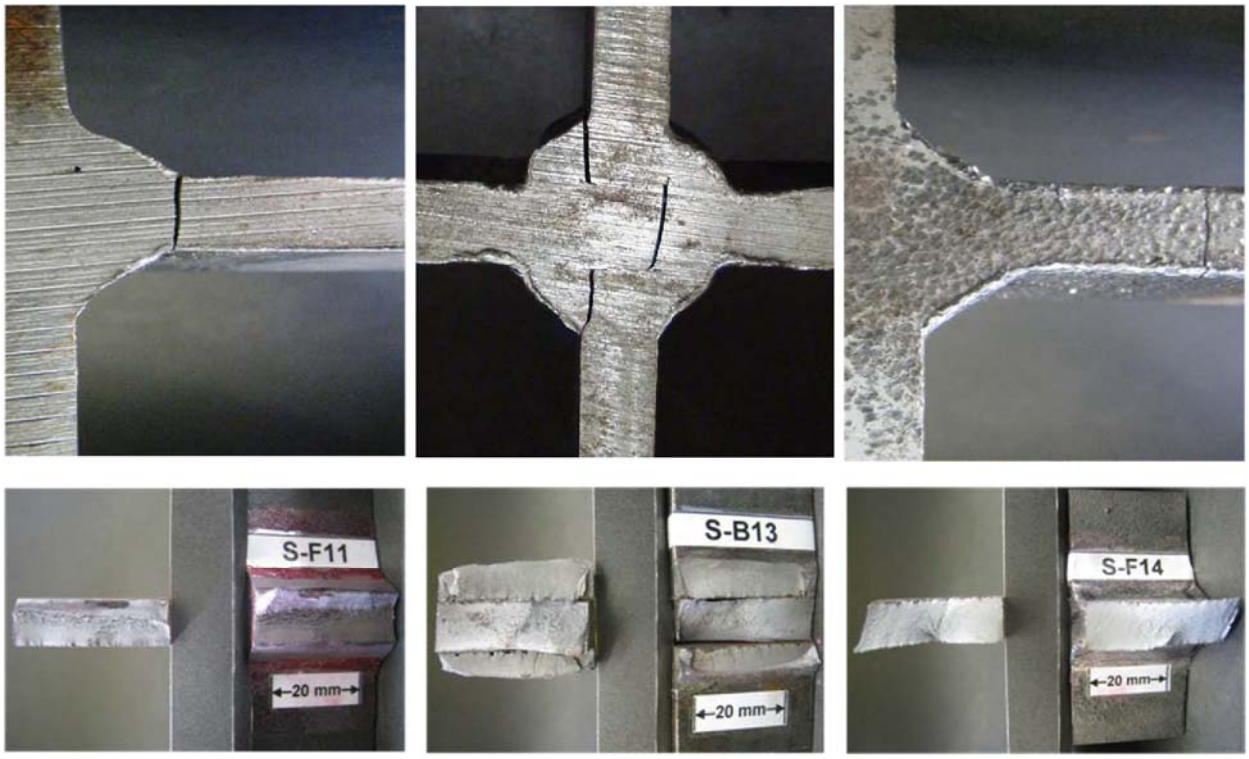

Figure 4.1: Fatigue cracks; Left: in loaded weld toe, Middle: in stiffener weld toe, and Right: in base metal

4.2.1 Constant amplitude (CA) tests

Fig. 4.2 presents all 24 constant amplitude (CA) loading fatigue tests conducted in this study along with similar results of fatigue tests from a previous study performed at three different stress amplitudes:

- 15 fatigue tests at a stress range of 180. Six of them, 3 untreated and 3 normally peened, were conducted by (Walker et al. 2008) at R = 0.1. The other nine tests consist of three untreated, three normally peened, and three peened under 135 MPa prestress at stress range of 180 MPa, but at stress ratio of R = 0.4.

- 15 untreated, normally peened, peened under 45 MPa and 135 MPa prestress fatigue tests at stress range of 270 MPa and R= 0.1.

- Three untreated tests and three treated were performed at a stress range of 400 MPa and a stress ratio of R = -1.

Design S-N lines for Detail Categories 'A', 'B', and 'C' (CAN/CSA-S6-06) are also plotted for comparison purposes.

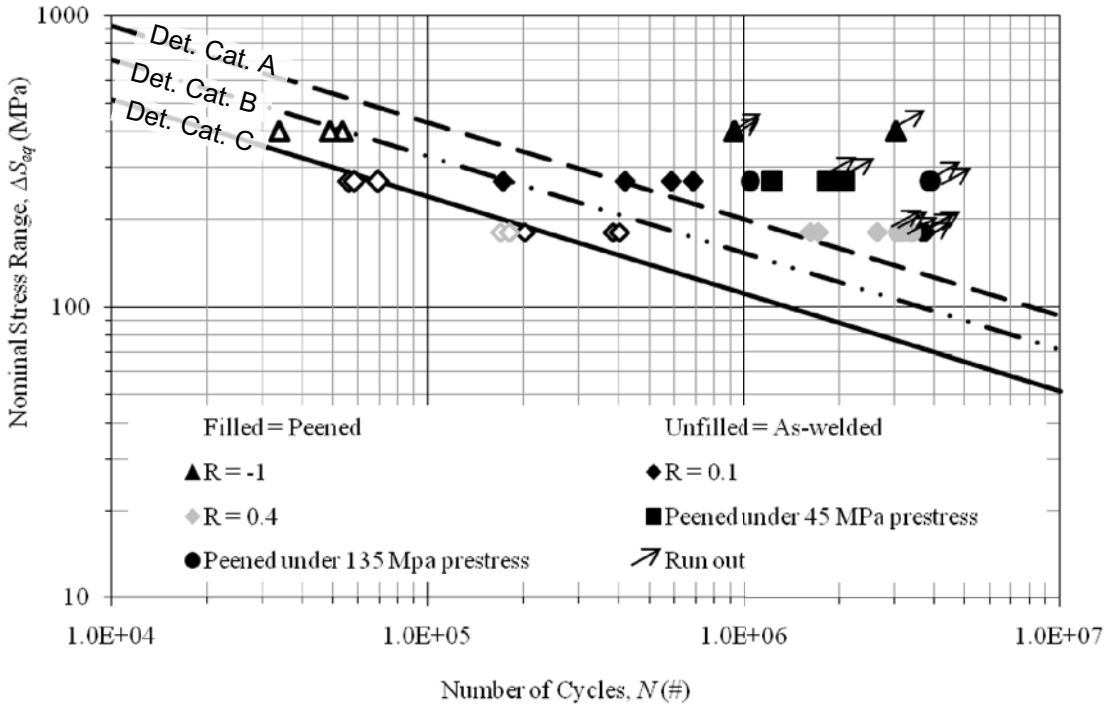

Figure 4.2: Constant amplitude (CA) fatigue test results

All as-welded and most of normally peened specimens failed at the weld toe of the loaded plate at all three stress ranges. Two treated under load specimens failed at the weld toe of the loaded plate before 3 million cycles, two failed in the stiffener weld toe while the other specimens endured more than three million load cycles.

The untreated specimen fatigue lives all lie near the design curve for Detail Category 'C', while all except one result for the treated specimens lie above the Detail Category 'A' design curve. This suggests that the peening resulted in a significant increase in fatigue life. Additionally, as

the results of Figure 4.2 imply, the treatment is even more efficient when applied under load. Only two of the specimens treated under load failed in the peened region (after more than a million load cycles). The other four either endured more than 3 million load cycles or failed at a location other than peened weld toe. These results match well with the general trends for hammer and ultrasonic treatments applied under load reported in [Maddox 1998] and [Ummenhofer et al. 2006a].

Figure 4.3 proposes an explanation for the performance improvement of the peened welds treated under load. In this figure, σ_{weld} is the tensile residual stress due to the welding process, σ_{pwt} is the compressive residual stress introduced by the post-weld treatment and σ_{dead} is the stress due to the dead load, which is simplistically assumed to be tensile and uniform. Simply stated, if a tensile dead load stress is introduced after the treatment, then the mean compressive stress level at the surface (and as a result, the treatment effectiveness) is reduced. On the other hand, if the tensile dead load stress is applied first, then the stress introduced by the treatment effectively negates any tensile dead load stress near the surface of the treated weld. This implies that treatment effectiveness can be increased by increasing the prestress level.

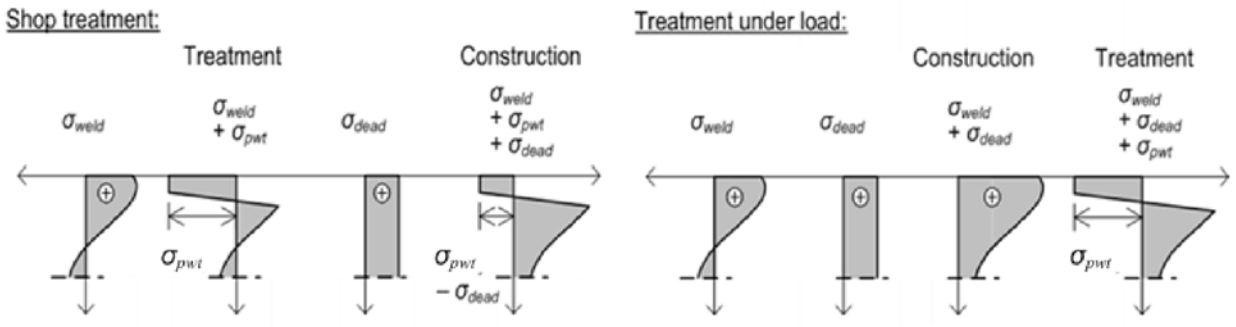

Figure 4.3: Residual stress distributions; Left: Shop treatment, Right: Treatment under load

The fact that peening treatments can be even more effective when applied under load, suggests that these treatments are well suited for the rehabilitation of existing bridges.

While no significant difference is observed between fatigue tests at the same stress range but with different R ratios for the untreated case, for the normally peened specimens tested at the 180 MPa stress range, the R ratio seems to play a key role. All three specimens tested with R = 0.4 had finite fatigue lives. However, for those tested at R = 0.1, no failure was reported. The fact that the stress range was identical, this suggests that behaviour can be attributed to the mean

load, which is higher for the higher R ratio. As a result, cracks spend a larger part if the cycle open when loaded with the higher R ratio.

4.2.2 Constant amplitude with periodic underload (CA-UL) tests

Fig. 4.4 presents results for the tests conducted under CA-UL loading at two different stress ranges:

- Six tests were conducted in (Walker et al. 2008) with an equivalent stress range of 186 MPa. A repeating 1000 cycle loading block consisting of 990 load cycles with ΔS = 180 MPa and R = 0.1 followed by 10 underloads with ΔS = 400 and R = -1 was applied.
- Six tests conducted in this study at the equivalent stress range of 279 MPa. A repeating 1000 cycle loading block consisting of 990 load cycles with ΔS = 270 MPa and R = 0.1 followed by 10 under loads with ΔS = 600 of 600 and R = -1 was applied.

As Figure 4.4 shows, specimens receiving no treatment had a fatigue life close to the Detail Category 'C' design curve. But for the peened specimens, the three test results lie under the Detail Category 'B' design curve, one between 'B' and 'A' and only two treated specimens lie above the Detail Category 'A', design curve. Comparing to CA loading case where almost all treated specimen had fatigue lives greater than the life expected by the Detail Category 'A' design curve, it can be concluded that peening was less effective for this loading spectrum. In other words, compressive overloads made the peening less effective. Additionally, analyzing this graph it is obvious that needle peening was far less effective for the loading spectrum with the higher effective stress range, i.e. ΔS = 279 MPa. This might be attributed to the extremely large load cycles, 600 MPa, present in that loading. Moreover, a portion of the peening-induced compressive residual stresses in the weld toe region may have been cancelled by the large compressive overloads in the loading spectrum.

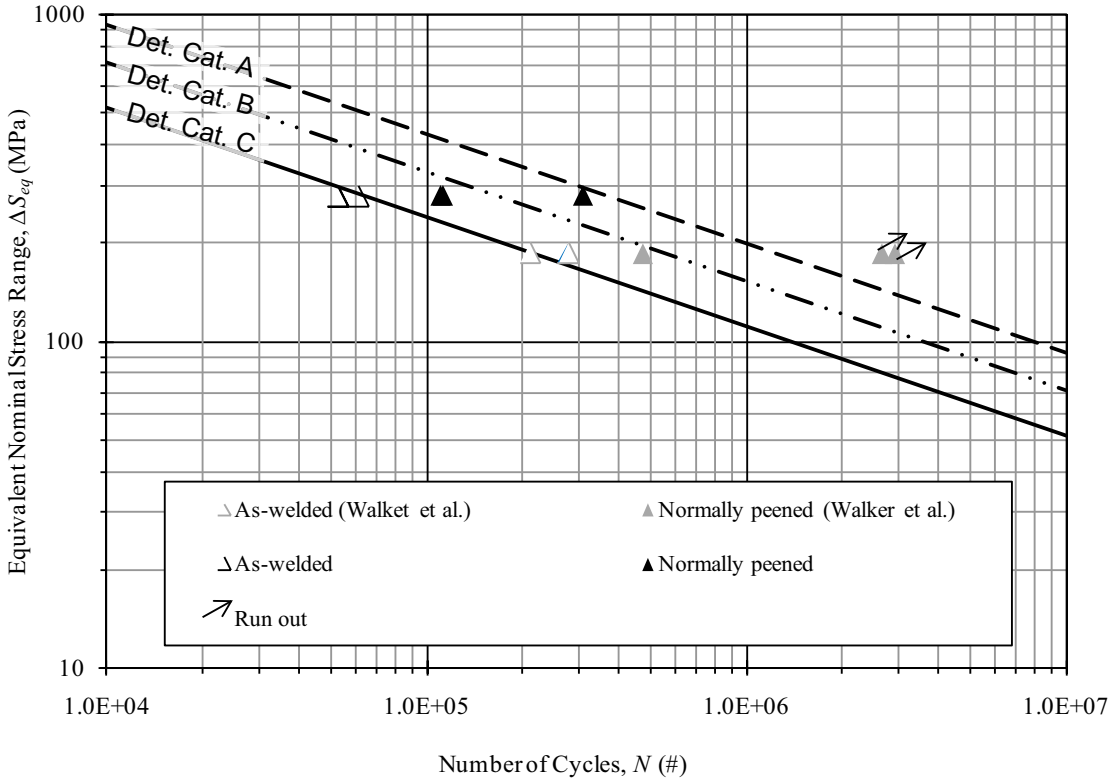

Figure 4.4: Constant amplitude with periodic underloads (CA-UL) fatigue test results

4.2.3 Variable amplitude (VA) tests

Figure 4.5 presents tests results for the variable (VA) amplitude loading fatigue tests. Similar to the previous graphs, the untreated specimens all had a fatigue life close to the life by the Detail 'C' curve. One of the peened specimens tested under the VA2 load history failed below the Detail 'A' design curve while all others either lasted for more than 3 million load cycles or failed at location other than the loaded weld toe. It was noticed that three tested specimens under the VA1 loading history lasted for more than three million cycles while the other two VA2 specimens eventually cracked in the base metal.

The fact that needle peening was less effective for the second load history, VA2, than for VA1, can be explained by comparing these two loading segments. One significant difference is that the VA1 load history can be characterized as more narrow-banded. In this case, passing a truck over the bridge generally results in only a single load cycle. In the VA2 load history, each axle load causes a small cycle as it comes on or off the end of the bridge resulting in a more wide banded

load history with more cycles that resemble overload events. Consequently, under VA2 loading history, fatigue cracks propagate at a higher rate making the treatment less effective.

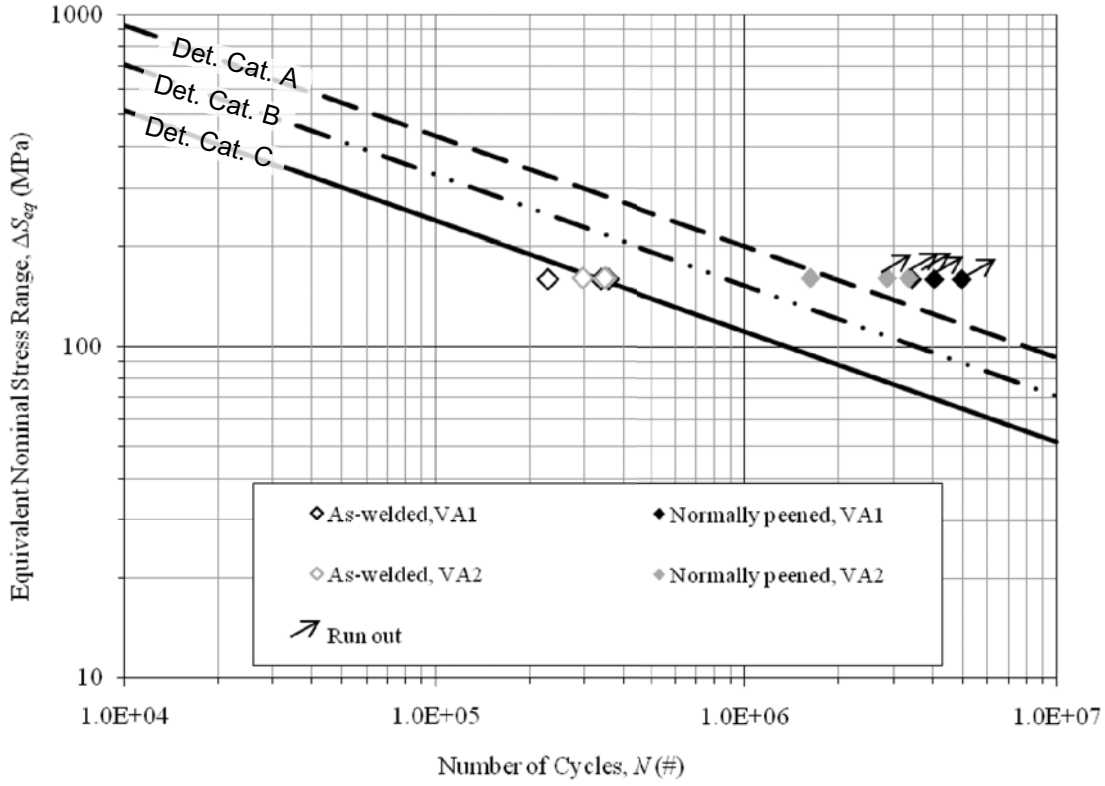

Figure 4.5: Variable amplitude (VA1 and VA2) fatigue test results

4.2.4 As-welded tests

All of the as-welded test results are reported in Figure 4.9. All of the specimens had fatigue lives more or less similar to those predicted by CAN/CSA-S6-06 Detail Category C.

All three specimens tested at R = -1 lie above the design curve. The tests at R = 0.1 lie around the design curve (some are above and some below). The only series for which all three specimens lie below the design curve is the CA loading at R = 0.4. This highlights the effect of R ratio, and consequently the mean stress, on fatigue life. Three sets of fatigue tests were conducted at a stress ranges of 180 MPa; constant amplitude with R = 0.1 and 0.4 and constant amplitude with periodic underloads. The mean fatigue life of the R = 0.1 series is the largest, followed by the CA-UL series, indicating the damaging effect of compressive underloads added to the loading spectrum. As expected, the R = 0.4 series had a shorter average fatigue life than

the previous two series. The two variable amplitude histories, VA1 and VA2, had fairy similar mean lives, without any meaningful deviation.

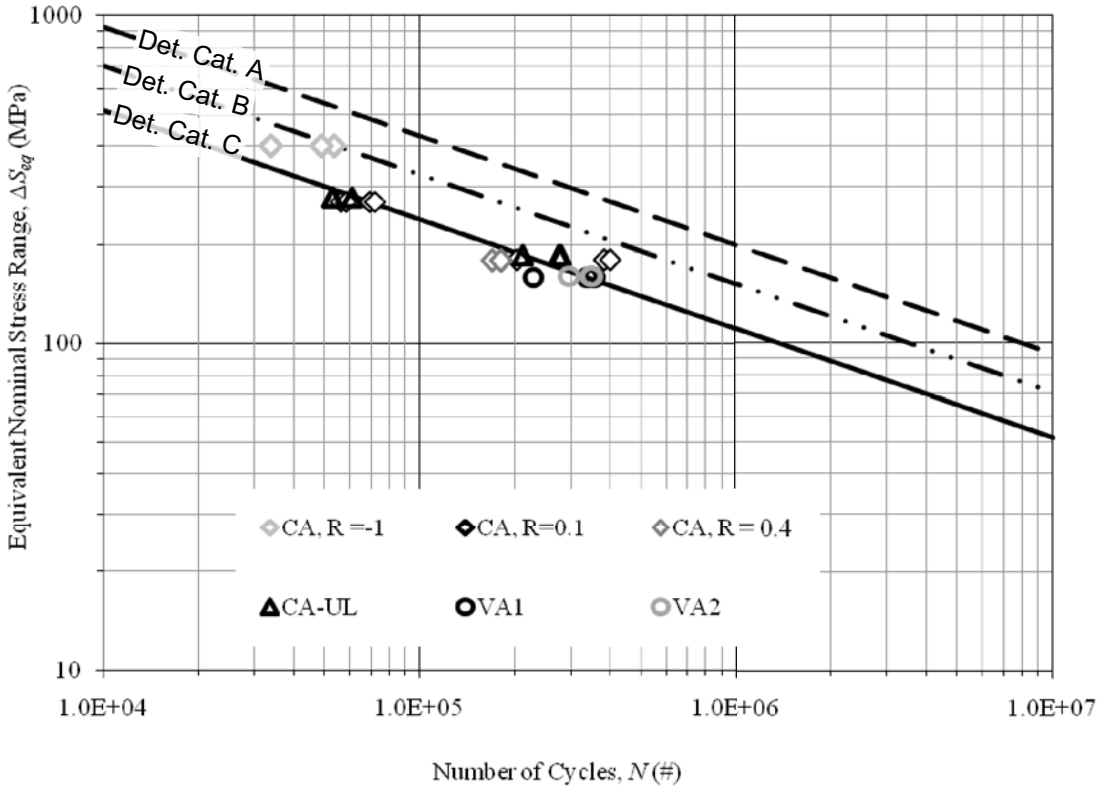

Figure 4.6: As-welded fatigue test results

4.2.5 Normally peened tests

All of the normally peened test results are presented in Figure 4.10. Although the tests results are more scattered than the as-welded results.

Needle peening was least effective for the CA-UL series with ΔS_{eff} = 279 MPa and all three specimens fell below the Detail Category A design curve, contrary to the CA-0.1 series with almost the same ΔS_{eff}. Similarly to the as-welded case, three different test series are presented for ΔS_{eff} close to 180 MPa and a similar trend is observed. Normally peened specimens tested under CA-0.1 did not fail after three million load cycles. All CA-UL loaded specimens were run outs or failed before, but close to, three million load cycles. The CA-0.4 specimens had the shortest fatigue lives in this category, showing the damaging effect of a higher mean stress with a similar stress range. Finally, all three VA1 test results endured more than three million load cycles, two

out of three VA2 specimens failed at the base metal after almost three million load cycles while the other one failed at the weld toe just below the Detail Category A design curve. The fact that the second variable load history was a wide banded one, might help to explain this trend.

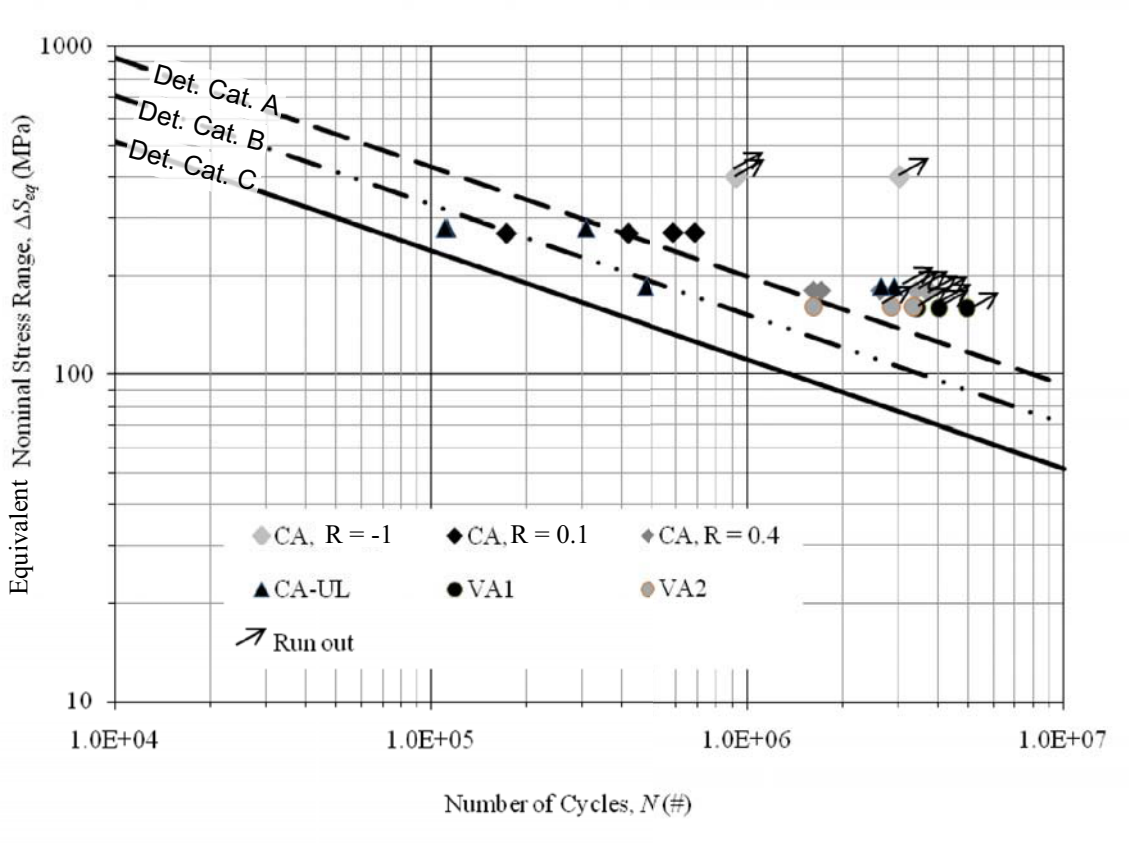

Figure 4.7: Normally peened fatigue test results

4.2.6 Peened under prestress tests

Figure 4.8 illustrates the effect of peening when applied under load, simulating the application of a post-weld treatment to already loaded structures, under different loading spectrums and under different prestress levels.

No failure was observed for specimens peened at the mean axial load level (210 MPa prestress), for R = 0.4 test series with ΔS_{app} = 180 MPa. For the constant amplitude tests with ΔS_{app} = 270 MPa and R = 0.1, however, one of the three specimens treated under load failed before three million cycles at each of the two examined prestressing levels. The other three specimens prestressed to 15% of S_{max} (45 MPa) failed in the stiffener weld toe and the other two specimens prestressed to mean axial stress (165 MPa) did not fail at all after more than three million load

cycles. In summary, peening under load resulted in a greater fatigue life improvement than peening without prestress and as a general trend, the more prestressed the specimen was upon receiving the treatment, the longer the fatigue life increase.

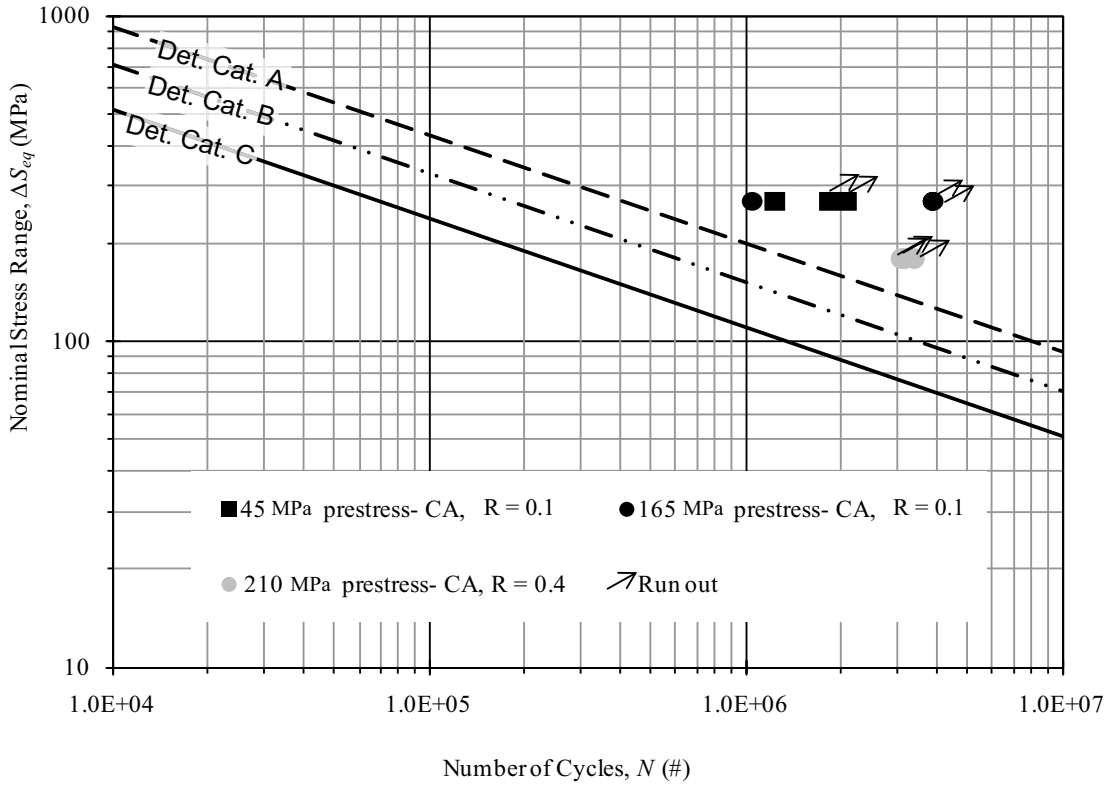

Figure 4.8: Peened under prestress fatigue test results

4.3 Material tests results

Two different sets of static and cyclic parameters are determined based on static and cyclic material tests. These parameters are used as material properties in the analytical models discussed in Chapters 5 and 6.

Figure 4.9 shows a typical stress – strain curve obtained for the 360W steel base metal tested in the study. As a general trend, the graph starts with a straight portion, showing a linear relationship between stress and strain. A plateau is then reached representing "yielding" of the material at a stress slightly less than 400 MPa. After yielding, the graph is no longer linear. However, upon unloading and then reloading, the material behaves linearly with a slope similar to the initial loading curve. Applying more load to the specimen results in more "elongation"

with a decreasing slope until reaching the absolute maximum in the graph, showing the ultimate stress. As the applied strain further increases, necking starts and eventually the specimen breaks at the rupture strain, which is ≈ 0.3 mm/ mm.

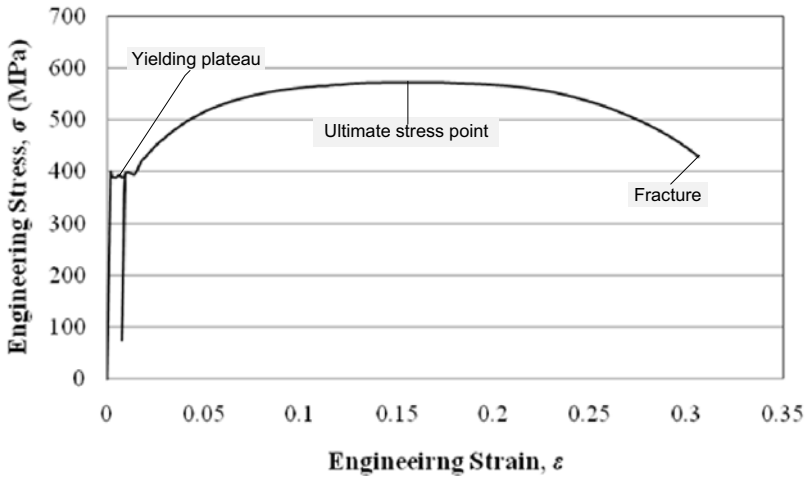

Figure 4.9: Stress – strain curve for Specimen S3 (350W steel)

Based on the obtained graphs, the following material properties were calculated for all five specimens. The results are summarized in Table 4.1:

- Modulus of Elasticity ***(E)***; defined as the ratio of nominal engineers stress to corresponding strain while the material is in the linear elastic range. This parameter was estimated by minimizing the least squares parameter (R^2) and assuming linear stress-strain behaviour (see Figure 2.2)
- Yield stress ***(σ_y)***; defined as the average of the stress values for points in the "yielding plateau".
- Yield strain ***(ε_y)***; is the strain to the nominal yield stress level.
- Ultimate stress ***(σ_u)***; is the maximum nominal stress that the material can endure without significant change in its cross sectional area. This point is the absolute maximum stress on the stress – strain curve.
- Fracture strain ***(ε_f)***; is defined as the strain at fracture.

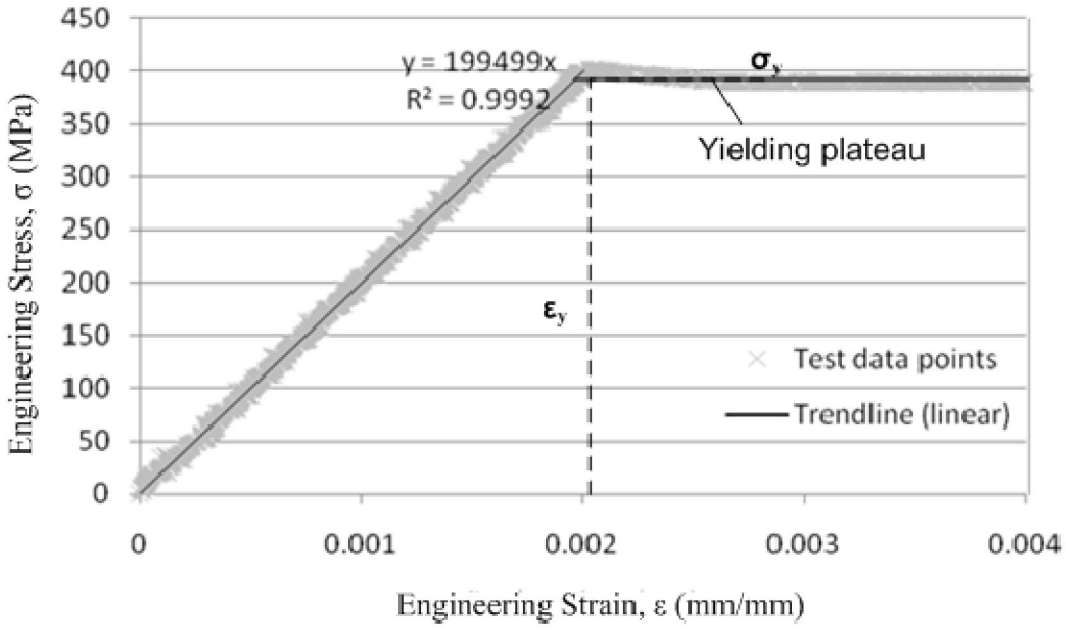

Figure 4.10: Calculating E constant for Specimen S3 (R = regression)

Table 4.1 summarizes results obtained for each test specimens. The results are fairly precise and the coefficients of variation (C.V) for E, σ_y, and σ_u are less than or close to 0.02, showing a low-variance distribution.

Table 4.1: Static material properties base on steel coupon tests

Specimen	**Modulus of Elasticity E** (GPa)	**Yield Stress** σ_y (MPa)	**Yield Strain** ε_y (mm/mm)	**Ultimate Stress** σ_u (MPa)	**Fracture Strain** ε_f (mm/mm)
S1	196.5	401.1	0.000200	571.8	0.3073
S2	200.3	418.9	0.000215	570.5	0.3165
S3	199.5	400.9	0.000205	572.1	0.3063
S4	206.6	397.1	0.000193	571.7	0.2941
S5	205.2	408.8	0.000203	585.3	0.3261
Mean	***201.6***	***405.4***	***0.000205***	***574.0***	***0.3101***
C.V	***0.0285***	***0.0214***	***0.0387***	***0.00108***	***0.0387***

Fully reversed cyclic loading tests were conducted at seven different prescribed strains on two base metal specimens. Figure 4.11 shows typical cyclic stress-strain curve results obtained for the 350W steel used. Ramberg- Osgood cyclic stress-strain curve constants were determined by graphical curve fitting and minimizing the least squares parameters. K' and n' values were determined for the two specimens and are summarized in Table 4.2. Average values for these parameters are as follows: *K'* =1153.8 MPa, and *n'* = 0.165.

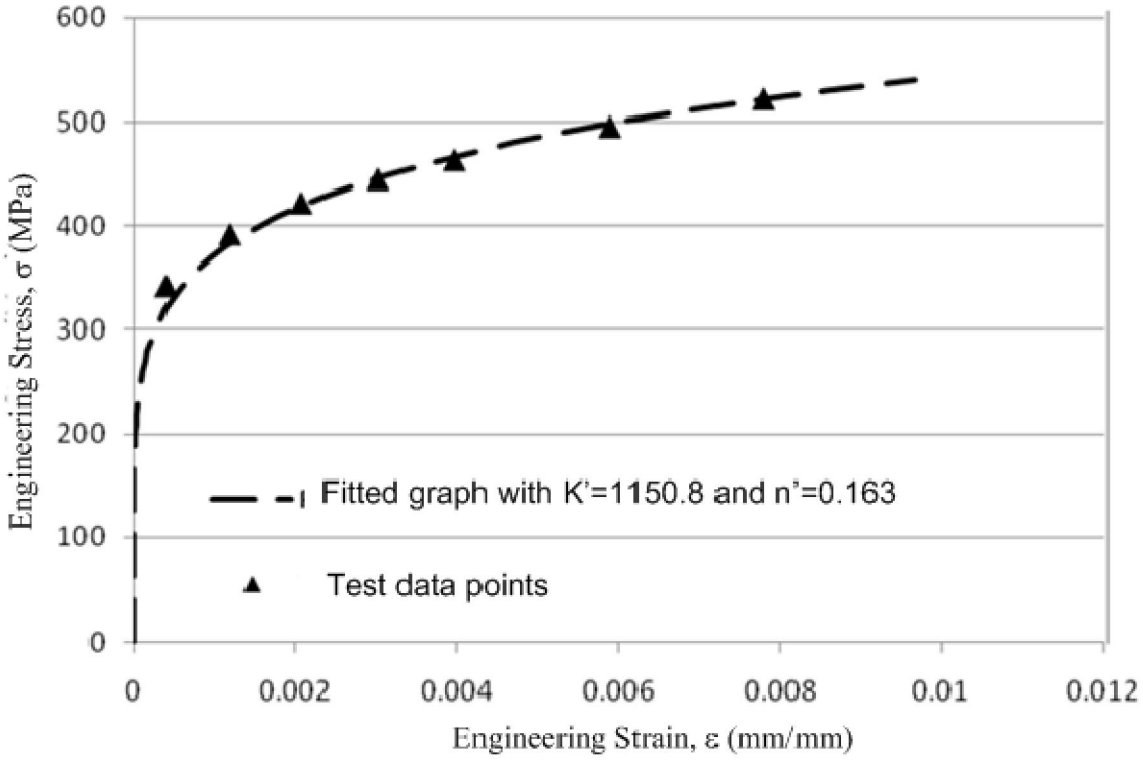

Figure 4.11: Cyclic stress – strain curve for Specimen C1 (350W steel)

Table 4.2: Cyclic material properties base on steel cyclic tests

Specimen	Cyclic Hardening Coefficient, *K'*	Cyclic Hardening Exponent, *n'*
C1	1150.8	0.163
C2	1156.9	0.166
Mean	1153.8	0.165

4.4 Crack growth measurements

Fig. 4.12 shows three stained specimens, two as-welded (one CA tested and one VA tested) and one normally peened (CA tested). As the ink marking suggests and based on other observations, the cracks tended to propagate linearly in the as-welded specimens at the visible crack depths (i.e. > 1.0 mm), while curved cracks were mostly observed in the peened specimens.

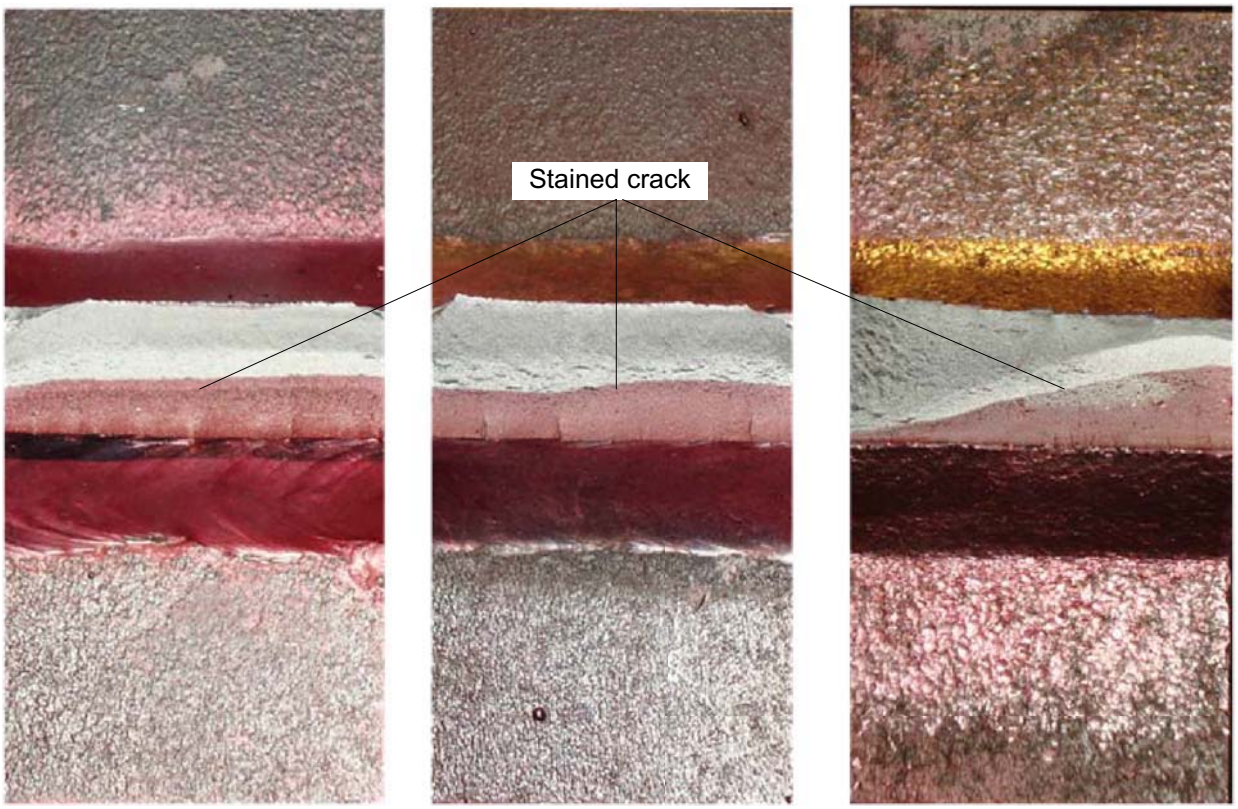

Figure 4.12: Fractured surfaces of stained specimens; as-welded CA (right), as-welded VA (middle), normally peened CA (right)

Figure 4.13 shows two fractured specimens fatigue tested under crack front marking (CA-M) loading. The beach-marks are indicated in the picture and similar to the ink marking results, the crack fronts are linear for untreated specimen and curved for peened ones. Beach-marks are thicker and more visible in the peened specimens than in the as-welded one. The fact that a special loading condition (change in the stress amplitude) being applied for a larger number of load cycles for the treated case (100,000 load cycles) than for the as-welded case (10,000 load cycles) and consequently, the crack propagation having more opportunity to form distinct crack fronts in the S-E32 specimen.

The peening induced-compressive residual stresses present at the weld toe surface appear to make it easier for the already initiated surface cracks to grow vertically in depth rather than horizontally in width. This might explain the linear crack propagation in the as-welded specimens and the curved crack propagation in the treated specimens, apparent in both the ink marking and crack front marking results.

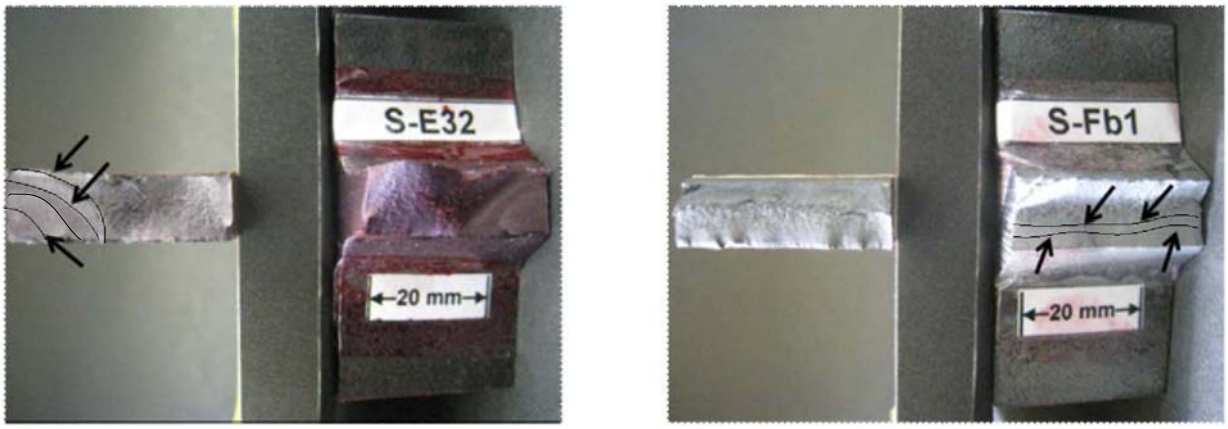

Figure 4.13: Fractured surfaces of two CA-M fatigue loaded specimens, normally peened (right) and as-welded (left)

ACPD crack growth measurements were obtained for six test series:

- untreated, normally treated, and treated under load for fatigue tests under CA loading with R = 0.1 and ΔS_{app} = 270 MPa,
- untreated specimens under both VA1 and VA2 loadings,
- a peened specimen under VA2 loading (the only failed specimen in that category).

Sample results for each case are shown in Figures 4.14 to 4.19. In these figures 'Pt. 1' and 'Pt. 2' refer to the depth readings for the two measurement sites on the weld toe that eventually cracked.

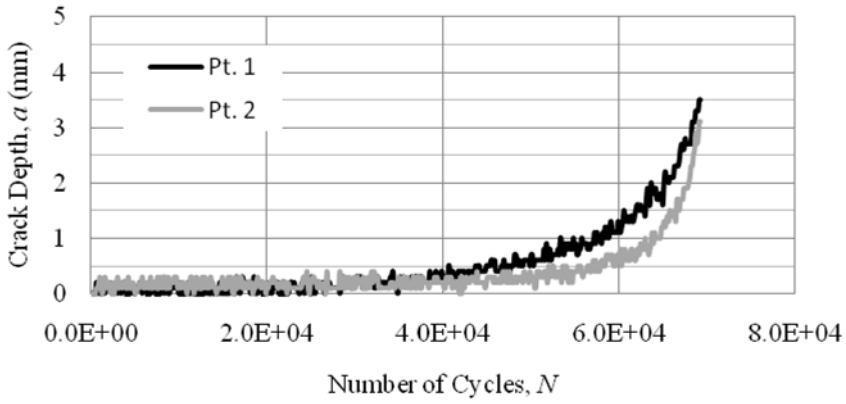

Figure 4.14: Crack depth measurements for as-welded specimen under CA loading

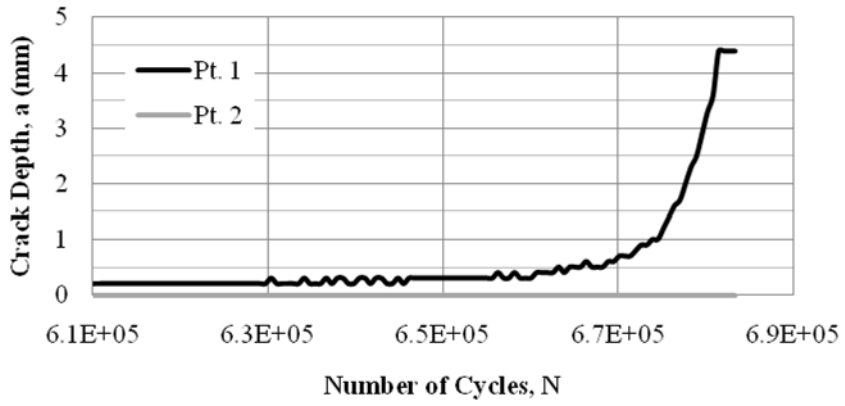

Figure 4.15: Crack depth measurements for normally peened specimen under CA loading

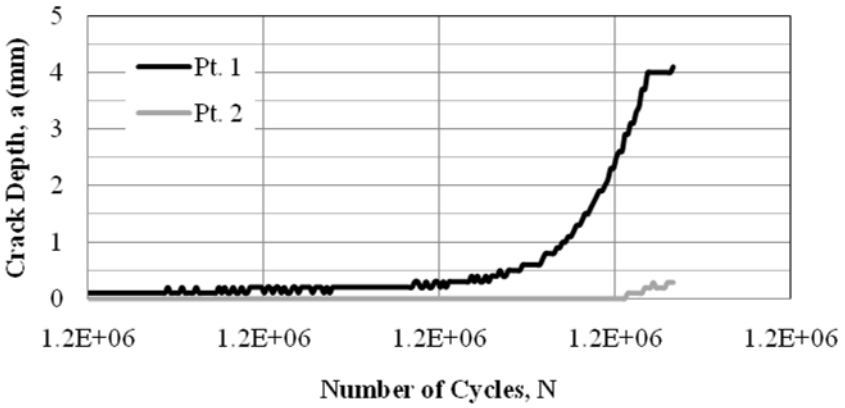

Figure 4.16: Crack depth measurements for peened under 15% prestresss specimen under CA loading

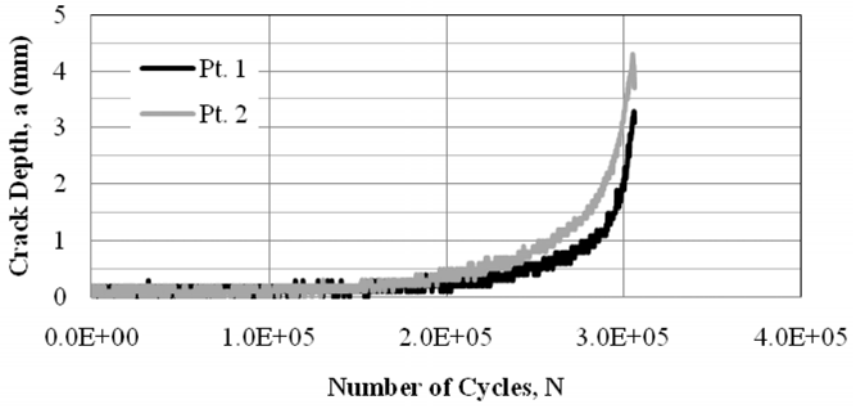

Figure 4.17: Crack depth measurements for as-welded specimen under VA-1 loading

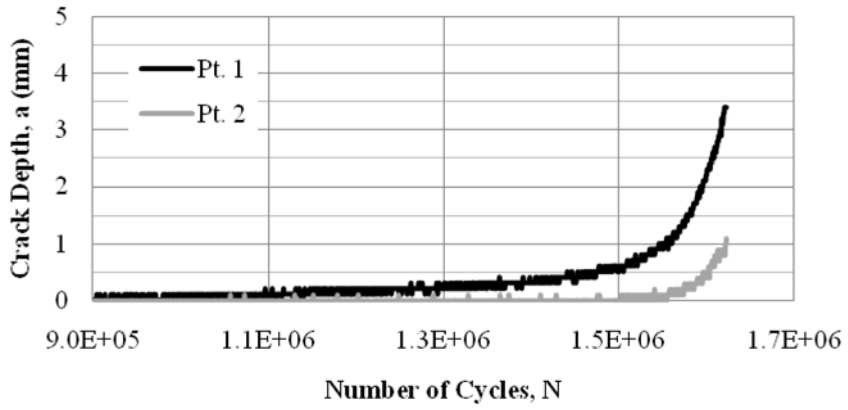

Figure 4.18: Crack depth measurements for as-welded specimen under VA-2 loading

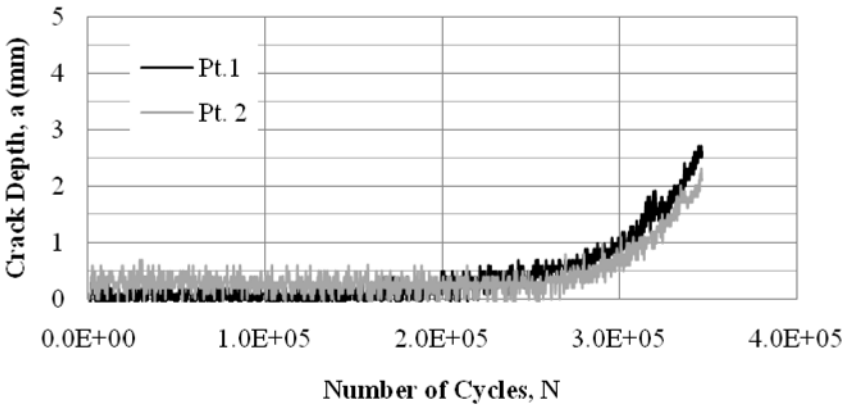

Figure 4.19: Crack depth measurements for normally peened specimen under CA loading

By comparing these figures, the following conclusions can be made:

- Cracks propagated at slower rates in the treated under load specimen than in the normally peened and as-welded specimens. This shows the effect of peening on retarding crack growth. However, this was the case only for crack depths smaller than ~ 0.5-1.0 mm.
- Similar behaviour is observed for crack depths larger than 0.5-1.0 mm, regardless of the treatment type they received (see Figure 4.20).

This implies that the needle peening treatment is effective in slowing the growth of small cracks up to roughly 0.5-1.0 mm.

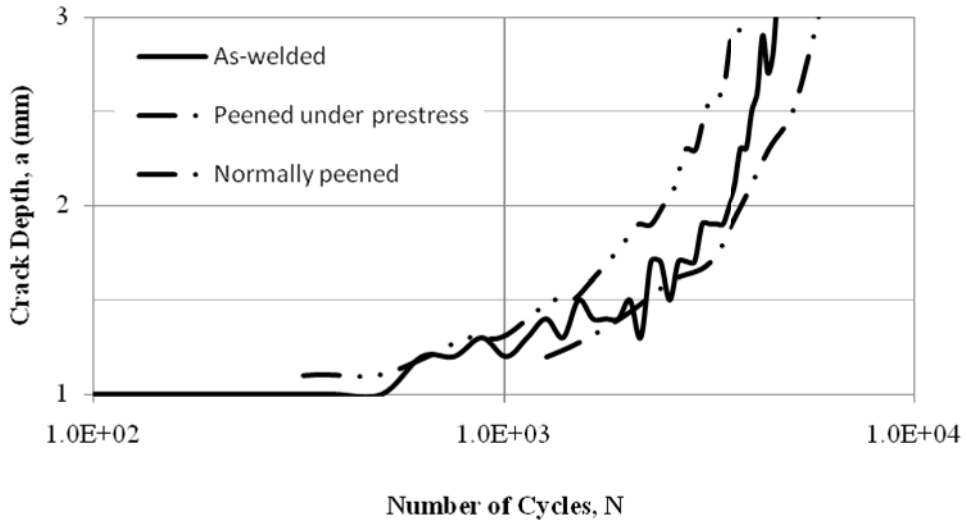

Figure 4.20: ACPD crack growth measurement results, CA loading at ΔS = 270 MPa, for a > 1.0mm

To evaluate the device accuracy, dye penetrant staining was used upon crack detection in three specimens and the actual crack depths (measured with calipers) were compared with the ACPD readings after complete specimen fracture. Two additional fatigue tests employing the crack front marking technique were also conducted to provide a second means of validating the ACPD device. In both cases, the ACPD measurements were found to give accurate predictions of the actual crack depth, especially for cracks with small aspect ratios.

Table 4.3 compares the results obtained using different methods. The vertical lines on the figure show the locations of the probe needles attached on the specimens. This comparison was made for three specimens; an as-welded specimen (S-Fm1) and a normally peened specimen (S-E32) under CA-M loading and a peened under load specimen (S-G14) tested under CA loading.

4.5 Microhardness measurements and microstructure

Although peening has been shown to improve the fatigue performance of welds primarily by introducing beneficial compressive residual stresses, which cause cracks to grow at a slower rate during the early stages of crack propagation, depending on the peening method, secondary treatment effects such as modification of the weld toe geometry and near-surface hardness may also have an influence on fatigue behaviour. Herein, the effect of peening on the near-surface hardness of the fatigue specimens was investigated by conducting microhardness tests on the base metal and heat affected Zone (HAZ) of the untreated (AW) and needle peened (NP) welds.

Table 4.3: Crack depth measurement comparison

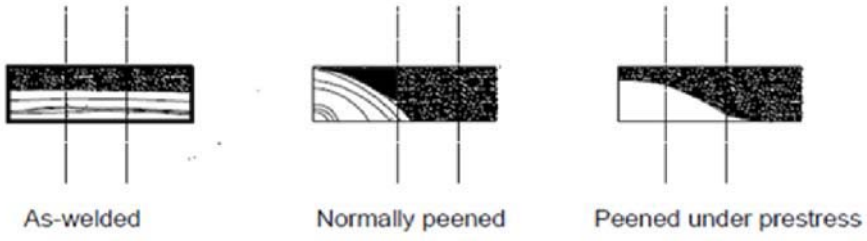

		Pt.1	Pt.2		Pt.1	Pt.2		Pt.1	Pt.2
Specimen	**S-Fm1**			**S-E32**			**S-G14**		
N(cycles)	63,352			2,643,354			577,421		
ACPD(mm)	1.4	0.4		0.6	0		5.8	1.3	
CALIPER(mm)	1.67	0.55		0.68	0		6.05	1.3	
N(cycles)	67,672			2,648,250					
ACPD(mm)	2.1	1.1		2.5	0				
CALIPER(mm)	2.34	1.28		2.68	0				
N(cycles)	67,975								
ACPD(mm)	2.4	1.2							
CALIPER(mm)	2.63	1.37							
N(cycles)	71,814								
ACPD(mm)	3.8	3.8							
CALIPER(mm)	4.04	3.95							

As discussed in Chapter 3, indentations were made at a depth of ~0.1 mm below the surface and then every 0.2 mm up to ~2 mm in depth and were repeated three times for the HAZ of the untreated and treated welds. Average HV values for each depth then calculated. Based on the measured indentation dimensions, the Vickers hardness (HV) was calculated for each depth. The results are presented in Figure 4.20.

As Figure 4.21 shows, needle peening resulted in a considerable increase in the near-surface hardness. However, the hardness decreases rapidly below the surface, to that of the as-welded HAZ at a depth of ~0.6 mm. Similar general trends are reported in [Branco et al. 2002] and [Ummenfofer et al. 2006b] for welds treated by hammer peening and UIT.

Moreover, these results can be used to estimate values for a number of cyclic material parameters for as-welded and peened HAZ material.

Figure 4.21 shows an image of the near surface microstructure of a needle peened weld. The compressed region near the surface is apparent in this figure. Two indentations are also clear in this picture and, under close inspection; the top indentation is noticeably smaller than the bottom one, indicating the higher HV number near the surface due to peening.

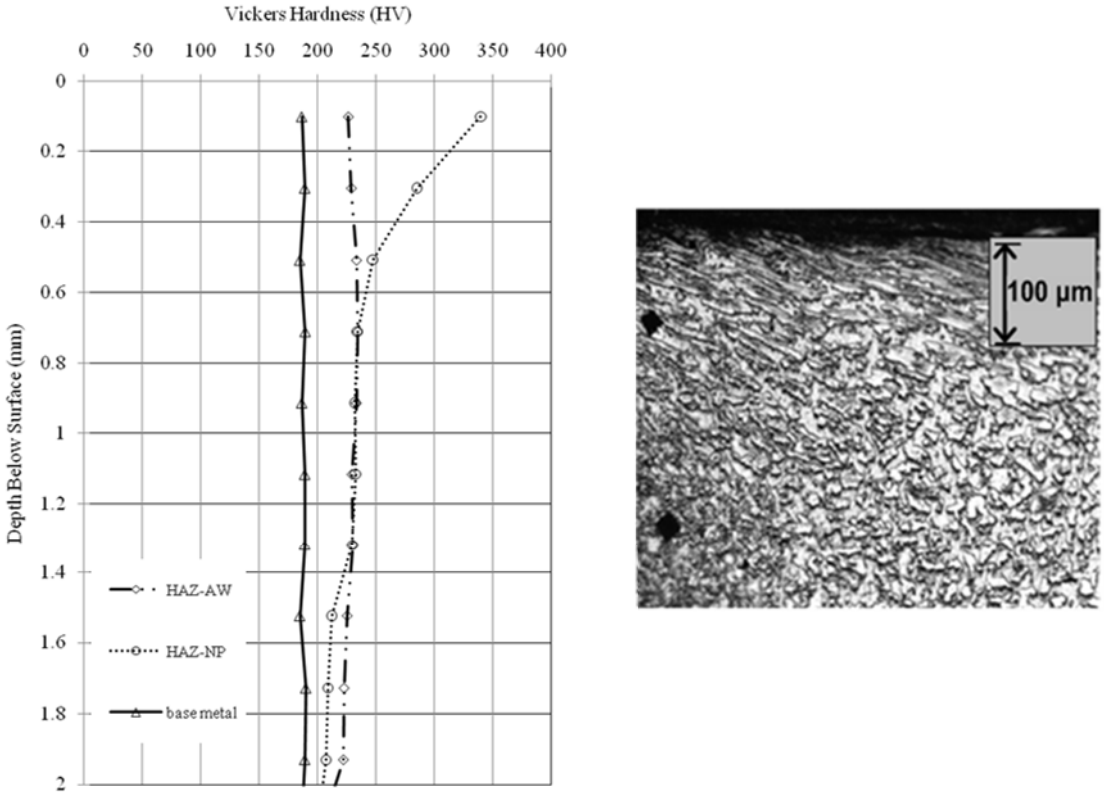

Figure 4.21: Microhardness measurements (left) and microstructure of needle peened weld (right)

A roughly similar depth affected by needle peening, ~0.2 mm, in hardness measurements also can be deduced by examining the microstructure of the peened weld in Figure 4.21. This conclusion correlates well with the fact that similar behaviour was observed for crack depths larger than 0.5-1.0 mm.

4.6 Weld toe geometry

Figure 4.22 illustrates how weld toe angle and radii were defined and measured. Distributions of the measured weld toe angles and radii are summarized in Figure 4.23 and statistical data are presented in Table 4.4. Based on presented data, the following conclusions are made:

- The Measured weld toe angles for the untreated specimens are generally slightly smaller than those for peened specimens.
- Though the measured weld toe angles are more scattered for the peened specimens than for as-welded specimens, no significant systematic difference is observed.

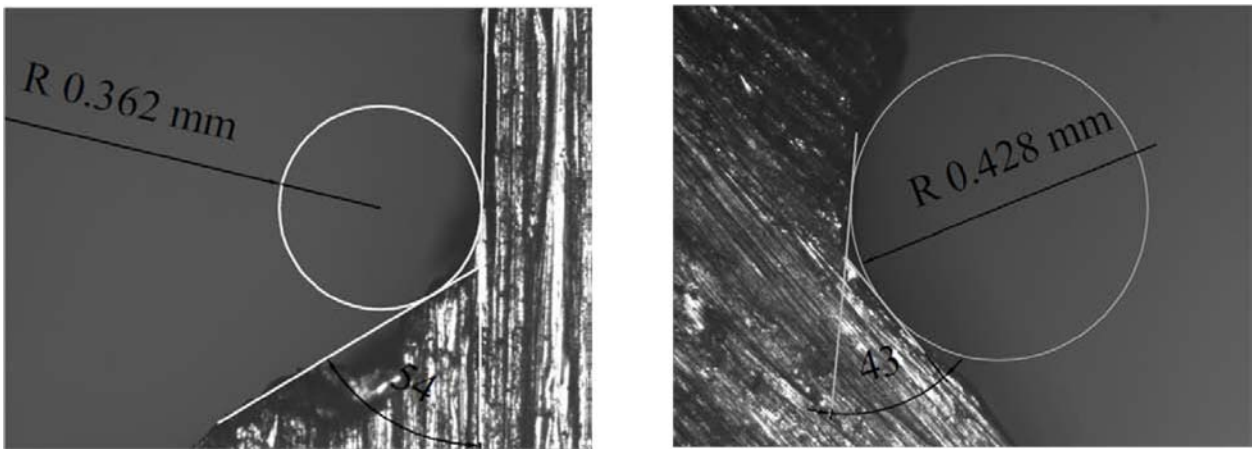

Figure 4.22: Measuring weld toe angle and radius for as-welded (left) and peened (right) specimen

Table 4.4: Statistical data of the weld toe geometry measurements

		No. of measurements	Minimum value	Maximum value	Mean value	VAR	S	COV
Weld toe angle (°)	As-welded	35	26	56	39.76	47.64	6.9	0.17
	Normally peened	29	14	50	29.00	91.53	9.5	0.33
Weld toe radius (mm)	As-welded	31	1.21	0.21	0.65	0.09	0.3	0.47
	Normally peened	21	2.09	0.17	0.68	0.16	0.4	0.59

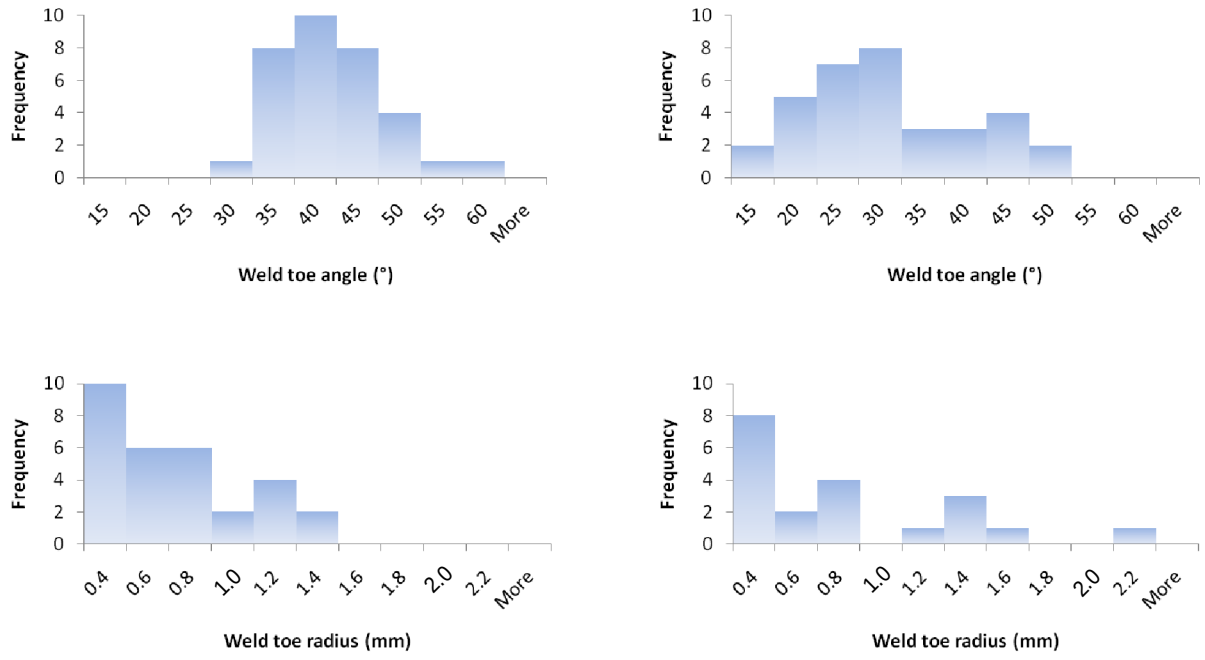

Figure 4.23: Distributions of weld toe angles and radii for as-welded (top and bottom left) and needle peened (top and bottom right) specimens

In summary, peening resulted in a slight flattening the weld toe by around 10 degrees, leaves the weld toe radius more or less unchanged.

By carefully examining the pictures used for measuring the weld toe geometry, a number of typical weld toe defects were also detected. Figure 4.24 shows samples of these "initial defects" that were generally smaller than ~ 0.08 mm.

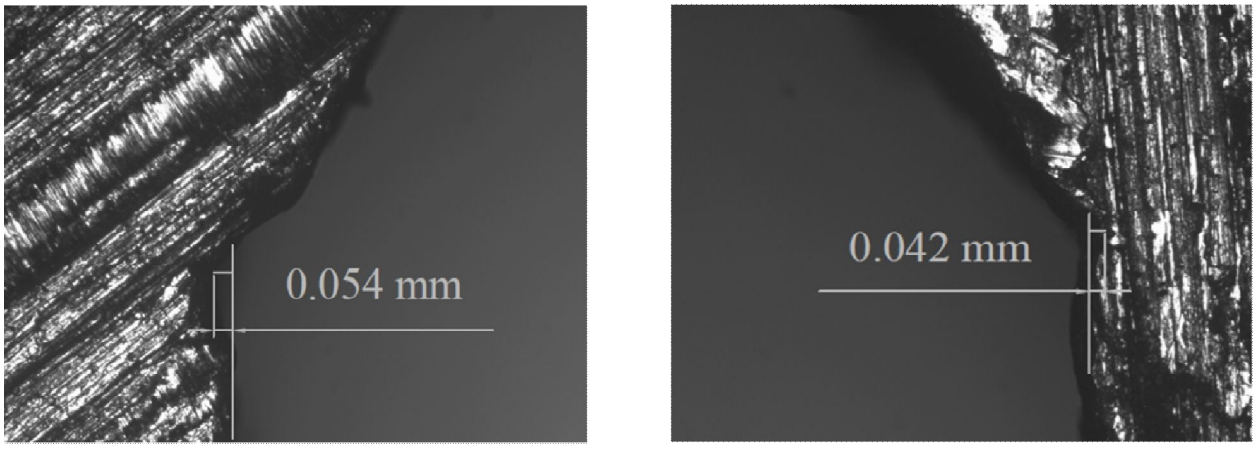

Figure 4.24: Defects present at the weld toe (untested specimens)

Cracked weld toes were also examined. Figure 4.25 shows pictures of two cracked specimens. On the left, arrows show small cracks initiated at the weld toe and on the right, a large crack, possibly formed by the connection of small cracks can be seen.

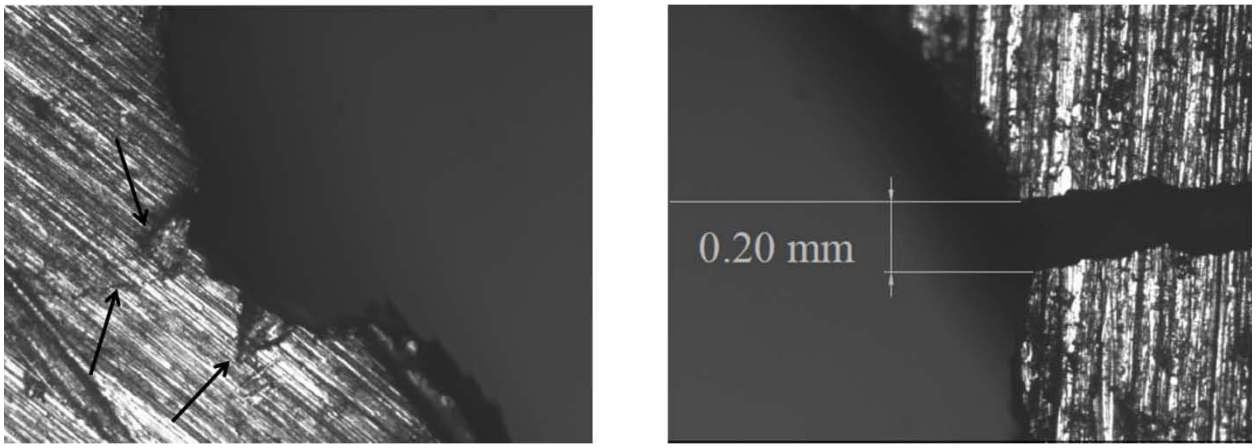

Figure 4.25: Cracks initiated and propagated at the weld toe (cracked specimens)

4.7 Crack profiles

As previously noted, generally two types of crack were observed, linear cracks in the untreated specimens and curved cracks in the peened ones. Figure 2.26 shows how crack profiles were measured for the cracked surfaces. For the linear cracks, crack depths were measured at three different points (left end, maximum depth, and right end) and are summarized in Table 2.5. For the curved cracks, the deepest point, a, and crack width, c, were measured for the final crack. Using these two measured values, the crack front ratio, *a/c*, was calculated. The results are presented in Table 4.6.

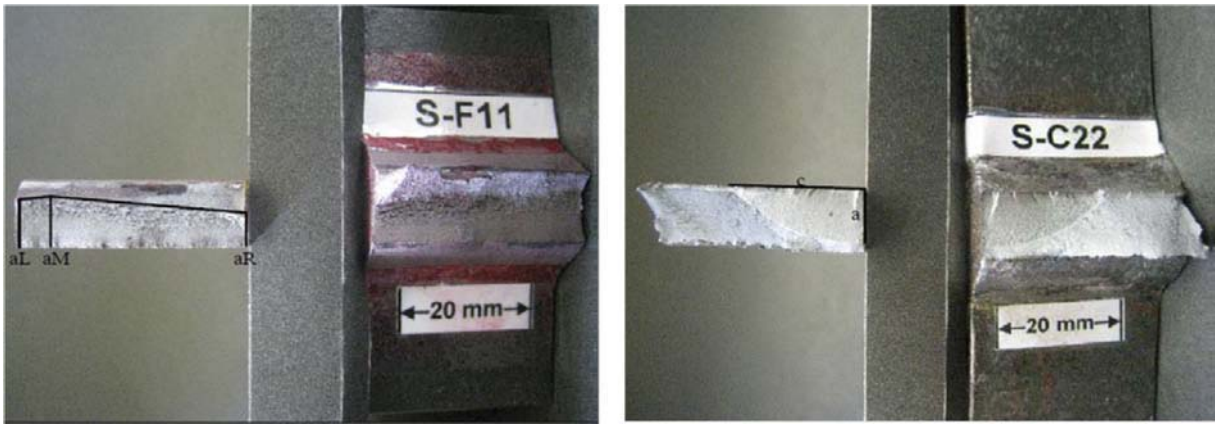

Figure 4.26: Crack profile parameters, linear crack (left) and curved crack (right)

Table 4.5: Crack depth measurements for linear cracks

Specimen	Peened/ As Welded	Crack depth (mm)		
		aL	*aM*	*aR*
S-C11	AW	3.78	5.45	4.51
S-C21	AW	6.11	6.11	4.44
S-B21	AW	4.58	6.11	4.58
S-B22	P	4.87	5.53	4.00
S-A21	AW	4.29	5.82	5.02
S-B11	AW	5.38	5.96	4.44
S-A31	AW	5.82	5.82	2.91
S-E31	AW	4.87	5.89	4.87
S-F11	AW	6.40	6.40	3.49
S-Fb1	AW	4.44	6.11	4.36

Table 4.6: Crack front ratio measured for curved cracks

Specimen	Peened/As Welded	*a*	*c*	Note	*a/c* ratio
S-E32	P	9.24	16.00		0.58
S-G14	P	8.22	21.82		0.38
S-C22	P	6.85	15.27		0.44
S-C12	P	7.71	16.00		0.48
S-A22	P	7.13	21.82		0.32
S-B12	P	5.96	30.55	2*c*	0.40
S-A12	P	6.91	29.09	2*c*	0.48
S-A13	P	7.78	21.91		0.36

As noted earlier, the deepest point was always on the side surface for the curved cracks, therefore, the small specimens size can be a source of error in the test results. Crack front ratios were measured based on final crack shapes and were all close to 0.40. To obtain a better understanding of the crack front ratio value during fatigue testing, beach-marks in the fractured surface for the specimen tested under the crack front marking loading scheme, were used to calculate *a/c* at different stages. Results are presented in Figure 4.27.

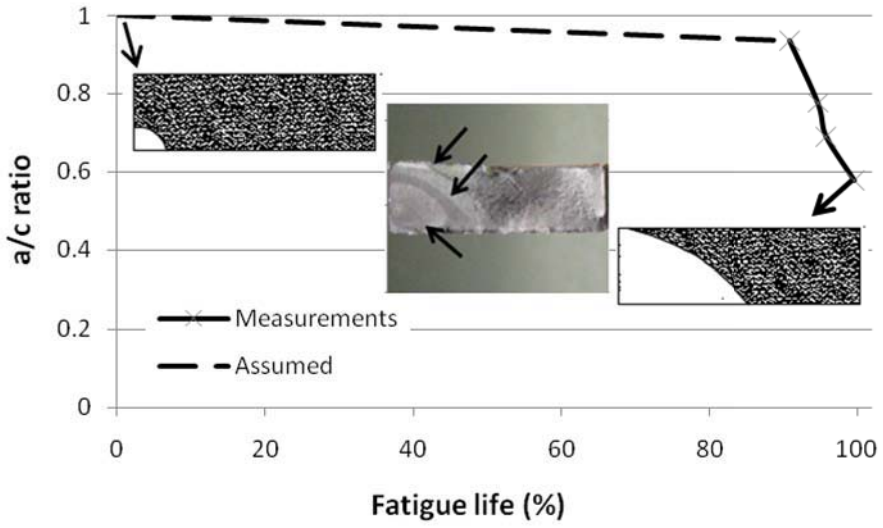

Figure 4.27: a/c ratio in different test stages for a crack front marked specimen

As the graph suggests, cracks propagated with a nearly circular profile, *a/c* ratio close to 1, at the early stages and through testing, and especially during the last 10% of its fatigue life, that ratio decreased and an elliptical crack was formed. Eventually, like the other peened specimens, the aspect ratio was around 0.40 at the time of failure.

4.8 Residual stress measurements

Measured residual stresses for three specimen with different loading and treatment conditions types are summarized in Table 4.7 and Figure 4.28.

- The measurements showthat there is an approximately uniformly distributed tensile residual stress with the magnitude of 15~20 % of yield stress present near the surface of the untreated specimen. This tensile residual stress can be referred to as the "welding residual stress".
- Needle peening the specimen resulted in a significant change in the residual stress distribution through the specimen thickness with a magnitude as high as -500 MPa (compressive) near the weld toe surface. It then gradually decreases for about a millimeter until reaching an almost uniform tensile residual stress greater than that in the untreated specimen (because of the stress redistribution due to the peening).

- The measured residual stresses for the tested peened-specimen were close to and slightly higher than those for untested peened-specimen. This implies that residual stress relaxation was negligible during testing. The fact that needle peening was performed by two different operators for the tested and untested (tested specimen treated by Walker) specimens might be an explanation for higher residual stress measured at the surface of the tested specimen.

Table 4.7: Residual stress measurements

	Location 1		Location 2	
	Depth (mm)	**Residual stress (MPa)**	**Depth (mm)**	**Residual stress (MPa)**
As-welded	0.00	+28 ± 7	0.00	+34 ± 7
	0.10	+34 ± 7	0.10	+55 ± 14
	0.21	+48 ± 7	0.21	+103 ± 7
	0.50	+55 ± 14	0.49	+90 ± 7
	0.99	+21 ± 7	1.05	+55 ± 7
	1.49	+48 ± 14	1.51	+55 ± 14
	1.75	+34 ± 7	1.75	+55 ± 14
Normally Peened	0.00	-200 ± 7	0.00	-269 ± 14
	0.09	-421 ± 7	0.10	-400 ± 14
	0.20	-317 ± 7	0.20	-317 ± 7
	0.49	-296 ± 7	0.51	-255 ± 7
	1.00	+62 ± 7	1.01	+165 ± 14
	1.51	+138 ± 14	1.49	+76 ± 7
	1.80	+165 ± 7	1.89	+221 ± 7
Normally Peened (CA-UL tested)	0.00	-276 ± 14	0.00	-228 ± 14
	0.13	-448 ± 7	0.11	-496 ± 14
	0.19	-448 ± 7	0.21	-490 ± 7
	0.51	-269 ± 14	0.51	-407 ± 14
	1.10	+28 ± 14	0.98	-28 ± 14
	1.55	+172 ± 14	1.49	+255 ± 14
	1.79	+186 ± 7	1.75	+262 ± 7

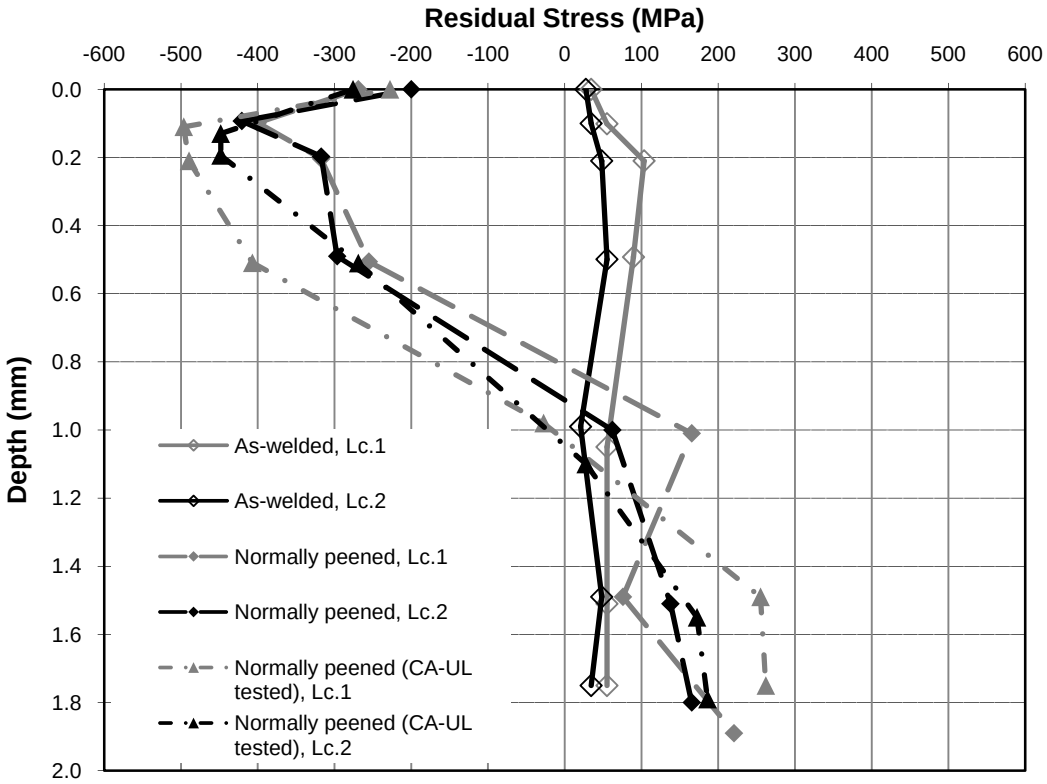

Figure 4.28: Residual stress profiles

Chapter 5

Fracture Mechanics Analysis

5.1 Introduction

In this Chapter, a previously developed strain-based fracture mechanics (SBFM) model [Lam and Topper 1998, Khalil and Topper 2003, and Walbridge 2008] is used to analyze the fatigue specimens. The model's ability to predict the fatigue performance under different loading and treatment conditions is evaluated by comparing the predicted results with the test results.

The SBFM model is first described in Section 5.2 and its input parameters are explained in Section 5.3. The model predictions of fatigue crack growth are then compared with the ACPD-derived crack growth measurements in section 5.4. Section 5.5 compares the test results with the model fatigue life predictions for different CA and VA loading and conditions. Finally, model predictions of the effectiveness of needle peening treatment applied under load are presented in section 5.6.

5.2 Description of strain-based fracture mechanics model

The model employed herein is basically a linear elastic fracture mechanics (LEFM) that is modified to consider non-linear material effects. By applying the Paris-Erdogan crack growth law, modified to account for crack closure effects and a threshold stress intensity factor (SIF) range, the number of cycles to failure, N, is calculated by numerically integrating the following expression over a crack depth range, a_i (initial crack depth) to a_c (critical crack depth).

$$N = \int_{a_i}^{a_c} \frac{da}{C \cdot MAX(\Delta K_{eff}^m - \Delta K_{th}^m, 0)} \qquad (5.1)$$

where a is crack depth, C and m are the Paris constants, and ΔK_{eff} and ΔK_{th} are the effective and threshold stress intensity factor ranges, respectively.

Crack closure effects are considered in calculation of ΔK_{eff} by using the following expression to calculate the effective stress intensity factor range, ΔK_{eff}:

$$\Delta K_{eff} = K_{max} - MAX(K_{op}, K_{min}) \qquad (5.2)$$

where K_{max} and K_{min} represent the SIFs at the maximum and minimum load levels in each load cycle, and K_{op} is the SIF corresponding to the crack opening stress level in that load cycle.

Each SIF is determined using the following expression:

$$K = Y \cdot E \cdot \varepsilon \cdot \sqrt{\pi \cdot a} \qquad (5.3)$$

where Y is a correction factor that accounts for the crack shape, the free surface on one side of the crack, and the finite thickness of the plate, E is the module of elasticity of the material, a represents the (crack) depth below the surface, and ε is the local strain at that depth.

A cyclic Ramberg-Osgood material model is used to determine the stresses and strains for each load cycle:

$$\Delta\varepsilon = \frac{\Delta\sigma}{E} + 2\left(\frac{\Delta\sigma}{2 \cdot K \cdot}\right)^{1/n'} \qquad (5.4)$$

ε and σ are strain and stress, respectively, and K' and n' are material constants.

Neuber's rule is used to calculate strain histories at various depths below the surface of the weld toe. Neuber's rule for monotonic stress-strain curve is as follows:

$$\varepsilon\sigma = \frac{(kS)^2}{E} \qquad (5.5)$$

where k is the theoretical stress concentration factor and S is the nominal applied stress.

For cyclic loading, instead of stress and strain values (ε, σ and S), stress and strain ranges are used ($\Delta\varepsilon$, $\Delta\sigma$ and ΔS):

$$\Delta\varepsilon\,\Delta\sigma = \frac{(k\Delta S)^2}{E} \qquad (5.6)$$

Formulas proposed in (Newman 1984) are used to model crack closure:

$$S_o/S_{max} = A_0 + A_1R + A_2R^2 + A_3R^3 \qquad for\ R \geq 0 \qquad (5.7)$$

$$S_o/S_{max} = A_0 + A_1 R \qquad for\ -1 \le R < 0 \qquad (5.8)$$

where R is the stress ratio, and S_{max} is the maximum local stress level, and S_o is the crack opening stress, when $S_o > S_{min}$.

The coefficients are:

$$A_0 = (0.825 - 0.34\alpha + 0.05\alpha^2) \cdot [\cos(\pi\ S_{max}/2\sigma_0]^{i/\alpha} \qquad (5.9)$$

$$A_1 = (0.415 - 0.071\alpha) \cdot S_{max}/\sigma_0 \qquad (5.10)$$

$$A_2 = 1 - A_0 - A_1 - A_3 \qquad (5.11)$$

$$A_3 = 2A_0 + A_1 - 1 \qquad (5.12)$$

σ_0 is the flow stress (usually taken as the average of the yield and ultimate strength) and α is the plastic constraint factor. Herein, α is calculated using a formula proposed in [Wang et al. 2002].

$$\alpha = 1.78 - 0.628\ (\sigma_{max}/\sigma_Y) \qquad (5.13)$$

Based on [McClung 1994], the σ_{max}/σ_0 ratio is multiplied by Y, the correction factor in the crack closure equation (5.6). the Newman formula is also modified slightly by imposing an upper limit so that the $Y \cdot \sigma_{max}/\sigma_0$ ratio cannot exceed 1.0.

Along with the described crack closure model, a model proposed in [Khalil and Topper 2003] is used for the crack opening stress evolution following overload events under VA loading.

$$\sigma_{op} = \sigma_{cu} + \mu \cdot (\sigma_{ss} - \sigma_{cu}) \qquad (5.14)$$

where σ_{cu} is the crack opening stress before the current load cycle, σ_{ss} is the crack opening stress if the crack was cycled under CA loading at the current stress range, and μ is a material constant. For SAE 1045 steel $\mu = 0.002$ is recommended [Khalil and Topper, 2003].

During the analysis, the material is cyclically loaded at various depths below the surface of the weld toe and strain parameters are determined for each load cycle. The local elastic stress (σ_{el}) is calculated by adding up the local elastic residual stress ($\sigma_{el,res}$) due to welding (and peening in the case of peened specimens) and local elastic stress due to the applied load ($\sigma_{el,app}$).

Using the approach described in [Dabayeh et al. 1998], a stress concentration factor, k_p, that considers the presence of the crack in the weld toe, is used to determine the local elastic stresses. To calculate k_p, the following expression is used:

$$k_p = k_{el} \cdot \frac{K_{el}}{Y \cdot \sqrt{\pi \cdot a}} \qquad (5.15)$$

where k_p is the modified stress concentration factor (SCF), k_{el} is the SCF for the uncracked weld toe, and K_{el} is the elastic stress intensity factor that considers the non-uniform stress distribution along the crack path.

Elastic weight functions, m(x, a, a/c, a/t), from [Shen and Glinka 1991] for semi-elliptic cracks in finite thickness plate, are used to calculate K_{el}:

$$m(x, a, a/c, a/t) = \frac{2}{\sqrt{2\pi(a-x)}} \left[1 + M_{1A}\left(1-\frac{x}{a}\right)^{1/2} + M_{2A}\left(1-\frac{x}{a}\right) + M_{3A}\left(1-\frac{x}{a}\right)^{3/2} \right] \qquad (5.16)$$

where a is the crack depth, t is the thickness of the plate, c is half of the width of the semi-elliptical surface crack, and M_{1A}, M_{2A}, and M_{3A} are model parameters.

Using (5.16), K_{el} can be determined by following expression:

$$K_{el} = \int_0^a k_{el}(x).m(x,a,c) \cdot dx \qquad (5.17)$$

where x is the depth below the surface of the plate.

Now, by using (5.15), the local elastic stress (σ_{el}) corresponding with S can be calculated as follows:

$$\sigma_{el} = k_p \cdot S \qquad (5.18)$$

Stress-strain hysteresis loops are generated by calculating the local nonlinear stress-train history for the given nominal stress history. Each time a hysteresis loop is closed, σ_{max}, ε_{max}, σ_{min}, ε_{min}, σ_{op}, and ε_{op} are calculated. Using these parameters, ΔK_{eff} and da/dN are then determined. Finally, the fatigue life is calculated by numerical integration of Eq. 5.1.

The model requires the residual stress distributions for the fatigue detail due to both welding and the applied post-weld treatment method. As a simplification, the residual stress is introduced by

shifting the stress monotonically from zero to the specified residual stress level. In this way, the effect of any strain hardening due to peening is conservatively ignored.

5.3 Input parameters

Where applicable, laboratory test results were used to determine model input parameters. For those parameters without experiment-based measurements, proper values were assumed and then justified. Table 1 summarizes the assumed values for the various input parameters.

Table 5.1: Assumed values for model input parameters

Input parameter	Assigned Value	Units	Source
T	*9.5*	*mm*	nominal
θ_w	*45*	°	
ρ_w	*0.5*	*mm*	
E	*201.6*	*GPa*	
σ_y	*405.4*	*MPa*	
σ_u	*574.0*	*MPa*	
n'	*0.165*	-	
K'	*1153.8*	*MPa*	
C	$2.8 \cdot 10^{-13}$	*N, mm*	
m	*3*	-	[Walbridge 2008]
ΔK_{th}	*80*	$MPa \cdot \sqrt{mm}$	[Walbridge 2008]
μ	*0.002*	-	[Khalil and Topper 2003]
a_i	*0.15*	*mm*	[Walbridge 2008]
a_c	*T/2*	*mm*	[Walbridge 2008]

- Note: source of parameter value is the current study, unless noted otherwise.

The elastic modulus (E), yield stress (σ_y), ultimate strength (σ_u), Ramberg-Osgood material constants (K' and n'), weld toe radius (ρ_w) and angle (θ_w), are determined based on the test results presented in Chapter 4. The average base metal values are used for the material

parameters. For the weld toe geometry parameters (weld toe angle and weld toe radius), values slightly greater than the mean measured values are used (45° and 0.5 mm, respectively).

In order to determine $k_{el,app}$, two approaches were considered. In [Walbridge 2008], parametric equations from [Monahan 1995] for T-butt welds are used to calculate the $k_{el,app}$ distribution. This distribution was also determined by 2D (plain strain) finite element analysis using the ABAQUS 6.7.4 software. To do this, the uncracked specimen geometry was modeled and analysed to locate the peak surface stress. A line of nodes was then placed perpendicular to loading direction passing the location of the peak stress, followed by a new mesh generation and analysis. Results obtained by these two methods were in close agreement to each other, as shown in Figure 5.1. However, the FEA-based results were used in the susequent analytical work.

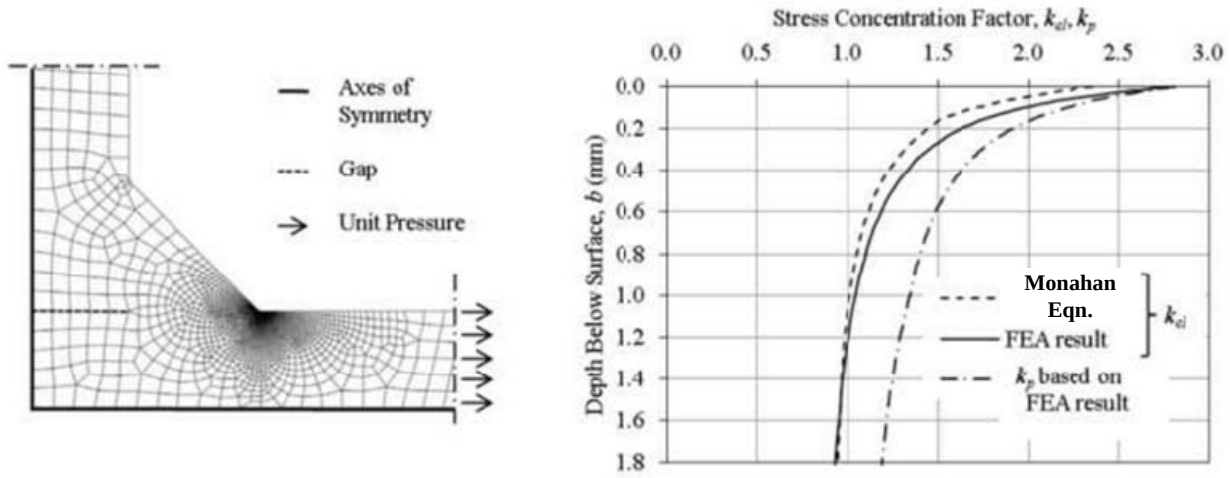

Figure5.1: $k_{el,app}$ distribution determination; FEA model (left),calculated distributions (right)

Herein, the residual stress distributions due to welding and needle peening (in the case of treated specimens) are based on the residual stress measurements reported in Chapter 5. The assumed values, along with the actual measurements, are presented in Figure 5.2.

For the other parameters, following assumptions are made:

- An initial crack depth of a_i = 0.15 mm is assumed. Reasonably close values are also reported in [Radaj, 1990], and [Walbridge 2008].

- Typical large crack values for structural steel are used for the Paris m constant (m = 3) and threshold stress intensity range (ΔK_{eff} = 80 MPa·$\sqrt{mm}$) based on reported value in [Walbridge 2003] and [Lam et al. 1998],
- A critical crack depth (a_c) of T/2 is assumed, and
- A value of 0.002 is assigned for SAE 1045 steel for the μ parameter, based on [Khalil and Topper 2003].

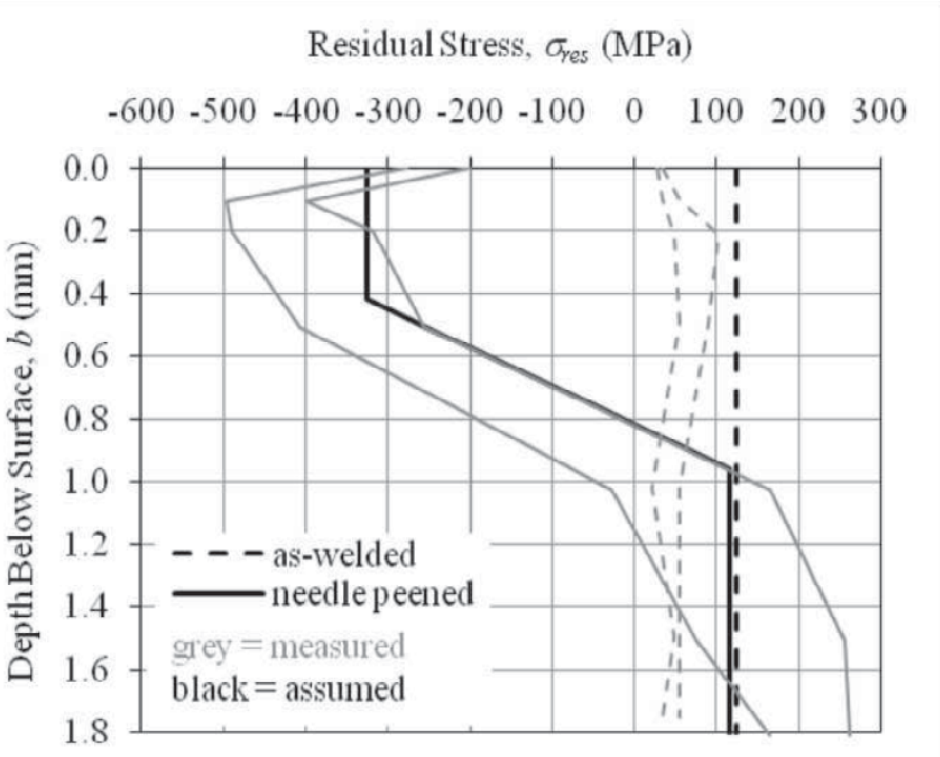

Figure 5.2: Measured and assumed residual stress distributions

In order to determine the crack shape versus depth function and Paris C constant, fatigue test results of an untreated specimen tested under ΔS_{app} = 270 MPa and R = 0.1, were closely examined. An essentially "through crack" was observed for this specimen for a visible crack depth of a = 1.0 mm and beyond. Close fatigue life predictions were obtained by using this assumption, with the aspect ratio varying linearly from $(a/c)_i$ = 0.6 to a/c = 0.0 at a = 1.0 mm. Based on the results presented in Chapter 4, higher a/c ratios were observed for cracks larger than 1 mm deep in peened specimen, however, a conservative assumption was made by not considering this trend in the analysis.

The Paris C constant was then determined by fitting the crack growth curve, predicted by the SBFM model to the ACPD-based one. Close predictions were obtained by choosing a value of $2.8 \cdot 10^{-13}$ (N·mm) for this parameter, as can be seen in Figure 5.3.

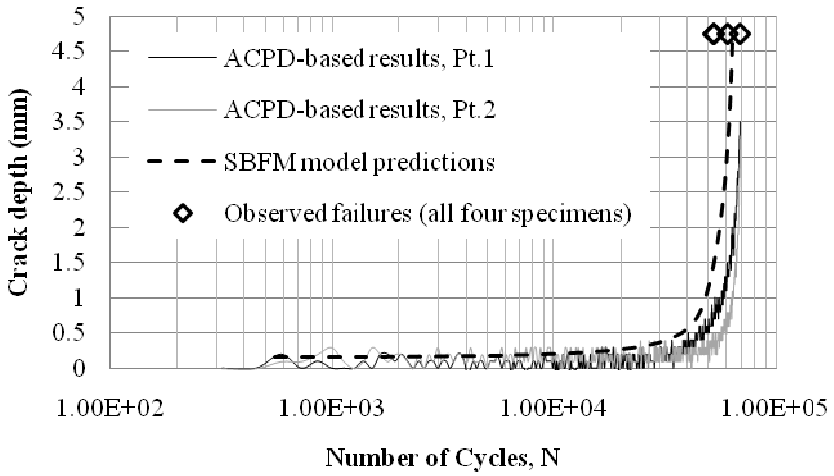

Figure 5.3: Measured and predicted crack growth curves for as-welded specimen, tested under ΔS_{app} = 270 MPa and R = 0.1

5.4 Comparison of model predictions and test results

Model predictions and test results for as-welded specimens tested under CA loading are presented in Figure 5.4. As can be seen in this figure, the model closely predicts the applied stress ratio (R) effects on the fatigue lives of the specimens. In general, the average fatigue lives are also closely predicted for each loading condition

Figure 5.5 shows a comparison of model predictions and test results for the peened specimens tested under CA loading. As can be seen in this figure, at ΔS = 180 MPa, the model is able to predict the finite fatigue lives for the peened specimens at R = 0.4 and runouts for the peened specimens at R = 0.1. Additionally, the mean fatigue lives for all test types are closely predicted. However, the average fatigue lives for the peened specimens tested at R = -1 are underpredicted slightly.

Figure 5.6 presents a similar comparison for the untreated specimen under constant amplitude loading with periodic underloads (CA-UL), and variable amplitude loadings (VA1 and VA2). The model does a good job in predicting the fatigue lives of the specimens in all cases.

Specifically, it correctly predicts the greater fatigue lives of the specimens tested under VA2 compared to those tested under VA1.

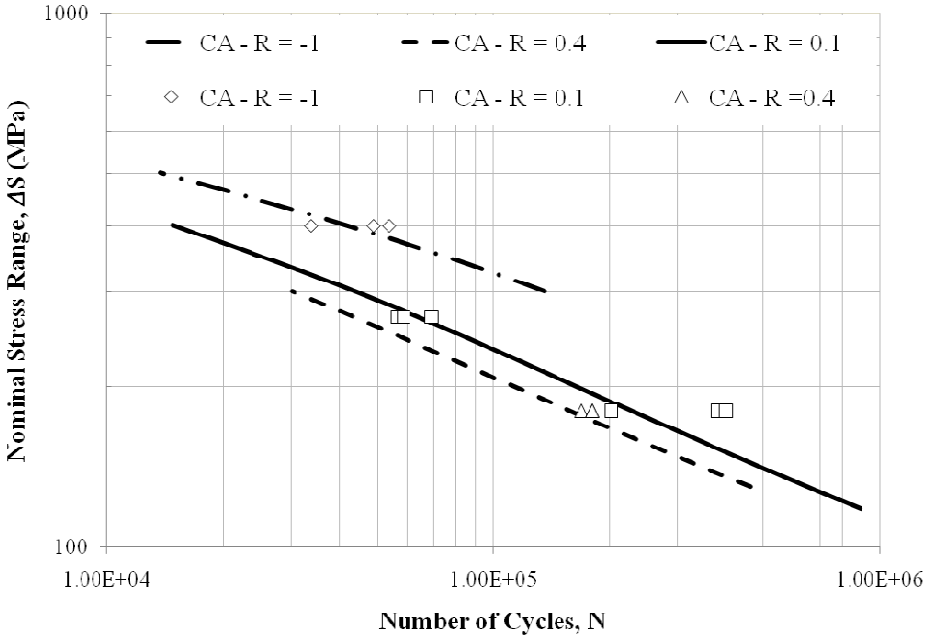

Figure 5.4: SBFM and fatigue tests results for as-welded specimens tested under constant amplitude (CA) loading

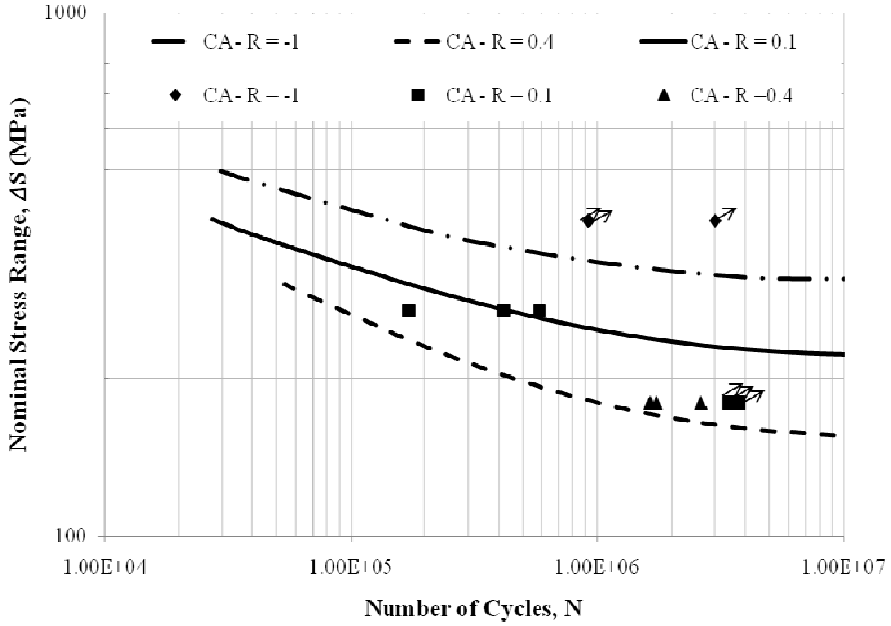

Figure 5.5: SBFM and fatigue tests results for needle peened specimens tested under constant amplitude (CA) loading

In Figure 5.7, the SBFM predictions are compared with the test results for the peened specimens tested under CA-UL and VA loading. The model predictions are in good agreement with the test results. In particular, the model correctly predicts lower fatigue lives under the VA2 loading history than under VA1 loading (i.e. the reverse of the trend observed for the untreated case). The fatigue lives are also closely predicted or conservatively underestimated for the peened welds under CA-UL and VA loading.

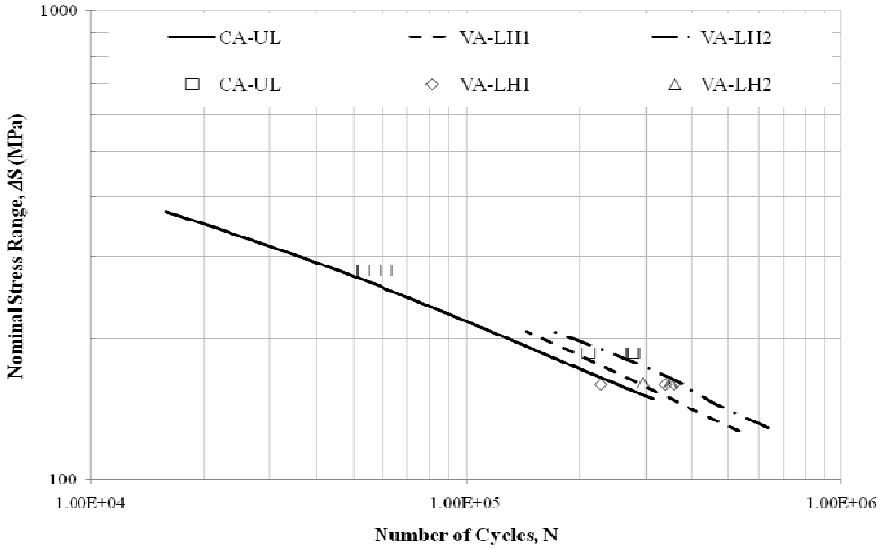

Figure 5.6: SBFM and fatigue tests results for as-welded specimens tested under variable amplitude (VA) loading

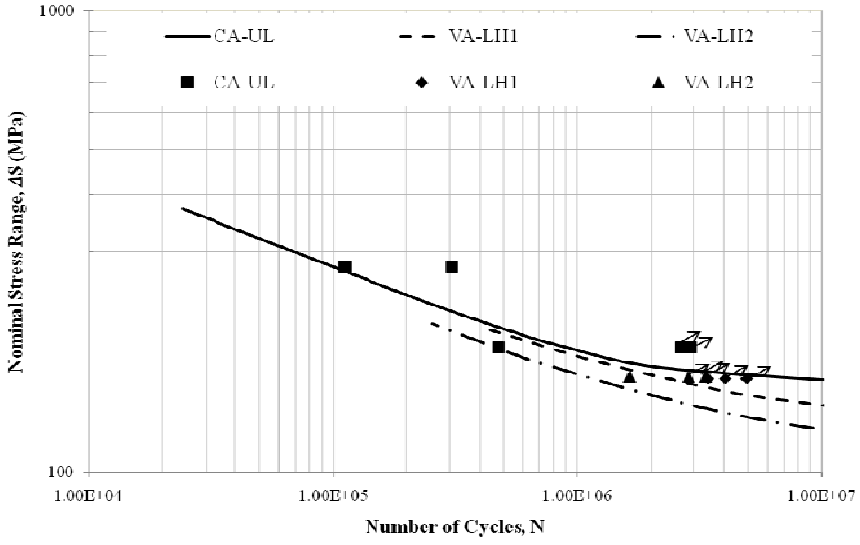

Figure 5.7: SBFM and fatigue tests results for needle peened specimens tested under variable amplitude (VA) loading

5.5 SBFM predictions for peening under load

Model predictions for as-welded, normally peened, and peened under two prestress ratios are summarized in Figure 5.8, along with the peened-under load fatigue test results. For analyzing the specimens treated under load, it is assumed that the effect of prestressing, treating, and then fatigue testing can be modelled by simply adjusting the assumed R-ratio for the analysis. Thus, for example, for a test conducted at $R = 0.1$, prestressing to the mean stress level, treating, and then testing can be modelled by analyzing the specimen under the same stress range, but with the R-ratio shifted to -1.0.

As noted earlier, the SBFM model accurately predicts the average fatigue lives of the untreated and normally peened specimens. It also correctly estimates the additional benefit of peening under load for a 45 MPa prestress. However, for the specimens treated under a 165 MPa prestress, the model predicts an infinite fatigue life under tension only loading at $\Delta S = 270$ MPa, but one specimen in this series failed after almost 1 million load cycles. Further testing is needed, to determine whether or not the single failure observed for the case of peening under a 165 MPa prestress was an anomaly.

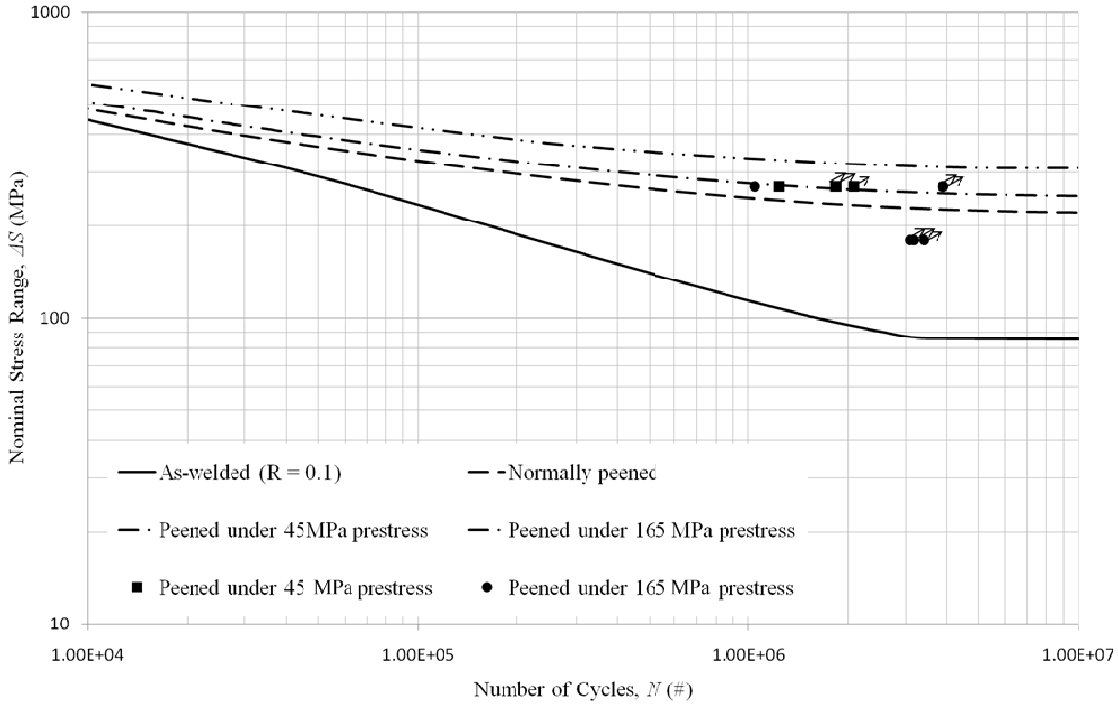

Figure 5.8: Fatigue tests results and SBFM model predictions for specimens peened-under load

The model predicts more than a 100% increase in the CA fatigue limit as a result of normal peening. That number can be increased to more than 200% if peening is applied under high prestress ratios. Also, peening effectiveness is correlated with the applied nominal stress range, and as the applied stress range decreases, the peening becomes more effective.

Figure 5.9 compares the effectiveness of needle peening when applied under different prestress ratios. The fatigue life improvement is calculated using following expression:

$$\%\, imp_N = \frac{N_P - N_{AW}}{N_{AW}} \text{ x } 100\ \% \qquad (5.19)$$

where N_P and N_{AW} are fatigue lives corresponding to the peened and as-welded cases, respectively.

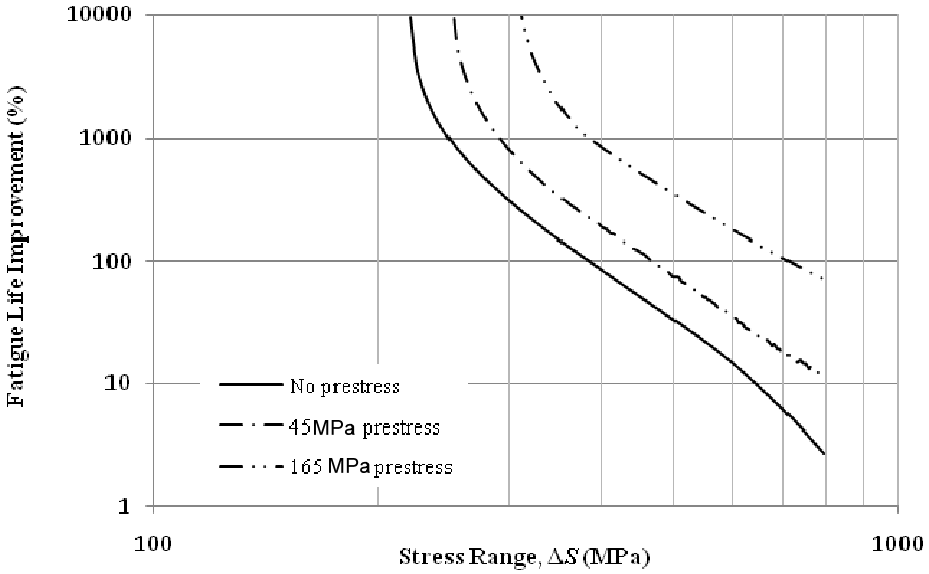

Figure 5.9: Comparison of effectiveness of needle peening applied under prestress

As can be seen, peening is more effective at low stress ranges than at high stress ranges. Moreover, by increasing the amount of prestress, a greater improvement in fatigue life will be achieved.

Chapter 6

Modelling of Fatigue Crack Growth with a Cohesive Zone Model

6.1 Introduction

As explained in Section 2.2, Paris model, [Paris and Erdogan, 1963] and [Paris et al. 1961], is dominantly used to predict fatigue crack growth. Fatigue life predictions are mainly based on Paris equation which correlates the crack growth rate (da/dN) to the stress intensity range (ΔK):

$$da/dN = C \cdot \Delta K^m \qquad \textit{(repeated in 2.6) (6.1)}$$

Paris constants, C and m, account for the characteristics of the applied loading and the specimen geometry. Various models are proposed to accommodate complex conditions that influence the crack growth rate; however, their parameters still depend on properties of the applied loading and/or the environment. As an example, as seen in Section 5.2, the fracture mechanics model is able to consider crack closure only if ΔK is modified to account for threshold stress intensity range. Hence, Paris model and similar approaches based on Equation 2.6 are valid as long as the ideal conditions of linear elastic fracture mechanics (LEFM) are met. These conditions are: small scale yielding, constant amplitude cyclic loading, and long cracks. Otherwise, these formulations lose their predictive capability. Specifically, if they cannot be paired with a plasticity model, they will not be able to model crack retardation. Other approaches are developed recently to address these deficits and one of the novel approaches is the cohesive zone approach. Cohesive fatigue models have widely been implemented as cohesive interface finite elements.

The cohesive zone approach for fracture problem was initiated back in 1960's, when [Dugdale 1960 and Barenblatt 1962] for the first time introduced two models that included a cohesive zone in front of the crack tip. However, those models and most of the models developed after considered monotonic fracture problems only. Cyclic fracture problems of stage II fatigue crack growth were addressed in later studies including [De-Andres et al. 1999, Nguyen et al. 2001, Roe and Siegmund 2003, and Ural and Papoulia 2004]. It has been claimed that cohesive zone models are able to capture the nonlinear behaviour in the process zone when considering the process zone as a zone of zero thickness. Additionally, they can be paired up with a plasticity model in the bulk material and are thus able to predict the fatigue behaviour of materials, even if the small scale yielding assumptions at the crack tip are violated.

The model used herein to simulate fatigue crack growth in the steel specimens, is a damage-based cohesive model proposed in [Ural et al 2009]. The model exhibits a bilinear traction-separation monotonic behaviour (Fig. 6.2). Under cyclic loading, the model shows a nonlinear cyclic behaviour due to damage accumulation within the monotonic cohesive envelope.

In this chapter, the cohesive model is described in section 6.2 and its input parameters are explained in section 6.3. The finite element model used in this study is explained in Section 6.4 and fatigue crack growth predicted by the model is compared with ACPD-based results. Finally, model responses to changes in applied stress range, R ratio, and residual stress fields are investigated in Section 6.5.

6.2 Model description

In the proposed model, traction and displacement are correlated with a degrading linear traction-separation relationship, as follows:

$$T = F(\kappa)\,\delta \qquad (6.2)$$

where T is a scalar effective cohesive traction, $F(\kappa)$ is the elastic coefficient as a function of the damage variable, κ, and δ is the effective opening displacement, as defined in [Ortiz and Pandolfi 1999].

The elastic coefficient function is defined as follows:

$$F(\kappa) = \frac{\sigma_c(1-\kappa)}{\kappa\left(\delta_u - \delta_c\right) + \delta_c} \qquad (6.3)$$

where σ_c is the initial peak traction, which represents the maximum strength of the cohesive model, δ_c is the critical displacement at which damage starts to accumulate, and δ_u is the ultimate (failure) displacement, i.e., the crack opening displacement at which the traction becomes zero and a complete crack forms.

Under cyclic loading, both the peak traction and stiffness degrade as the damage accumulates, and κ increases. The change in the peak traction and the stiffness as a function of κ are denoted by $C(\kappa)$ and $F(\kappa)$, respectively. The peak traction C as a function of the damage parameter κ is defined as follows:

$$C(\kappa) = \sigma_c\,(1-\kappa) \qquad (6.4)$$

Consequently, the effective cohesive traction T (Equation 6.2) must satisfy the following inequality:

$$T \leq C(\kappa) \qquad (6.5)$$

Figure 6.1 schematically represents the proposed relationships.

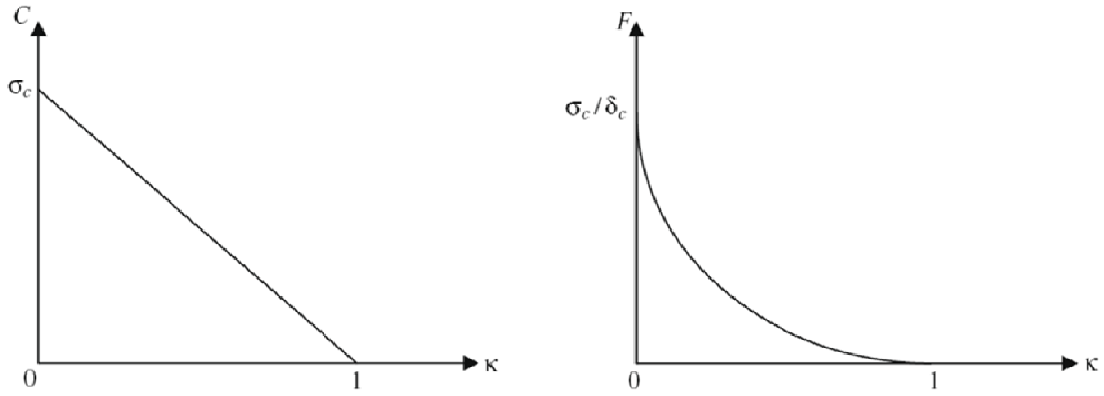

Figure 6.19: Evolution of peak traction (left)and stiffness (right) with accumulation of damage [Ural et al., 2009]

The damage parameter, κ, takes values between 0 (representing no damage) and 1 (representing complete fracture when no load is transmitted between the interfaces). As seen in Figure 6.1, $F(\kappa)$ is strictly decreasing. Thus, $C(\kappa)$, and consequently $T(\kappa)$, take values between σ_c at $\kappa=0$ and 0 when $\kappa=0$.

Under monotonic loading, like other cohesive models, the response of the model (T-δ curve) comprises of an ascending and a descending branch. On the ascending branch, while $\kappa = 0$, F is a fixed constant and Equation 6.2 results in a linear relationship between the traction, T, and the opening displacement, δ. When the traction reaches its capacity, σ_c, and the opening displacement reaches the critical value, δ_c, the inequality 6.5 becomes binding, and substituting $T = C(\kappa)$ into the Equation 6.2 yields to a new equation:

$$C(\kappa) = F(\kappa)\delta \qquad (6.6)$$

Substituting equations 6.3 and 6.4 results in another relationship between the displacement and the damage parameter on the descending branch, as follows:

$$\delta = \kappa(\delta_u - \delta_c) + \delta_c \qquad (6.7)$$

Substituting T into Equation 6.4 also results in a linear relationship between T and δ, confirming that T, κ, and δ are all linearly related.

Figure 6.2 shows a schematic illustration of the described cohesive traction-separation relationship.

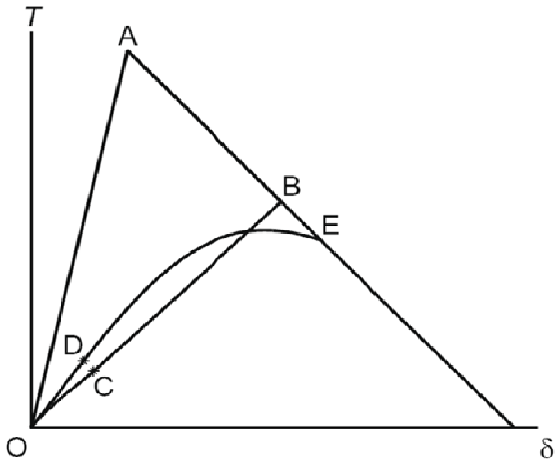

Figure 6.2: A schematic representation of the proposed cohesive traction-displacement relationship [Ural et al., 2009]

In Figure 6.2, OA is the ascending branch, on which no damage occurs. Damage initiates at point A, when the traction reaches its capacity. The damage parameter, κ, keeps increasing continuously along AB (the descending branch) upon further loading. Upon unloading, damage value is not changed along BC until the threshold C. However, it decreases from C to O. Upon reloading, the damage value does not change during OD, until the threshold D. Damage increases along DE, resulting in a decrease in the traction capacity. After reaching the descending branch in the monotonic traction-displacement envelope, κ continues to increase and causes T to decrease until there is a complete loss of load transmitting ability of the interface.

The evolution of the damage variable is ruled by the following equations:

$$\begin{aligned} \dot{\kappa} &= \alpha^* \kappa\,(T-\beta C)\,(\dot{\delta}) && \text{if } (T-\beta C)\,(\dot{\delta}) > 0, \\ \dot{\kappa} &= 0 && \text{if } (T-\beta C)\,(\dot{\delta}) < 0, \\ \dot{\kappa} &= \dot{\lambda} && \text{if } T=C \text{ and } \dot{\delta} > 0 \end{aligned} \qquad (6.8)$$

where α^* and β are material parameters, representing the rate of damage evolution and the threshold for initiation of damage, respectively, and $\dot{\lambda}$ is a free variable. Depending on loading

conditions, α^* takes two different values; denoted by α for the loading case (when $\dot{\delta} > 0$) and by $-\gamma$ for the unloading case (when $\dot{\delta} < 0$). Both α and γ are also material properties.

Evolution equations 6.8 are similar to damage plasticity [Lubliner et al. 1989] in many ways. The first and second equations in (6.8) allow damage acceleration (when $\dot{\delta} > 0$) or healing (when $\dot{\delta} < 0$) to occur only when the traction is larger or less than the threshold throughout loading and unloading, respectively. Since crack retardation sources can be considered inactive when the opening displacement is not small enough [Ural et al. 2009], the evolution equation for crack healing is set to be active only when the traction drops below the threshold value. Similar to classical plasticity theory, in which a free parameter $\dot{\lambda}$ is chosen to maintain the stress on the yield surface, a free parameter is foreseen in the third equation in 6.8 so that $\dot{\kappa}$ will not be constrained. In fact, during loading, if T reaches C, the traction will be forced to trace the monotonic envelope, i.e. $T = C(\kappa)$ holds, and thus κ will increase.

In summary, when the traction is moving along the monotonic cohesive curve, the evolution of κ depends only on the plasticity parameter, λ. When unloading, damage decreases if the value of the traction is less than the threshold value. During reloading, κ is a function of cohesive traction, rate of deformation, previous damage value, and threshold value. Lastly, to prevent the crack faces from interference, a penalty stiffness is included in the formulation in case of negative values of the relative (or, you can say, opening) displacement.

6.3 Finite element implementation and input parameters

The cohesive model described in the previous section is implemented as a constitutive relationship governing interface elements in a finite element mesh. A model with geometry similar to that of the fatigue specimens is created in the finite element program ABAQUS 6.7-1. Due to symmetry, only half of the specimen is modeled. Figure 6.3 shows the finite element model dimensions, the loading direction, and the pre-crack location. Based on our experimental observations, it is assumed that the crack path will be as shown in the figure.

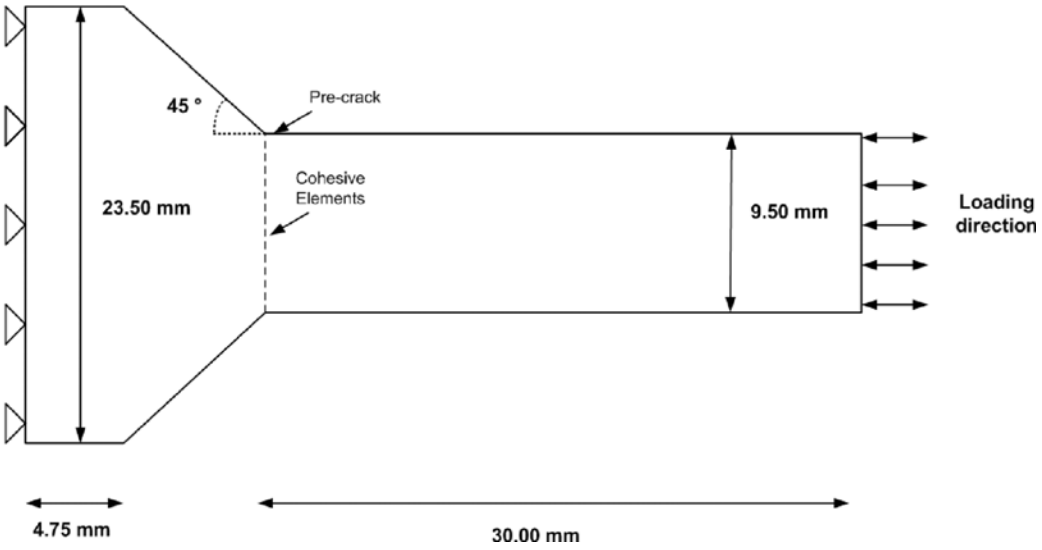

Figure 6.3: Finite element model dimensions

Figure 6.4 shows the finite element mesh, which consists of 4650 CPS4R (4-node bilinear plane stress quadrilateral) elements. Right below the weld toe in the model, a 0.19mm pre-crack is placed. A set of 49 cohesive interface elements are then placed vertically which can be considered as the predefined crack path (see Figure 6.5).

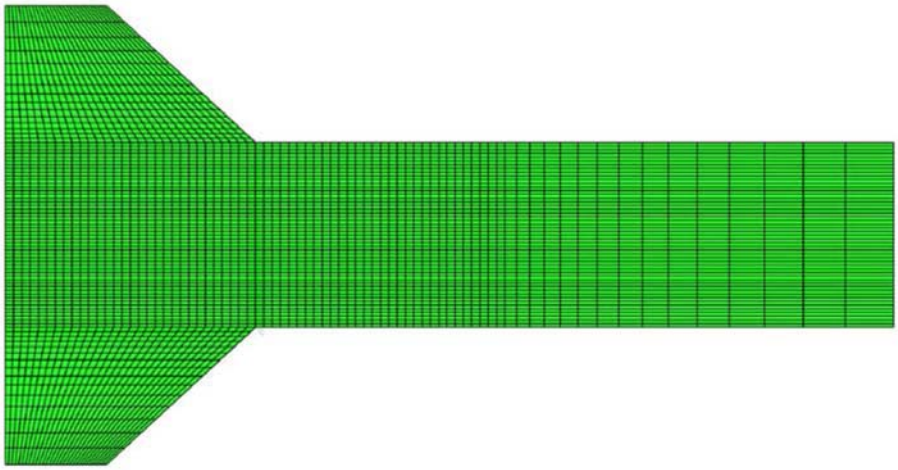

Figure 6.4: Finite element mesh

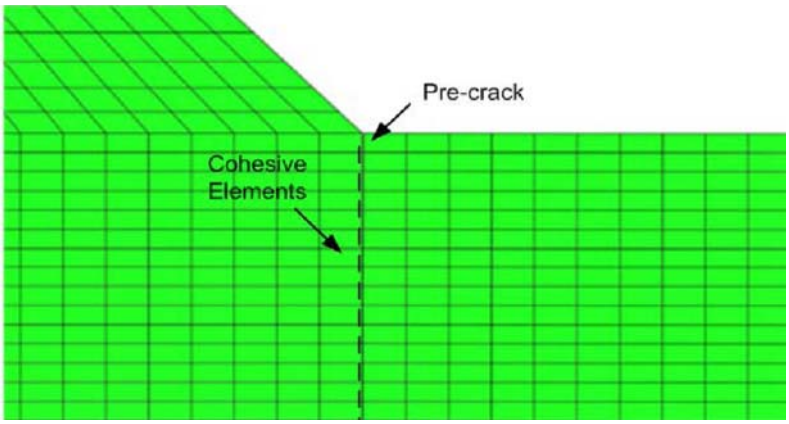

Figure 6.5: A close-up of the pre-crack and cohesive elements placement

The model needs a number of material properties to simulate the fatigue test. Where applicable, laboratory test results are used to determine model input parameters. For those parameters without experiment-based measurements, proper values are assumed and then justified. Table 6.1 summarizes the assumed values for the various input parameters.

Table 6. 2: Assumed values for model input parameters

Input parameter	Assigned Value	Units
E	*201.6*	*GPa*
σ_y	*405.4*	*MPa*
σ_u	*574.0*	*MPa*
G_c	*15.89*	*N/mm*
σ_c	*450.0*	*MPa*
δ_c	*0.00050*	*mm*

- The elastic modulus (E), yield stress (σ_y) and ultimate strength (σ_u) are determined based on the test results presented in Chapter 4. The average base metal values are used for material parameters.
- The bulk material is defined as a elastic-plastic material with various amounts of hardening.
- To determine G_c, the work of separation per unit area, the following formula is used under plane strain conditions:

$$G_c = \frac{K_{IC}^2}{E(1-\nu^2)} \qquad (6.9)$$

where K_{IC} is the fracture toughness of the material and ν is the Poisson's ratio. Room temperature Poisson's ratio value for steel is typically 0.30 [Calister 2007], however, choosing a value for fracture toughness is not that straightforward. In the absence of any test-based fracture toughness measurements for the material used for fabrication of the specimens, a room-temperature plane strain fracture toughness value of 54 $MPa\sqrt{mm}$ reported in [Calister 2007] for Steel Alloy 1040 is assumed. Steel 1040 has similar mechanical properties to ST 350W steel. The chosen value is also validated by comparing with other reported ranges for K_{IC} elsewhere, e.g. [Ashby et al. 2007].

- The local cohesive strength of the material, σ_c, is required to lie between the yield stress and the ultimate stress (Ural et al., 2009). A value of 450 MPa is assigned for σ_c, also known as the critical stress.
- Since the slope of the ascending branch of the monotonic envelope is a penalty parameter that ensures minimal separation before the critical stress is reached, the assigned value for the critical displacement, δ_c, is the smallest possible number that can be used in the model so that the model converges.

Under plane strain assumptions, the cohesive zone size can be estimated using the following expression (de Andres et al., 1999):

$$r_{coh} = \frac{\pi}{8}\frac{E}{1-\nu^2}\frac{G_c}{\sigma_c^2} \qquad (6.10)$$

which results in a cohesive zone size of 6.82mm. This zone is spanned by 35-36 interface elements and the size of the interface elements is small enough to resolve the cohesive zone [Ural et al., 2009].

Having all other parameters assigned, the triple parameters, α, β, and γ, are determined by simulating the fatigue test performed on an as-welded specimen under CA loading with nominal applied stress range of 270 MPa at R = 0.1.

To avoid a cycle-by-cycle simulation of high-cycle fatigue applications, an extrapolation scheme is required. Extrapolation is done by choosing a scaling function, like *f(k),* in such a way that

instead of simulating *N* cycles of a material whose parameters are (α, β, γ), only N/k cycles can be simulated with the parameters *(f(k)α, β, f(k)γ)*. A simple but effective extrapolation scheme reported in [Ural et al., 2009] is used herein in which *f(k) = k*; i.e. N cycles with the parameters (α, β, γ) is equal to *N/k* cycles with the parameters *(αk, β, γk)*.

The model is implemented in the finite element program ABAQUS and all analyses are performed under plane strain assumptions. A uniform, tensile, prestress field equal to 100 MPa is also added to the elements adjacent to the cohesive interfaces to simulate the residual stresses due to the welding process. In total, 100 displacement control load cycles are applied, simulating almost 70,000 cycles in the actual experiment. Thus, *k = 700* is used for extrapolation.

Since a tension-only fatigue test is simulated, no crack closure occurs and the γ parameter does not affect the results. By using a trial and error method, the other two damage parameters, i.e., α and β, are then chosen by fitting the model predictions for fatigue crack growth to the ACPD-based crack growth curve (see Figure 6.6).

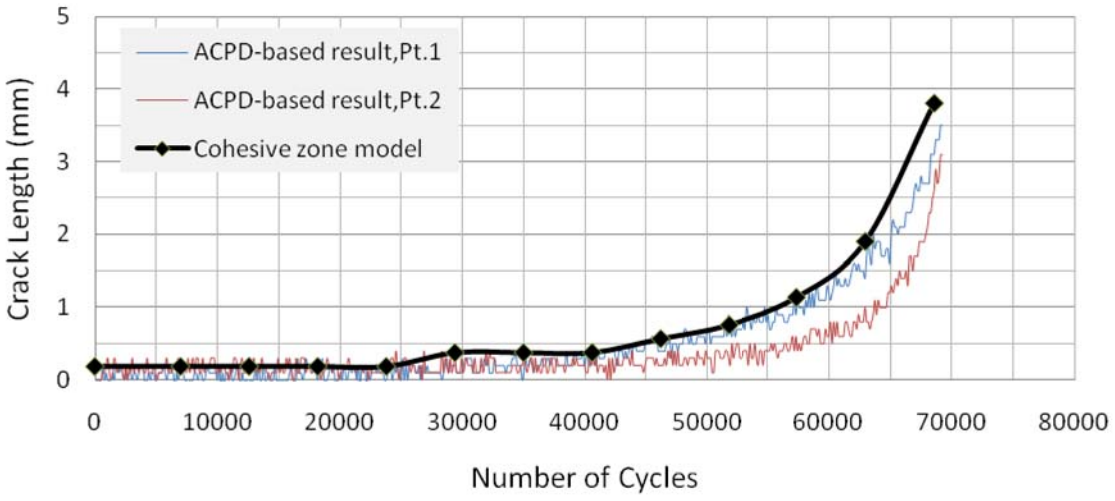

Figure 6.6: Fitted crack growth curve to the ACPD-based test results

In Figure 6.6, α is 0.020 and β is 0.038. Considering the extrapolation scheme with k = 700, the real value for α can be calculated to be 0.0000286.

6.4 Simulations of fatigue tests

Various fatigue tests are simulated and the effects of changing the R ratio, the applied stress range, and the prestress value on the response of the model are studied. Due to lack of

experimental results, the previously described SBFM model predictions are used to evaluate the cohesive model response. For all analyses, $\alpha = 0.0000286$ is assumed.

6.4.1 Effect of nominal applied stress range

Figure 6.7 compares the predictions of SBFM and of the cohesive model for fatigue tests under two applied stress ranges: 270 and 180 MPa, both at R = 0.1.

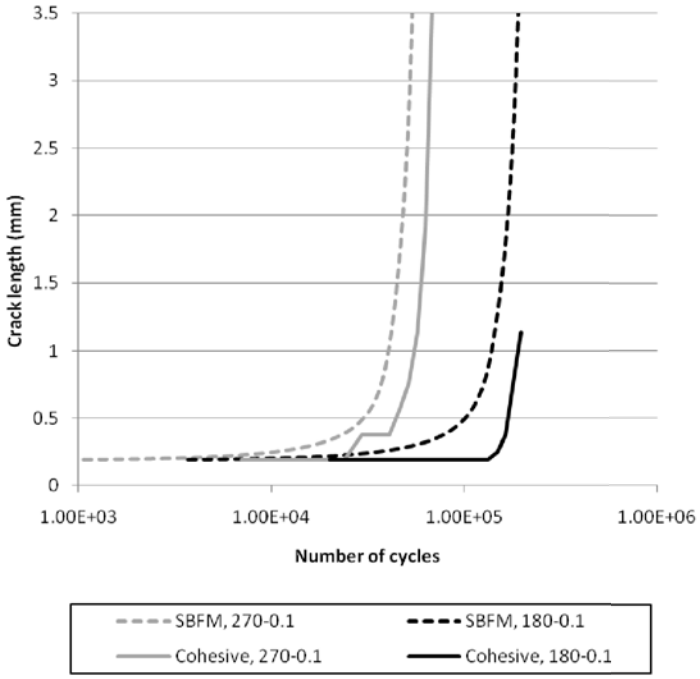

Figure 6.7: SBFM and Cohesive Zone models predictions comparison for different stress ranges

As Figure 6.7 implies, the cohesive model predicts a longer fatigue life then the SBFM model under $\Delta S = 180$ MPa. Overall, the cohesive model's predictions are consistent with the SBFM predictions for both applied stress ranges.

6.4.2 Effect of R ratio

Figure 6.8 compares SBFM and cohesive models predictions for fatigue testing under a 180 MPa applied stress range at two different R ratios of 0.1 and 0.4.

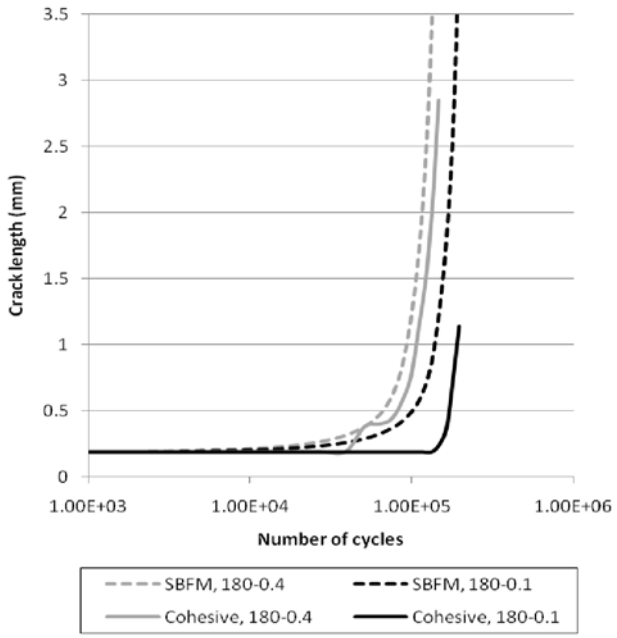

Figure 6.8: SBFM and Cohesive Zone models predictions comparison for different R ratios

It is seen that the cohesive model is able to represent the effect of R ratio. For R = 0.4, the cohesive model predictions match well with the SBFM results and good consistency is also seen for the R = 0.1 case.

6.4.3 Effect of prestress

Figure 6.9 compares both SBFM and cohesive model predictions for two different prestress fields: a uniform 100 MPa tensile prestress field accounting for welding procedure residual stresses, and a bi-linear residual stress field simulating the effect of peening, similar to Figure 5.2, with a compressive 300 MPa prestress portion on top.

As shown in Figure 6.9, the cohesive model predicts the effect of peening on delaying fatigue crack growth. Results presented in this figure are also consistent with two previous figures and the cohesive model predictions are less conservative than SBFM predictions.

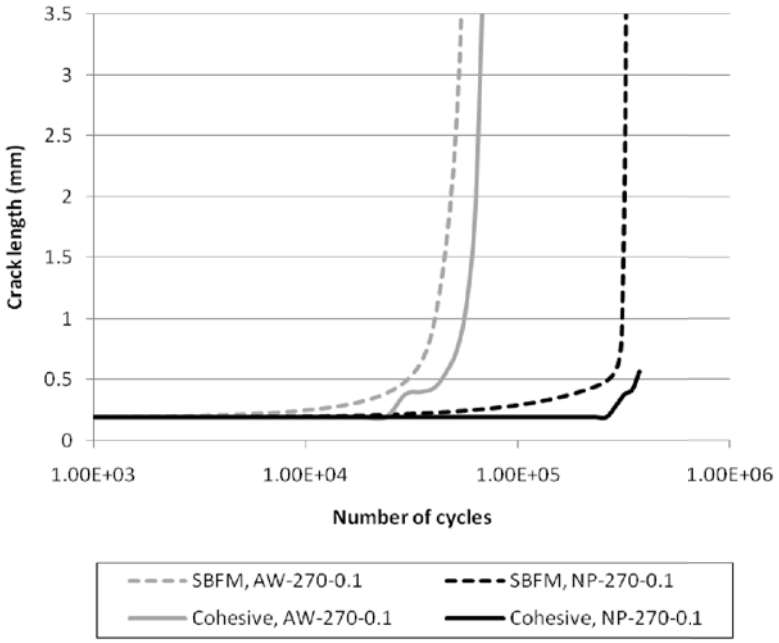

Figure 6.9: SBFM and Cohesive Zone models predictions comparison for different residual stress fields

Chapter 7

Conclusions and Recommendations

7.1 Conclusions

The conclusions presented in this chapter are divided according to the three main areas of the research work: those resulting from (i) the experiments and measurements, (ii) the strain-based fracture mechanics analysis, and (iii) the cohesive zone studies.

7.1.1 Experiments and measurements

The following conclusions are drawn based on the experiments and measurements, which are described in Chapter 3 of this thesis, with the results presented in Chapter 4:

- Material tests were conducted and the mechanical properties of the steel base metal used for specimen fabrication were accurately determined. Modulus of elasticity and yield and ultimate stresses were determined from tension coupon tests. Cyclic material constants were determined from cyclic material tests. Based on these tests, the average measured material properties were as follows: E = 201.6 GPa, σ_y = 405.4 MPa, σ_u = 574.0 MPa, K' = 1150.8 MPa and n' = 0.165.

- Fatigue tests were conducted on welded steel specimens, simulating different loading and peening conditions. In general, there was a good agreement between the mean fatigue lives of the as-welded specimens and the CAN/CSA-S6-06 Detail Category C design curve. Of the specimens tested under constant amplitude loading, those peened under load had the largest fatigue lives. In all cases, peening resulted in a significant fatigue life increase. However, greater fatigue life improvements were observed at the lower stress ranges.

- Both as-welded and needle peened specimens tested under CA-UL loading, had mean fatigue lives less than those tested under CA loading. The difference for the as-welded specimens was negligible, but this difference was significant for the peened specimens. This suggests that the peening effectiveness can be decreased considerably under cyclic loading spectrums that contain large compressive underloads.

- For the variable amplitude loading tests, the untreated specimens had mean fatigue lives slightly less than observed in the constant amplitude tests. Two loading histories were studied. The mean fatigue life for the untreated specimens under VA1 loading was slightly less than under VA2 loading. However, the reverse trend was seen for the peened specimens.
- Among all of the peened specimens, the specimens peened under load had the largest fatigue lives and the normally peened specimens tested under CA-UL loading had the shortest lives. For the normally peened species, the treatment benefit decreased with an increase in the R ratio.
- Dye penetrant was used to stain cracked specimens upon the detection of cracks. It was observed that through cracks eventually form in the as-welded specimens. However, curved crack fronts were usually seen in the peened specimens. It is concluded that the peening induced-compressive residual stresses present at the weld toe surface appear to make it easier for the already initiated cracks to grow vertically in depth rather than horizontally in width.
- A crack front marking loading scheme was also used to study the crack front shape for as-welded and peened specimens. Beach-marks indicating through crack were observed for the untreated specimens while curved beach-marks were observed for peened specimens. Additionally, the crack aspect ratio, a/c, was seen to change at different stages of fatigue testing. Crack profile measurements showed that for peened specimens the aspect ratio was around 0.40 at the time of failure.
- The alternating current potential drop (ACPD) method was used for continuous crack growth monitoring for both as-welded and peened specimens under various loading schemes. Cracks propagated at slower rates in specimens treated under load than in the normally peened and as-welded specimens. This confirmed the effect of peening on retarding crack growth. However, this was the case only for crack depths smaller than ~ 0.5-1.0 mm as similar behaviour was observed for crack depths larger than 0.5-1.0 mm, regardless of the treatment type. It is concluded that the needle peening treatment is effective in slowing down the growth of small cracks up to roughly 0.5-1.0 mm.

- Microhardness measurements were conducted on untreated and peened HAZ material and on the base metal. Needle peening resulted in a considerable increase in the near-surface hardness. However, the hardness decreases rapidly below the surface to that of the as-welded HAZ at a depth of ~0.6 mm. Studying an image of the near surface microstructure of a needle peened weld showed a compressed region near the surface up to a depth of ~0.2 mm. Compressed grain boundaries due to needle peening confirmed the effect of post weld treatments on surface microstructure of the material.

- Weld toe measurements showed that the weld toe angles for the untreated specimens are generally slightly smaller on average than those for the peened specimens. No meaningful difference for the weld toe radius was seen.

- A number of typical weld toe defects were detected. These "initial defects" were generally smaller than ~0.08 mm.

- Residual stress measurements showed that there is an approximately uniformly distributed tensile residual stress with the magnitude of 15~20 % of yield stress present near the surface of the untreated specimen. Needle peening a specimen resulted in a significant change in the residual stress distribution through the specimen thickness, with a stress magnitude as high as -500 MPa (compressive) measured near the weld toe surface. Measured residual stresses for the tested peened-specimen showed that residual stress relaxation during testing was negligible.

7.1.2 Strain-based fracture mechanics model

A previously developed strain-based fracture mechanics (SBFM) model was used to estimate analytically the effectiveness of peening applied to welded details. The following conclusions are drawn as a result of the SBFM analyses:

- Results from the conducted laboratory tests and crack growth measurements were used to establish the model input parameters. The Paris C constant was determined by fitting the predicted crack growth curve to the ACPD-based curve. Using this approach a value for the Paris C constant of $2.8 \cdot 10^{-13}$ (N, mm) was established.

- Comparison of the model predictions and test results showed that the model was able to predict the fatigue lives for both the as-welded and peened specimens for all loading

conditions. It also correctly estimated the additional benefit of peening when applied under a relatively small prestress level (45 MPa).

- The model predictions were then used to estimate the additional benefit of peening under load. More than a 100% increase in CA fatigue limit is expected as a result of normally peening, while that number can be increased to more than 200% if peening is applied under high prestress ratios. Moreover, peening effectiveness is correlated with the applied nominal stress range: as the applied stress range decreases, the peening becomes more effective. Based on SBFM predictions, an almost 100% fatigue life improvement can be achieved by needle peening under 45 MPa prestress at the stress range of 500 MPa, however, that number is about 1000% at the stress range of 300MPa.

7.1.3 Cohesive zone model

A previously developed cohesive zone model was introduced and applied to predict fatigue crack growth in a weld detail under cyclic loading. Fatigue tests were simulated using the finite element program ABAQUS. Based on this work, the following conclusions are drawn:

- Values were assumed for those parameters without experiment-based measurements, and then justified. These values were found to be G_c = 15.89 N/mm, σ_c = 450.0 MPa, and δ_c = 0.00050 mm.
- The material parameters α and β were chosen by iteration. Using values for these parameters of α = 0.0000286 and β = 0.038, the model closely estimated the ACPD-based fatigue crack growth curve for an as-welded constant amplitude fatigue test.
- Other fatigue tests were simulated and the model correctly predicted the effects of varying the applied stress range, R ratio, and residual stress level on the fatigue behaviour.

7.2 Recommendations for future work

7.2.1 Experiments and measurements

The following recommendations for the future research are made based on the experiments conducted and measurements made:

- Fatigue testing of large scale specimens is recommended to study the effects of specimen size and also the effects of the loading interactions in real welded structures.
- Peening under other prestress ratios is advised to verify the correlation between the prestress and the effectiveness of peening when applied under load.
- Both qualitative and quantitative quality control methods for peening should be investigated to ensure the predicted improvement in fatigue performance is accurate.
- The effectiveness of other peening methods under simulated in-service VA loading conditions, especially Ultrasonic Impact Treatment (UIT), should be further studied.
- Further testing to study the fatigue behaviour of welds peened-under load and then subjected to variable amplitude loading histories is recommended.

7.2.2 Strain-based fracture mechanics model

Regarding the strain- based fracture mechanics studies conducted in this research work, the following recommendations are made:

- The effects of assuming different crack shape ratios for different treatment and fatigue testing conditions should be considered in the fracture mechanics model.
- Further experiments are recommended to validate other input parameters. Specifically, crack propagation tests could be performed to better characterize the Paris constants and the μ parameter.
- Further work is recommended to develop S-N design curves for peened welded details, similar to the existing curves for as-welded details currently in the design codes.

7.2.3 Cohesive zone model

The following recommendations for future research are made based on the damage based cohesive zone modelling work performed within the scope of this thesis:

- Further experiments are recommended in order to validate other input parameters. In particular, the values for G_c and σ_c need to be accurately determined.

- Other extrapolation schemes should also be studied. Specifically, in order to predict the effects of peening in long life fatigue tests, an alternative extrapolation scheme is needed, as the linear scheme used in this study does not seem to be accurate enough.
- It is recommended to modify the cohesive zone finite element model by introducing actual residual stress distributions for the different treatment conditions. Fatigue testing on welds peened-under load can be then precisely simulated.

References

Abtahi, A., Albrecht, P., and Irwin, G. R., "Fatigue of periodically overloaded stiffener detail." J. Struct. Div., 102_11_, 2103–2119, 1976

Agerskov, A., "Fatigue in steel structures under random loading" Journal of Constructional Steel Research 53, 283–305, 2000.

Albrecht, P. and Yamada, K., "Rapid calculation of stress intensity factors, J. Structural Division, ASCE 103, pp. 377–389, 1977.

Albrecht, P., and Friedland, I. M., "Fatigue-limit effect on variable-amplitude fatigue of stiffeners." J. Struct. Div., 105_12_, 2657–2675, 1979.

Albrecht, P., and Lenwari, A., "Variable-amplitude fatigue strength of structural steel bridge details: review and simplified model." Journal of Bridge Engineering, July/August 2009, 226-237, 2009.

Albrecht, P., and Rubeiz, C., "Variable-amplitude load fatigue, Task A—Literature review, Volume III—Variable-amplitude fatigue behavior." Rep. No. FHwA-RD-87-061, Federal Highway Administration, McLean, Va., 1990.

American Association of State Highway and Transportation Officials, Standard Specifications for Highway Bridges, 4th Draft Edition, AASHTO, Washington D.C., April, 1992.

Anami K., Miki C., Tani H., and Yamamoto H., "Improving fatigue strength of welded joints by hammer peening and TIF-dressing" JSCE, Vol. 17, No.1. 57s-68s, April 2000.

Ashby M., Hugh Sh., Cebon D., "Materials- engineering, science, processing and design", Butterworth-Heinemann 2007.

ASTM E3-01: Standard Guide for Preparation of Metallographic Specimens. American Society for Testing and Materials, 2007.

ASTM E384 – 10: Standard Test Method for Knoop and Vickers Hardness of Materials, American Society for Testing and Materials, 2010.

ASTM E-8: Standard Test Methods for Tension Testing of Metallic Materials. American Society for Testing and Materials, 2004.

Braid, J.E.M., Bell, R., and Militaru, D.V., "Fatigue Life of As-Welded, Repaired, and Hammer-Peened Joints in High Strength Structural Steel". Welding in the World, 39(5), 248-261, 1998.

Branco, C.M., Infante, V., and Battista, R., "Fatigue Behaviour of Welded Joints with Cracks, Repaired by Hammer Peening". International Institute of Welding, Doc. XIII-1992-03, 2002.

Bremen, U. 1989. “Amelioration du comportement à la fatigue d’assemblages soudés : étude et modelisation de l’effet de contraintes residuelles”. EPFL Thesis No. 787, Lausanne, Switzerland, 1989.

Calister W.D., “Materials science and engineering”, John Wiley and Sons, 2007.

Canadian Standards Association (CSA), “Canadian Highway Bridge Design Code.” CAN/CSA-S6-06, 2006.

Canadian Standards Association (CSA), “Welded Steel Construction (Metal Arc Welding)”, CSA Standard W59-03, 2003.

Cheng, X., Fisher, J.W., Prask, H.J., Gnäupel-Herold, T., Yen, B.T., and Roy, S., “Residual stress modification by post-weld treatment and its beneficial effect on fatigue strength of welded structures”, International Journal of Fatigue, Vol. 25, No. 9-11, pp. 1259-1269, 2003.

Costa Borges L.A. , “Size Effects in the Fatigue Behaviour of Tubular Bridge Joints”, EPFL Thesis No. 4142, Lausanne, Switzerland, 2008.

Dabayeh, A.A., Berube A.J., Topper, T.H., “An experimental study of the effect of a flaw at a notch root on the fatigue life of cast Al 319”, Int. J. Fatigue;20(7):517-530, 1998.

de Andres, A., Perez, J.L., Ortiz, M., “Elastoplastic finite element analysis of three-dimensional fatigue crack growth in aluminum shafts subjected to axial loading”, Int. J. Solids Struct. 36, 2231–2258, 1999.

ESDEP Lecture notes, ESDEP WG 12.

European Convention for Constructional Steelwork, “Recommendations for the fatigue design of steel structures”, ECCS Technical Committe 6, Rotterdam, 1985.

Gurney, T. R. “Fatigue of Welded Structures”, Cambridge University Press, UK, 1979.

Gurney, T. R. “Theoretical Analysis of the Influence of Toe Defects on the Fatigue Strength of Fillet Welded Joints”, Report No.E/32/1977, March 1977.

Haagensen, P.J. and Maddox, S.J., “IIW Recommendations on the Post Weld Improvement of Steel and Aluminum Structures”, International Institute of Welding, Doc. XIII-1815-00, 2000.

Haagensen, P.J., Statnikov, E.S., and Lopez-Martinez, L., “Introductory fatigue tests on welded joints in high strength steel and aluminium improved by various methods including ultrasonic impact treatment (UIT)”, International Institute of Welding, Doc. XIII-1748-98, 1998.

Huo, L., Wang, D., and Zhang, Y., “Investigation of the fatigue behaviour of the welded joints treated by TIG dressing and ultrasonic peening under variable-amplitude load”, International Journal of Fatigue, Vol. 27, pp. 95-101, 2005.

Husset, J., Lieurade, H., Maltrud, F. and Truchon, M., “Fatigue crack growth monitoring using a crack front marking technique”, Welding in the World, pp. 276–282, 1985.

International Institute of Welding (IIW), “Recommendations for fatigue design of welded joints and components”, IIW Doc. XIII-1965-03 / XV-1127-03, 2005.

Khalil M., Topper T.H., “Prediction of crack-opening stress levels for 1045 as-received steel under service loading spectra”, Int. J. Fatigue 25, 149-157, 2003.

Klippstein, K.H. and Schilling, C.G., “Pilot study on the constant and variable amplitude behaviour of transverse stiffener welds”, Journal of Constructional Steel Research, 12(3-4): 229-252, 1989.

Kudryavtsev, Y., Kleiman, J., Lugovskoy, A., Lobanov, L., Knysh, V., Voitenko, O., and Prokopenko, G., “Rehabilitation and Repair of Welded Elements and Structures by Ultrasonic Peening”, International Institute of Welding, Doc. XIII-2076-05, 2005

Kulak, G. L., and Smith, I.F.C., “Analysis and design of fabricated steel structures for fatigue: A primer for civil engineers”, Structural Engineering Report No. 190, Department of Civil Engineering, University of Alberta, 1993.

Lam, T.S., Topper, T.H., and Conle, F.A., “Derivation of crack closure and crack growth rate data from effective-strain fatigue life data for fracture mechanics fatigue life predictions”, International Journal of Fatigue, Volume 20, Issue 10, Pages 703-710, November 1998.

Lugg, M., “AN INTRODUCTION TO ACPD”, TSC 2002

Maddox, S.J. “Fatigue of steel fillet welds hammer peened under load”, Welding in the World, 41(4): 343-349, 1998.

Maddox, S.J., “Improving the fatigue strength of welded joints by peening”, Metal Construction (TWI), Vol. 17, No. 4, 1985, pp. 220-224.

Manteghi, S. and Maddox, S.J., “Methods for fatigue life improvement of welded joints in medium and high strength steels”, International Institute of Welding, Doc. XIII-2006-04, 2004.

McClung, R.C., “Finite element analysis of specimen geometry effects on fatigue crack closure, Fatigue Fract. Eng. Mater. Struct. 17:861-872, 1994.

Ministry of Transportation of Ontario “Truck Weight Survey”, 1995.

National Swedish Committee on Regulations for Steel Structures, Swedish Regulations for Welded Steel Structures 74 StBk-N2, 1974.

Office of the Auditor General of Ontario, “2009 Annual Report”, 2009.

Schilling, C. G., Klippstein, K. H., Barsom, J. M., and Blake, G. T., “Fatigue of welded steel bridge members under VA loadings.” NCHRP Rep. No. 188, Transportation Research Board, Washington, D.C., 1978.

Shen, G., Glinka G., “Weight functions for a surface semi-elliptical crack in a finite thickness plate”, Theor. Appl. Fract. Mech. 15(3):247-255, 1991.

Ummenhofer, T., Weich, I., and Nitchke-Pagel, T., “Life cycle extension of welded wind energy converters and other steel constructions by weld improvement techniques”. Stahlbau, 74(6): 412-422, 2006.

Ural A. , Krishnan V. R., Papoulia K. D. “A cohesive zone model for fatigue crack growth allowing for crack retardation”, International Journal of Solids and Structures 46, 2453–2462, 2009.

Ural, A. Papoulia, K.D., “Modelling of fatigue crack growth with a damage-based cohesive zone model”. Neittaanmäki, P. et al. (Eds.), Proceedings, European Congress on Computational Methods in Applied Sciences and Engineering, ECCOMAS 2004. Jyväskylä, Finland, 2004.

Ural, A., “Advanced three-dimensional simulations and cohesive modelling of fatigue crack growth”, Ph.D. thesis, Cornell University, 2004.

Walbridge, S., “Fatigue analysis of post-weld fatigue improvement treatments using a strain-based fracture mechanics model”. Engineering Experiment Fracture Mechanics, 75: 5057-5071, 2008.

Walbridge, S. and Nussbaumer A., “Probabilistic fatigue analysis of shop and field treated tubular truss bridges”. Journal of Constructional Steel Research, 64, 156-166, 2008.

Walker, M., Van Berkel, S., and Walbridge, S., “Needle Peening to Improve the Fatigue Performance of Existing Steel Bridge Welds”. CSCE Conference, Quebec City, Canada, 2008.

Wright W., “Post-weld treatment of a welded bridge girder by ultrasonic impact treatment”, Federal Highway Administration, Turner-Fairbank Highway Research Center, 1996

Yamada, K., “Fatigue behaviour of structural components subjected to VA loading.” Ph.D. thesis, Univ. Of Maryland, College Park, Md., 1975.

Yamada, K., Nagatsu, S., and Mitsugi, Y., “Evaluation of scatter of fatigue life of welded details using fracture mechanics”. Proceedings of the JSCE, 6(1), 13-21, 1989.

Zhang, Y.-H. Maddox, S.J., “Investigation of fatigue damage to welded joints under variable amplitude loading spectra”, Int. J. Fatigue 31(1):138-152, 2009.